Università degli Studi di Udine
PhD programme in
Environmental and Energy Engineering Sciences

Doctorate Chair Prof. Alfredo SOLDATI

The tracer method and conductance probes to study stratified-dispersed flows in near horizontal pipes

Dott. Enrico Pitton

EVALUATION PANEL

Prof. Marco FOSSA	Reviewer
Prof. Alessandro PAGLIANTI	Reviewer
Prof. Luca BRANDT	Committee member
Dr. Cristian MARCHIOLI	Committee member
Dr. Francesco PICANO	Committee member
Prof. Alfredo SOLDATI	Supervisor
Prof. Marina CAMPOLO	Co-Supervisor

Author's Web Page: http://158.110.32.35/PEOPLE/Pitton.html

Author's e-mail: enrico.pitton@uniud.com - pitton.enrico@gmail.com

Author's address:

Dipartimento di Ingegneria Elettrica
Gestionale e Meccanica
Università degli Studi di Udine
Via delle Scienze, 206
33100 Udine – Italia
mobile. +39 347 3021010
web: `http://www.diegm.uniud.it`

A Giulio e nonna Linda,
alba e tramonto della Vita.

Abstract

The tracer method has been adopted to study stratified-dispersed flow in a horizontal pipe, 80 mm in diameter and 50 m long, operating at 5 Bar with nitrogen-water mixtures. The use of the tracer method in a horizontal pipe required the development of a specially designed test section, the related electronics and a data acquisition system. The test section consists of a short pipe made of a non-conducting material installed in a flow rig designed to operate at an appreciable pressure (40 Bar). The flow loop is made of metallic pipes connected to the electrical ground. The conductance probes are made of three parallel, rigid wires spaced along the flow direction and have been used to measure the height or the electrical conductivity of the liquid layer. The three-electrode geometry is aimed at minimizing current losses toward ground. The simultaneous operation of all the probes of the array, without multiplexing, allows a substantial reduction of current dispersion and a good circumferential resolution of film thickness or conductivity measurements. The probe geometry may generate an appreciable disturbance to the gas-liquid interface. This aspect of the proposed method has been studied with an experimental and numerical investigation relative to free falling liquid layers.

It has also been necessary to develop a tracer injection system, which has been designed in order to obtain uniform tracer concentration in the liquid film immediately after its injection. The main flow parameters which can be measured with the present experimental set-up are the circumferential distribution of the film height, flow rate and tracer concentration, the rates of droplet entrainment and deposition and the split of the liquid phase between the wall layer and the entrained droplets. The average tracer concentration data have been interpreted with a new three-field model of the liquid phase in the stratified-dispersed flow pattern. In the present formulation, the model holds for steady, fully developed flow conditions and is based on a one-dimensional description of the flow system. The data cover a limited number of flow conditions.

Contents

List of Figures

List of Tables

Preface

This work has been developed during a three-years doctorate activity, in the frame of a collaboration between the University of Udine and TEA Sistemi spa, a spin-off company of the University of Pisa. The work has been conducted under the supervision of Prof. Alfredo Soldati and Prof. Marina Campolo (University of Udine) and Prof. Paolo Andreussi (TEA Sistemi, University of Pisa).

Part of results are going to be published as scientific papers (see List of Publications, Appendix B). The Financial contribution of ENI E&P and TEA Sistemi spa is gratefully acknowledged.

1 Introduction

1.1 Motivation

Pipeline transportation over long distances of natural gas in presence of a liquid phase (light hydrocarbons and/or water) is becoming a common practice in the oil industry and can be extremely challenging when a subsea pipeline is expected to operate at high pressure and low temperature (see for instance, Fig. 1.1). When this happens, the risks associated with the Flow Assurance issues and the high investment costs oblige to a very careful design of the flow lines.

In these near horizontal pipes, stratified flow conditions are encountered at moderate phase velocities. At increasing the gas velocity, only part of the liquid flows at the pipe wall, while the remaining liquid is entrained by the gas in the form of fast moving droplets which tend to deposit back onto the wall layer. The competing phenomena of droplet entrainment and deposition determine the liquid hold-up in the pipe and appreciably affect the pressure gradient.

At large gas velocities, the liquid film may cover the entire pipe wall and the resulting flow pattern becomes similar to annular flow in vertical pipes. However, horizontal annular flow typically occurs in heat transfer equipment, when small diameter pipes are employed. Also most of the available data are relative to small diameter pipes operating with air and water at atmospheric pressure. In natural gas pipelines the pipe diameter and the gas velocity are such that the continuous liquid phase mainly flows at the bottom of the pipe and the resulting flow pattern can be better classified as Stratified-Dispersed (SD) flow.

One-dimensional, multi-field, gas-liquid flow models reported in the literature (see for instance, Bendiksen et al., 1991), are based on a set of one-dimensional mass, momentum and energy conservation equations. The integration of these equations requires empirical methods or correlations to predict the transitions among the different flow patterns and to estimate flow parameters such as the rates of droplet entrainment and deposition. Recently, Bonizzi et al., (2009) have shown that the integration of con-

FIGURE 1.1 – Representation of a subsea pipeline for hydrocarbons transportation (Taken from http://subseaworldnews.com/).

servation equations directly provides a reliable detection of flow pattern transitions.

In both models cited above, stratified-dispersed flow in inclined pipes and annular flow in a vertical pipe are described by a similar set of conservation and closure equations. However, the closure equations required for these two regimes are quite different, due to the different effects of gravity. But while the data and correlations relative to vertical annular flow are abundant, there are almost no correlations for horizontal or inclined flow and very few data are available for the development or validation of flow models. These data are also lacking under conditions far from those of industrial interest, as far as pipe diameter and gas and liquid physical properties concern. The main objective of the present work is the development of a new experimental method able to provide these data. These data should include the measurement of the pressure gradient, the liquid holdup, the fraction of entrained droplets and the rates of droplet entrainment and deposition.

The critical flow parameters to be predicted in stratified-dispersed flow are the flow rate and thickness distribution of the liquid layer flowing at pipe wall and the fraction of liquid entrainment. This is because the split of the liquid phase determines the overall liquid hold-up in the pipe and the value of the frictional pressure losses.

Besides the fluid dynamic issue, a better understanding of the flow behavior of the dispersed phase has a wide number of implications in heat transfer and in the Flow Assurance studies.

The models developed for the prediction of liquid entrainment are based on the observation that in fully developed SD or annular flow the rate of droplet deposition becomes equal to the rate of entrainment and the entrained liquid fraction becomes approximately constant along the pipe. This allows the measurement of the entrained liquid and also the development of independent correlations for the deposition and entrainment rates to be

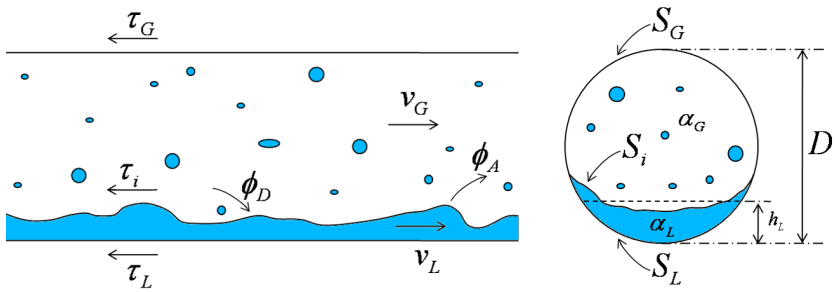

FIGURE 1.2 – Simplified scheme of stratified flow in atomization region.

performed.

1.2 Description of Stratified-Dispersed flow

Despite its apparent simplicity, the flow characteristics of SD flow (pressure drop, liquid holdup, interface shape, etc.) reveal complex behaviors at an accurate analysis. In the following the main characteristics of stratified and stratified-dispersed flows are summarised.

According to Andritsos and Hanratty, (1987b) and Tzotzi et al., (2011), four main subregimes of the stratified gas-liquid flow in horizontal and slightly downward pipes can be recognized. (1) A smooth region, occurring at moderate phase velocities, where the gas-liquid interface is smooth. (2) A two-dimensional (2-D) wave region, where the interface is covered by small amplitude, short wavelength regular disturbances. (3) A wavy region with large amplitude, irregular waves, with a steep front and a gradually sloping back. These structures are also found in the literature as roll waves or KelvinHelmholtz (K-H) waves. (4) An atomization region, where droplets or liquid filaments are torn off from the crests of large-amplitude waves and transported by the action of kinetic energy and turbulence of the gaseous phase, until they deposite back on the pipe wall at a certain distance downstream. In addition, the liquid starts climbing up the pipe walls and the interface shape is no longer approximated by a flat horizontal plane. In Fig. 1.2 a reference scheme of a stratified atomizing flow is depicted, along with the main parameters tipically involved for its modelisation.

Even though in the present study the declared range of interest of gas superficial velocity spans from 5 to 25 m/s, special attention was given to high gas flow rates, for which atomization occurs. All results shown in Chapter 6 focus on this flow pattern region.

1.3 Scope

The scope of this work is the development and validation of an experimental technique to characterize stratified-dispersed flow in near horizontal pipes. The main challenging task is the quantitative measurement of complex phenomena occurring in this flow pattern when pipe diameter and gas and liquid physical properties are close to those encountered in industrial applications, expecially in natural gas pipelines.

The principal quantities to be measured are:

- the liquid flow rate and film thickness distribution on the pipe wall, and consequently
- the liquid holdup;
- the amount of liquid entrained in the gas core;
- the rates of liquid entrainment and deposition;
- the gas-liquid interface shape;
- the pressure drop along the line.

1.4 Outline

The thesis is organized as follows:

- First, in Chapter 2 a literature review of the principal experimental methods used in the past to measure liquid film thickness, droplet entrainment and mass transfer rates in annular and stratified-dispersed flow is proposed. At the conclusion of the chapter the most suitable methodology for the present experiment is identified in the combination of conductance probes and tracer method.

  Then, the manuscript is structured in two main parts. Part I deals with the development of the conductance probes and is based on the paper Andreussi et al. (2014), currently under review:

- In Chapter 3 the design of the conductance probe test section is described in detail, along with theoretical considerations and numerical simulations of the electric field and probe intrusiveness. An entire section is dedicated to the desciption of the electronics developed for the data acquisition.

- In Chapter 4 the test section is validated in a free falling liquid flow. Results are compared with a theoretical model, numerical simulations and other experimental measurements available in the literature.

Part II is dedicated to the application of the tracer method to stratified-dispersed flow and is based on the published article Pitton et al. (2014):

- In Chapter 5 the theoretical description of the tracer technique in the study of vertical annular flow is recalled. Then, the design of the injection system is described, along with the experimental procedure.
- In Chapter 6 the results obtained from the flow tests are presented and discussed. A modified model of tracer transport is introduced to better fit the experimental data.

- Finally, Chapter 7 summarises the work performed and the main results obtained. Some proposals are presented for future improvements of the method.

2

Literature survey: experimental techniques

2.1 Introduction

In this chapter we propose a literature review of the principal experimental methods used in the past to measure liquid film thickness, droplet entrainment and rate of droplet entrainment and deposition in annular and SD flow. Obviously, the best technique does not exist, since each one presents advanteges and disadvantages, depending on the specific phenomena to be studied. This survey has the scope of giving to the reader a general overview of the main techniques developed until now and to identify the most suitable methodology for the present experiment.

2.2 Film thickness measurement

The importance of liquid films in a wide variety of industrial processes has led to extensive experimental investigations into the phenomenon of film flow. As film thickness in two-phase applications are generally less than a few millimiters, accurate measurementa are difficult, and this has led to the development of a variety of measurement techniques.

The most recent critical review on liquid film thickness measurements in multiphase systems has been carried out by Clark, (2002). In this section we do not examine in-depth each technique as done by this author, but we limit to highlight the most relevant methods suggested in his work, completed with the contribution of a wider literature research on the topic.

2.2.1 Hold-up measurements

Hold-up methods were arguably the preferred film thickness measurement techniques prior to the emergence of localised methods such as the conductance technique. These methods simply consisted on the isolation of a

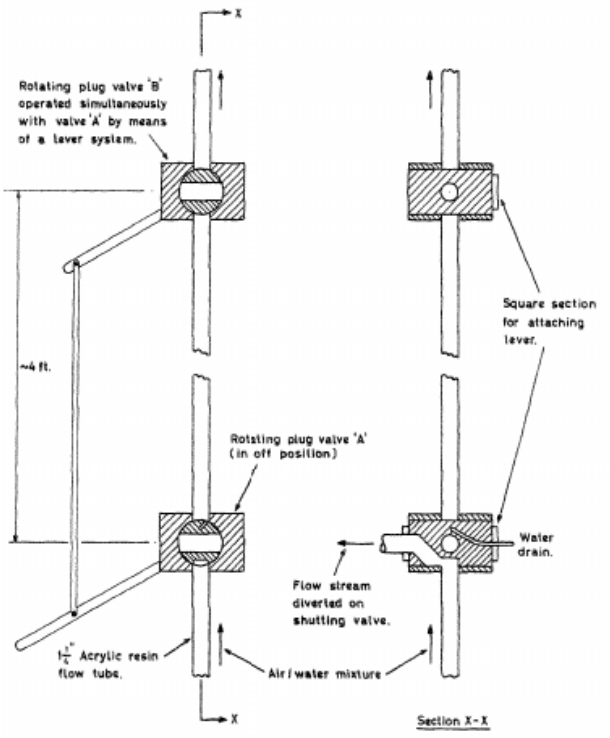

FIGURE 2.1 – Linked valve arrangements for hold-up measurements. Taken from Collier and Hewitt (1964).

section of film and on the measurement of the liquid volume within this isolated section, an early example of which is presented by Hewitt et al., (1961). It is in the isolation of the film where the main difficulties in implementation arise, and several techniques have been developed for different flow regimes.

Hewitt and Lovegrove (1963) give an example of the application of a manual hold-up system for film thickness measurement of air-water mixtures in upward annular flow in a 32 mm bore tube. They managed the rapid isolation of the section of tube by using two rotating plug valves operated by linked levers, shown schematically in Fig. 2.1. The total amount of liquid retained in the section is measured to determine the average film thickness. This method makes the assumption that the liquid extracted and measured consists entirely of liquid from the film. This is not strictly true, as part of the liquid will often flow in the gas core. The authors point out that this is negligible in climbing films at the low flowrates studied within their report but question the validity of the method at high mass flowrates, as in the case of the present work. Hughmark and Pressburg (1961) report a

similar study on vertical upward co-current air-liquid flow using electrical switching by solenoid valves.

2.2.2 Capacitance Probes

Capacitance probes are a popular alternative to Conductance Probes (Section 2.2.3) and Light Absorption Techniques (Section 2.2.7) where the test fluid is non-conductive, opaque, or immiscible with dyestuffs or a combination of these properties. The principle of this method is that, because of the usually significant difference in dielectric constant between a liquid and a gas, a pair of probes will give a localised measurement of the capacitance that will be function of the thickness of the film between them. Dukler and Bergelin (1952) and Tailby and Portalski (1960) report early applications of capacitance probes in measuring the thickness of falling films over flat vertical surfaces. Most recently, Ambrosini et al. (1998) used this capacitance probe technique for film thickness measurements of a water film falling down a flat plate. These studies and the other ones reported by Clark (2002) present results generally consistent with other studies using alternative film thickness techniques.

Ozgu et al. (1973) developed and tested two different electrode geometries, "ring"and "rod"probes. These geometries have been largely adopted also for conductance probes, as will be cleared in the next section. Ring probes are a pair of metallic electrode rings mounted flush into the tubular test section with their detecting surface shaped to match the contour of the surface over which the film flows. Rod probes are a pair of metallic cylindrical electrodes that are mounted flush into the test section at pre-determined distance in a similar manner to ring probes. Leskovar et al. (1979) and Sun et al. (1982) report improvements on the original design of ring and rod probes for application within vertical annular flows. They concluded that their ring arrangements were adequate for the measurement of film thickness from near zero up to a value of about 4-6 mm. The major advantage of rod probes over ring probes is that their spacing is easily adjustable, allowing optimisation of the signal for local film phenomena for improved resolution. However, it is also reported that rod probes have a lesser range of applicability in film thickness measurements than their ring counterparts (from near zero to 3 mm).

For the measurement of film thickness under transient conditions such as wavy flow, the response of the capacitance circuit and associated recorder must be sufficiently rapid to match the phenomenon. Another relevant task is the suppression of noise. Leskovar et al. (1979) mounted their probes with an attaching block that contained a metallic box designed to screen out local noise. All other literature sources studied for this review utilising capacitance probe have used similar shielding methods.

In the present review we do not focus on calibration procedure. We limit to state that a carefull calibration is a mandatory requirement for

every specific technique, expecially for those involving complex geometries. Calibration can be achieved using static and dynamic methods, depending on feasibility and on the precision to be achieved.

2.2.3 Conductance Probes

Conductance probes are probably the most extensively used time varying film thickness measuring device, and as such, a vast number of literature references on their use have been reported. The principle is similar to that of capacitance techniques and many of the problems of measurement are inherent in both techniques. Basically, conductance is measured using a circuit containing a pre-determined electrode configuration and the readings are amplified and displayed by some output devices.

Film thickness can be determined from these conductance measurements if a calibrated relationship, preferably linear, can be established between the two parameters within the range of measurements. Conductance probes are basically divided into two groups: flush-mounted probes and parallel-wire probes. Combinations of these two configurations have been also developed.

In the following the main configurations will be presented, going from simpler to more complex arrangements. All probe configurations have been grouped into two distinct sections: the basic two-electrode arrangement and more sophisticated multiple electrode set-ups.

TWO-ELECTRODE PROBES

Needle Contact Probe

The needle contact probe has always been a popular film thickness measurement device, and this popularity is probably due to the simplicity of its application to virtually any type and size of conducting liquid film flow. Recently, it has been primarily utilised as a calibration or comparative device for other more sophisticated probes. An example is reported in Fig. 2.2.

The probe usually consists of a needle, electrically insulated except for the tip, mounted on a moveable rod that can be brought to the surface of the film. An electrode is placed flush on the wall on which the film flows, directly opposite the needle tip. When the needle tip makes contact with the surface of the film a conduction path is made between the needle and the wall electrode allowing this contact to be recorded electronically. A micrometer or some form of dial gauge can measure the previously calibrated distance from the wall electrode.

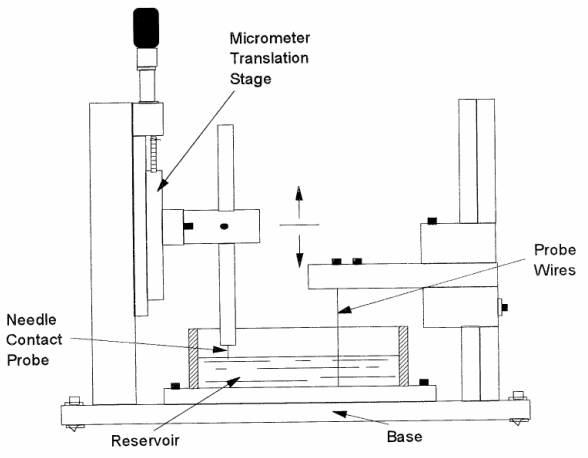

FIGURE 2.2 – Needle Contact probe used for wire probe calibration (Taken from Koskie et al., 1989).

Parallel-wire

Parallel-wire conductance probes consist of two thin parallel metallic wires stretched through the film normal to the wall over which the film flows, as shown in Fig. 2.3 (B). The wires are usually manufactured of platinum based alloys (e.g. platinum-rhodium) to ensure stable performance. The wires can be anchored in an insulating material at the wall and lacquered-insulated over one half of their length to allow thickness variations to be monitored on one side of a pipe only.

Parallel-wire conductance probes have been found to give a linear response in a wider range of film thickness and to allow a more localised measurement to be undertaken than their flush-mounted counterparts. For these reasons it is easy to understand why parallel wire probes have quickly become the most popular implementation of conductance film thickness measurement since their earliest reported applications by Swanson (1966) and Miya et al. (1971).

However, wire probes do have negative and potentially limiting features that should be considered before application. The most significant of these features are the inevitable disturbance of the flow and the modifications of the interfacial surface caused by the wetting of the wires. Naturally, the choice of wire thickness is critical to their successful operation. The wire diameter must be minimised to have negligible disturbance effect on the flow and yet large enough to be sensitive to electrical resistance with respect to the entire liquid film height.

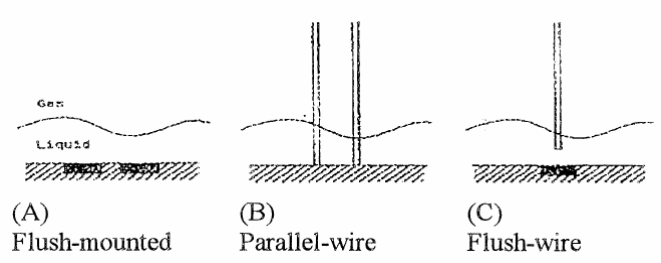

FIGURE 2.3 – Schematic diagram of differing conductance probe types.

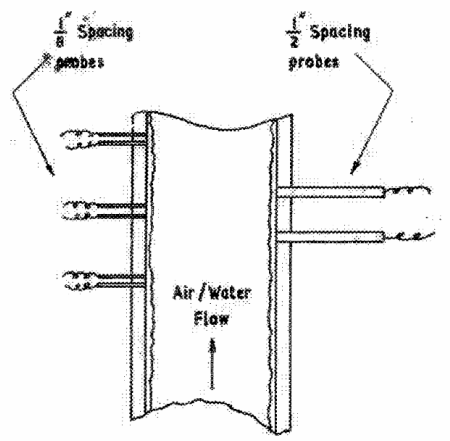

FIGURE 2.4 – Schematic of arrangement of two pin conductance probes at two different probe spacings. (Taken from Hewitt et al., 1962).

Flush-mounted

Flush-mounted probes have been first described by Coney (1973). These probes involve the measurement of conductance between two electrodes mounted flush in the insulated surface over which the film is passing (see Fig. 2.3 (A)). Contrary to wire probes, flush-mounted electrodes present a linear response only under specific conditions, i.e. above a determined distance between electrodes and below a value of film thickness. This drawback is compensated by their non-disturbance to the film flow, which is not true for the other conductance probe variants.

A number of electrode geometries for flush mounted conductance probes have been reported. Here we report the two configurations mainly adopted in the past:

- **Two pin electrodes.** These electrodes are probably the easiest to manufacture. Two metal pins/rods are mounted in the tube at a short distance between each other (circa 3-10 mm) and machined to match

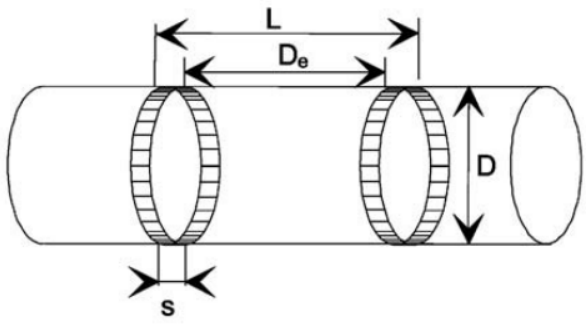

FIGURE 2.5 – Schematic of arrangement of a two ring conductance probe. (Taken from Devia and Fossa, 2003).

the shape of the surface. Numerous examples of the application of flush two-pin conductance probes for liquid film thickness measurements in vertical upflow and downflow of air-water mixtures, within the range of 30 mm to 42 mm i.d. vertical tubes, can be found in the literature. An example is shown in Fig. 2.4.

- **Two ring electrodes.** This configuration is comparable to the ring electrode geometry used in capacitance measurements (Section 2.2.2). These probes simply consist of two metal ring electrodes built flush with the tube inner surface at a set distance apart (see Fig. 2.5). Clearly this geometry is limited to measurement of the cross-sectional averaged thickness around the tube. The two-ring probe has been used by Asali et al. (1985) to measure the mean thickness of liquid films flowing in a vertical pipe. The electrical behavior and the application of ring probes to other flow patterns has been described in details by Andreussi et al. (1988) and Fossa (1998).

Among the numerous applications of conductance probes, the work by Geraci et al. (2007) is significant because these authors used both wire and flush-mounted probes for the measurement of the liquid film thickness distribution in stratified-dispersed flow.

Flush-wire

Murav'ev et al. (1984) first discussed and reported the combination of flush and wire conductance electrodes in the hope to create a probe configuration that would have the advantages, and limit the disadvantages, of both these electrodes. Kang and Kim (1992a) developed an alternative flush-wire conductance probe geometry (see Fig. 2.3 (C)) in an effort to increase the spatial resolution for continuous measurements of film thickness above what was available by conventional flush-mounted and wire probes. In this configuration the flush-wire conductance probe consists of an electrode mounted

flush to the wall over which the film flows and a vertical wire electrode inserted/suspended from the opposite wall. For flush-wire probes, many of the difficulties encountered with the utilisation of wire probes still exist. However, as the wire is only partially submerged in the film, wire induced drag phenomena are naturally less significant.

MULTIPLE ELECTRODE PROBES

Multiple needle contact

Sekoguchi et al. (1985) reports the development of a spatial measurement device, whose basic measuring element is the needle contact probe. This film thickness measurement device consists of 409 needle contact probes located strategically over the cross-section of interest, parallel to the wall, with an example of their arrangement shown in Fig. 2.6. The wires are electrically insulated, except for their tips, by coating with a thin resin film. They are assembled in 23 clusters of 17 probes and one cluster of 18 probes. The probes were arranged with spacings from 50 μm to 3.2 mm over a tube radius of 12.9 mm, with the bases of the clusters clamped in 24 equally spaced slots on the periphery of the tube. Sekoguchi and Takeishi (1989) report the development of a computer algorithm to process the data obtained with this sensor in order to determine the gas-liquid interface by comparing the signals of individual neighbouring probes.

Multiple needle contact probes have successfully been utilised by Sekoguchi and co-workers to improve knowledge of gas liquid interfacial characteristics in vertical flows, however, the devices are still open to potential areas of criticism. Firstly, they still retain the intrusive properties of their needle probe constituents. Moreover, Kang and Kim (1992b) criticised the resolution of this device, stating its limitation to identifying the liquid existence at only 17 fixed points along the film thickness direction.

Multiple parallel wire

Kang and Kim (1992b) report the development of a multi-conductance probe to measure the instantaneous spatial liquid film thickness, and in particular the three dimensional wave forms which are observed in thin liquid film flow. The probe is basically an extension of their development work on the flush-wire conductance probe (described above), and a schematic of their multi-conductance probe is presented in Fig. 2.7.

The probe consists of a large built-in flush electrode and eleven platinum wire electrodes. The front ten wire electrodes were uniformly aligned along the width of the flow, with the eleventh electrode located at a position downstream for wave velocity measurements.

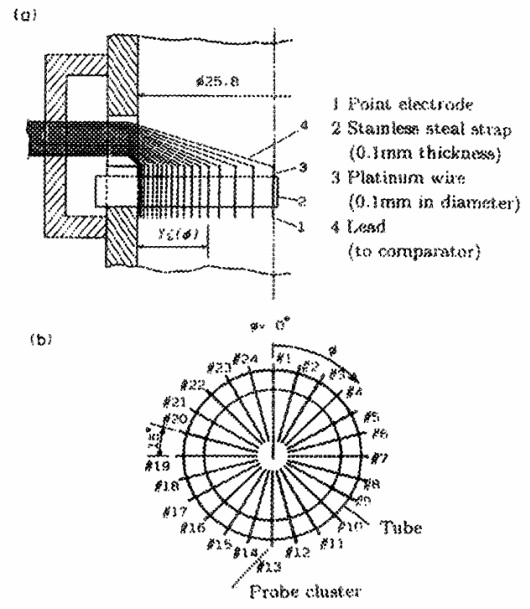

FIGURE 2.6 – Multiple needle probe: (a) arrangement of point-electrode probes on a strap; (b) arrangement of probe-clusters around the periphery. (Taken from Sekoguchi and Mori, 1997).

The measurement system was located at the centre of the measurement channel and the wire probes were connected to a translation stage for precision placement. Data processing provided three dimensional and contour maps of the interfacial surface.

Both horizontal and vertical liquid film experiments were conducted. This measurement technique is capable of giving an averaged thickness over a very small area for each wire, thought to be less than 0.1 mm, indicating a high accuracy. However, this application is restricted to 10 wires across a 150 mm wide duct resulting in a very poor global resolution.

Multiple flush-mounted

Multiple ring probes have been used by Nydal et al. (1992) to study slug flow in inclined pipes. Zhao et al. (2013) used a set of four flush-mounted probes to study the flow of large disturbance waves in a vertical film. In this paper, a thorough discussion on the signal saturation of flush-mounted probes at increasing the film thickness is reported.

In addition to the multiple needle contact probe, Sekoguchi and coworkers report also two multiple flush-mounted electrode devices, based on rings and rods electrode geometries, respectively.

Their multiple ring device simply consisted of 94 pairs of 5 mm spaced,

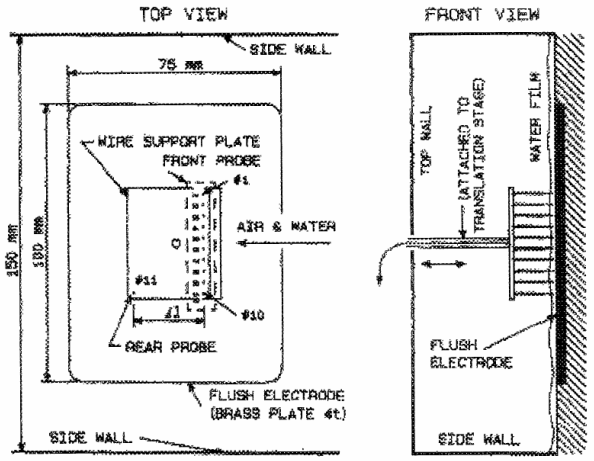

FIGURE 2.7 – Multiple parallel wire probe for film thickness measurement. (Taken from Kang and Kim, 1992b).

flush, 0.5 mm thick ring shaped electrode conductance probes arranged axially with a spacing of 25 mm over the tube length of 2325 mm. Each pair of ring electrodes can only provide the time-varying cross-sectional mean liquid holdup value at the locality, however, collectively can reveal limited information on the spatial distribution of hold up or film thickness along the tube length.

In order to obtain a higher spatial resolution, Sekoguchi and Mori (1997) report the implementation of an improved device, consisting of 266 pairs of 0.5 mm diameter brass rod electrodes, spaced 5 mm apart, and mounted flush with the inside wall of the tube. This provides a low resolution spatial picture of a vertical strip of the film.

Wire mesh sensor

Along with the development of multiple probe test sections, advanced conductance methods have also been proposed, such as the wire mesh sensor (WMS), Prasser et al., (1998). In Fig. 2.8 a schematic of the sensor used by these authors is reported. This technique has provided good results when studying bubble or slug flow and has been recently adopted by Vieira et al. (2014) to study stratified-dispersed flow in a horizontal pipe. Despite the method provides a good evaluation of quantities such as the mean and local void fraction distribution on the cross section, the rough discretization of the mesh (lateral distance between crossing points: 4.7 mm) does not allow an accurate measurement of the liquid thickness at the bottom of the pipe. On the other hand, a grid refinement would inevitably lead to heavy effects of intrusiveness, as for the other multiple electrode approaches.

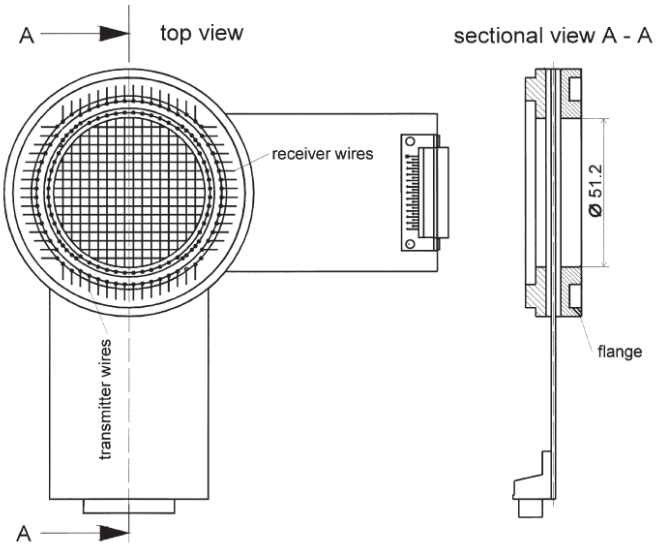

FIGURE 2.8 – Sketch of the wire-mesh sensor (16 x 16 sensitive points) developed by Prasser et al. (1998).

Recently a study on the intrusiveness of a three layer WMS has been presented by Ito et al. (2011). These authors observed an appreciable effect of the wire mesh on the velocity of gas bubbles crossing the mesh. This flow condition is quite different from the case of film flow, but the work of Ito et al. (2011) represents a serious warning against the use of intrusive probes.

As clearly stated by Vieira et al. (2014), they were not able at all to detect thin liquid films flowing in the upper part of the pipe, due to the scarsity of crossing points close to the duct surface. Moreover, all the points of the WMS closer to the wall than 1 mm were masked, in order to disregard the effect of sticking droplets on the pipe wall. These aspects pose a serious limitation to direct application of this technique to thin film flow.

This problem has been faced by Damsohn and Prasser (2009). These authors developed a multiple probe sensor, based on the wire mesh approach, which consists of a matrix of flush-mounted electrodes realized on a Printed Circuit Board (PCB).

This sensor, pictured in Fig. 2.9, is characterized by high time and spatial resolution, that allows a careful study of superficial waves over a wide range of wavelengths and wave velocities. On the other hand, this probe is limited by the saturation of its electrical response at increasing the film thickness. According to these authors, the maximum film thickness that can be measured with their sensor is 0.8 mm. The combined use of wire mesh and wall sensors may provide a complete picture of the liquid layer flowing at pipe wall in stratified-dispersed flow. Anyway, nobody seems to

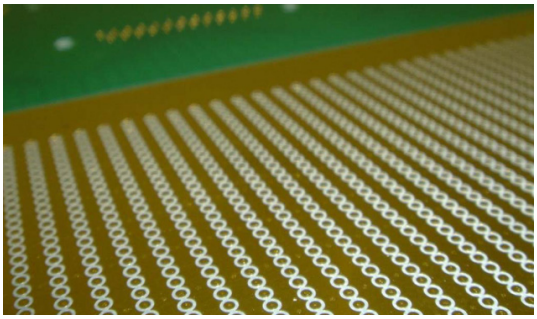

FIGURE 2.9 – Printed Circuit Board probe realized by Damsohn and Prasser (2009).

have implemented this concept so far.

Electronic circuitry

At the conclusions of this section on conductance method, few considerations on the electronic circuitry involved must be done. This latter has become more sophisticated in line with the rapid developments in electronics, generally. Tipically, the circuit arrangement utilised involves the application of a high frequency, constant amplitude A.C. voltage, produced in the from of a sine wave by a signal generator. The voltage is imposed across the electrode pair and the film thickness dependent electrical current is measured in the form of voltage drop across a reference resistor.

The choice of signal wave frequency is critical to the successful operation of the probe. Brown et al. (1978) and Kvurt et al. (1981) did extensive study on the influence of frequency on measurement results. These authors came to the conclusion that frequencies not lower than 50-100 kHz should be adopted to avoid that effect of "double layer"(due to ions transfer between electrodes) produces a long term drift of the probe response, affecting the reproducibility of measurements.

A final consideration about electronics goes to the use of multiplexing. When adopting multiple electrode probes, it may be possibile that the simultaneous use of all the electrodes leads to a mutual interference between them. In these cases, it is preferred to activate the electrodes one at a time. The most recent electronic circuitries are able to operate at a switching frequency of 10000 frames per second. However, the use of multiplexing implies a higher complexity in design and management of the electronics.

2.2.4 Absorption of Electromagnetic Radiation

A large number of measurement techniques are based on the measurement of the absorption of electromagnetic radiation, for which Lambert-Beer law applies:

$$\delta = -\frac{1}{\mu} \ln \left(\frac{I}{I_0} \right) \tag{2.2.1}$$

where, δ is the thickness, μ the linear absorption coefficient of the material, I the emergent intensity, and I_0 is the incident intensity of the monochromatic collimated beam. Therefore, in the determination of the thickness of a liquid film, if a collimated beam of radiation is passed through the liquid film, and the intensity of emergent radiation is measured by a suitable detector, Eq. 2.2.1 can be used to calculate the instantaneous film thickness δ, once μ is known.

Radiations of many bands of the spectrum have been used, from short wavelength radio waves (microwaves) through visible light to X-rays and radioactive emission (γ-rays). All the techniques essentially measure localised density (void fraction), and can only measure liquid film thickness in situations where all the liquid between emitter and detector is in the form of a single film. This causes difficulty in the case of annular flow in a pipe, since there are two films and liquid droplets entrained in the airflow involved along the pipe diameter.

X-ray Absorption

Solesio et al. (1978) developed this technique for film thickness measurements and reported success at measuring films of 1 mm average thickness flowing down an inclined plane at intervals of one millisecond with a precision finer than 50 microns. Their experimental set-up is shown schematically in Fig. 2.10.

The methodology consists of the production perpendicular to the film base of a fine collimated beam of X-rays, 0.5 mm in diameter, from the X-ray tube. This beam is partially absorbed by the film and the non-absorbed remainder is detected and measured on a photomultiplier. Solesio et al. (1978) found X-ray absorption not easy to utilise, but believed it provided a good comparative method for other techniques due to its fast response times and point information. This claim is supported by favourable comparison data obtained with a parallel conductance probe arrangement, recorded simultaneously with the X-ray data at virtually the same location.

A similar comparison has been performed recently by Zhang et al. (2013). They used simultaneously the ultrafast X-ray tomography and the wire-mesh sensor to study upward bubbly and slug flow in a vertical pipe. The authors concluded that comparison of gas fraction radial profiles gave in general good agreement and showed a maximum difference below 4%.

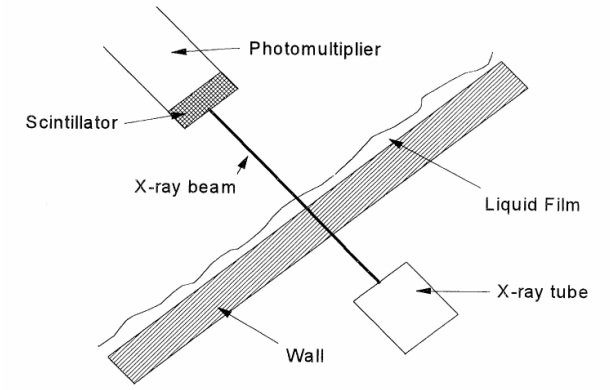

FIGURE 2.10 – X-ray absorption measurement technique.

β-ray Attenuation

Absorption of both beta and gamma rays has long been a traditional method for measuring the density of gas-liquid mixtures. Cravarolo et al. (1961) used β-ray absorption or "attenuation"for measuring the density of gas-liquid mixtures flowing in circular ducts in the dispersed region. The authors claim to have had reasonable agreement with other density measurement methods but do not include any data within their report. Recently, Bieberle et al. (2011) presented a high-resolution γ-ray computed tomography measurement system for the determination of cross-sectional time-averaged void distributions in thermo hydraulic facilities.

Anyway, applications of this method for liquid film-thickness measurements could not be found, and this is almost certainly due to the hazardous aspects of this technique and the wealth of alternatives.

Finally, it must be pointed out that when high frequency electromagnetic radiations are employed (X-γ-β-rays), a specific safety assurance is required. This may represent an additional limitation for their use.

Microwave Techniques

Roy et al. (1986) presented a simple experimental demonstration of how a microwave waveguide technique can be used for the non-intrusive measurement of the instantaneous local thickness of a falling liquid film. The concept behind the technique is that the loss of intensity of microwaves travelling along the wave guide and through the test section, i.e. between generator and detector, is a function of the local thickness of the film. The width of waveguide determines the local measurement spacing of the technique, and was 15 mm for this demonstration. Great care was taken in ensuring there was no leakage of energy from the measurement system, which could

detract from the accuracy of the measurements due to interference from nearby objects. The authors also gave consideration to the frequency of microwaves to be used, to ensure the frequency adopted was low enough that the depth of penetration and wavelength in the liquid are much larger than the thickness of the liquid film.

The authors state their belief that the method is suitable for both tubular and rectangular test sections. Disappointingly, little quantitative data are presented for comparison with alternative techniques.

2.2.5 Acoustic Method

The principle of this technique is that the variation of the ratio of energy transported and transmitted by the sound wave to that absorbed by the medium, is proportional only to the thickness and density of the medium. Bezrodnyy and Antoshko (1992) presented an experimental method for measuring the flow of falling films based on these acoustic properties of the liquid film. The authors claim the method be simple to implement, non-intrusive and have general applicability to falling film measurement in the range of 0 - 2.5 mm thick with an error not exceeding ±15%.

2.2.6 Ultrasonic Pulse-Echo Method

The basis of ultrasonic film thickness measurement is a pulse-echo approach, similar to sonar employed in naval applications. This involves the measurement of the transit time of a sound wave transmitted and received by a single ultrasonic transducer. The transit time can be combined with knowledge of the speed of sound in water to determine the liquid film thickness. This approach is complicated if the transducer is located external to the test section by the fact that the ultrasonic pulse will first be partly reflected by the solid wall/liquid interface before further partial reflection at the liquid/air interface, and also any subsequent interfaces.

The original study of Starkovich et al. (1980) presented results obtained for static and dynamic water films ranging between 1 and 10 mm in thickness on both horizontal and inclined surfaces, which were in good agreement with results obtained by needle contact probe. Dallman (1981) extended this original study to falling liquid films as thin as 0.02 mm in a cylinder and Chang et al. (1982) further developed the technique in liquid film thickness measurements in a variety of flow regimes in horizontal gas-liquid flows. More recently, Kamei and Serizawa (1998) used an ultrasonic device to measure the film thickness circumferential distribution of a two phase flow. They adopted a set of 40 sensors positioned on a simulated nuclear fuel rod, with time resolution of 250 Hz.

This technique have potentially advantages in industrial application: the ultrasonic transmitter can be easily attached/detached to the pipe without

the need for modification, and if the velocity of sound through the liquid under investigation is known, then no calibration is required.

2.2.7 Light Absorption Techniques

If the duct, or at least one section of the pipe, is made of a transparent material, optical methods can be applied to the study of the flow. Simple high-speed video recordings, even if performed with sophisticated cameras, are just able to provide qualitative behaviours of fluid mechanics and few quantitative measurable parameters. For example, Schubring et al. (2010b) used this technique to study disturbance waves in vertical annular flow. These authors could produce statistics on wave length, frequency and velocity whereas their videos did not provide any information about wave amplitude nor film thickness distribution. In order to obtain a deeper insight of the liquid layer, the method must involve the use of a collimated light beam to illuminate the specific portion of the film under study.

As stated for the other electromagnetic techniques, even light absorption methods are based on the well known Lambert-Beer law, see Eq. 2.2.1. In practice, this traditionally involves the passing of a monochromatic light beam through a liquid film and detecting the intensity of received light on the other side of the film by some form of photo device.

Practical problems in the implementation of the technique have shaped its design. One such problem is that the absorption coefficient of typical test liquids, such as water, for white light is too low to be capable of detecting small changes in the thickness of the liquid. This problem has been traditionally solved by the additions of small quantities of dye to the liquid film to dramatically increase the absorption of white light, however, this is potentially an area of concern about the validity of the technique. The addition of a dyestuff could potentially alter the test liquid properties, and of particular concern is the fact that a number of dyestuffs are very surface active and could artificially effect the interfacial shape.

Another potential experimental problem is that when using a vertical, tubular pipe geometry the light beam must be introduced in such a way that it can pass through the liquid film being measured without also travelling through the liquid film on the opposite wall. Introduction of the light beam in tubular geometries to avoid this problem has been attempted in a number of different ways.

Probably the largest area of concern in the utilisation of the light absorption technique in film thickness measurements is the reduction of the intensity of light received by the detector by means other than absorption, i.e. scattering and refraction at the air/liquid interface. In wavy flow, the surface of the film can be rough enough so that a potentially significant amount of the light contacting it will be scattered and refracted away from the detector. If the angle of the wave is sufficiently acute, even reflection of the light can become significant.

More recently, a novel light absorption technique has been developed by Wittig et al. (1992) and subsequently utilised by co-workers. In their arrangement, a laser using a near infra-red wavelength of 1462 nm replaces the white light source. At this wavelength strong absorption effects occur in liquids such as water, water/glycerin or alcohols without the need of enhancement with the addition of a dye. For example, a 1 mm thick water film leads to an intensity reduction of more than 95%, enabling high-accuracy thin film thickness measurements.

2.2.8 Fluorescence Technique

The fluorescence technique was developed and first reported by Hewitt et al. (1964) as a replacement for the traditional light absorption approach which was believed by these workers not to be applicable to thin liquid films. The principle of the technique is that a fluorescent dyestuff is added (e.g. 0.1 g/litre of sodium fluorescein by Hewitt et al., 1964) into the circulating liquid that forms the liquid film under study and this is irradiated with a beam of monochromatic light. The intensity of the light emitted by this irradiation of the film will proportionally increase with increasing film thickness. A portion of this emitted light is then collected and recorded, after separation from reflected and scattered components of the incident illumination.

More recently, this technique is evolved into the Planar Laser Induced Fluorescence (PLIF) (Schubring et al., 2010a; Cherdantsev et al., 2014; Zadrazil et al., 2014), in which the monochromatic light beam has been replaced by a laser sheet. The signal is usually captured by a CCD or CMOS camera and timing electronics is often used to synchronize pulsed light sources with intensified cameras.

PLIF is interesting because it allows to measure with good precision not only the thickness of the liquid layer, but also the concentration of a tracer dissolved into the fluid. This technique has been used with remarkable results for velocity, concentration, temperature and pressure measurements. Fig. 2.11 shows the scheme of the test section utilised in the work of Schubring et al. (2010a).

At the end of this section, a final note is directed to tomography, in general. A significant bottleneck of any tomographic method is that measurements must be post-processed by dedicated reconstruction algorithms, in order to produce decoded results in the form of images. This step is quite sophisticated and can introduce sistematic errors on data processing, as reported by most of the authors that performed tomographic measurements. Moreover, due to the complexity of image reconstruction, the process is often carried out off-line after all the data have been stored in a database.

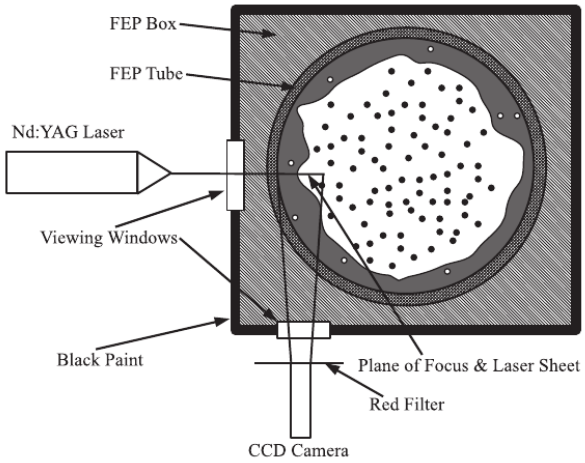

FIGURE 2.11 – Test section for PLIF measurements. (Taken from Schubring et al., 2010a).

Xu et al. (1997) described their efforts to optimize the numerical procedure with which they processed data. This aspect must be seriously considered when tomographic techniques are adopted.

Other minor or less used techniques for film thickness measurement are reported by Clark (2002). We send back to this author's review for any in-depth analysis and extensions about such methods.

2.3 Entrainment measurements

The methods originally developed to measure the liquid entrainment can be divided into two main groups: isokinetic sampling of the dispersed phase (Wallis, 1962) and extraction of the wall layer with a porous section of the pipe (Cousins and Hewitt, 1968). Both these methods present advantages and disadvantages.

- The **Isokinetic Probe** technique, also called the Sampling Probe Method, consists of droplet flux measurements at a number of positions on the tube cross section. After the pioneering work of Wallis (1962) and Gill et al. (1963-1964), this method has been adopted and improved by many scientists (Asali, 1984; Paras and Karabelas, 1991; Barbosa Jr et al., 2002). In Fig. 2.12 the setup used by these latter authors is reported. This technique, in addition to be intrusive, expecially in small diameter tubes, is particularly inaccurate when

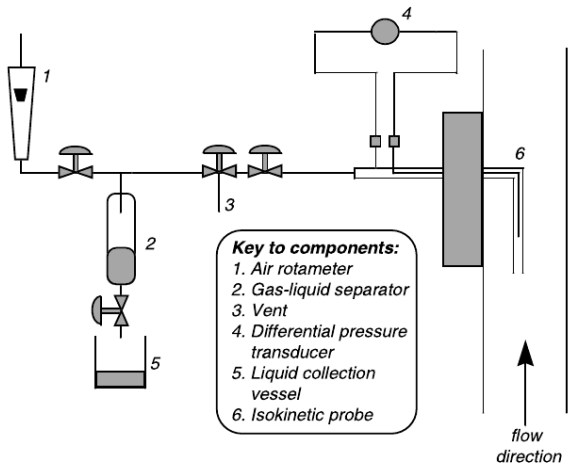

FIGURE 2.12 – Experimental setup for gas and liquid collection using the isokinetic sampling probe (Taken from Barbosa Jr. et al., 2002).

measurements are taken close to the gas-liquid interface, due to the sampling of part of the continuous liquid fraction, i.e. the wave crests. Moreover, the sampling probe method becomes more difficult to be used, and less accurate, in a horizontal pipe rather than in a vertical one, due to the loss of circular symmetry which obliges to sample in the entire cross-section. However, most of the data relative to horizontal flows have been obtained by the sampling probe method (Paras and Karabelas, 1991; Williams et al., 1996; Tayebi et al., 2000).

- The other common method reported in literature is the **Liquid Film Removal** (also known as the Liquid Film Extraction, or Liquid Film Withdrawal). It consists of the extraction of liquid film through a porous wall or a small opening on the pipe wall. Its first users included Cousins and Hewitt (1968), Webb (1970) and Whalley et al. (1973). The method has been adopted more recently by Fore and Dukler (1995), Lopez de Bertodano et al. (1997), and Assad et al. (1998). This method is limited by the necessity of visual observations to define the point of complete removal of the liquid film. This is very subjective and often results in large errors in the measurements. The removal of part of the gas along with the liquid also causes an additional uncertainty. Another source of error occurs close to the transition between ripple-annular flow and wispy-annular flow. It happens when the liquid flow increases and the film becomes frothy. The hypothesis is that there are large water ligaments attached to the film that cannot be removed (Assad et al., 1998). In Fig. 2.13 the experimental setup adopted by Lopez de Bertodano et al. (2001) is

shown.

- A third, less used, technique to measure the liquid entrainment is the **Tracer Method**. It was originally proposed by Quandt (1965) and has been adopted by Cousins et al. (1965), Jagota et al. (1973), Andreussi (1983) and Schadel et al. (1990) for the study of vertical annular flow. Leman et al. (1985) extended the method to developing flow conditions. This method provides a fairly accurate measurement of the fraction of entrained liquid, and good estimates of the entrainment and deposition rates, also under developing flow conditions, as shown by Leman et al. (1985). The tracer method consists of the continuous injection into the wall layer of a tracer which, in air-water flow, can be a salt solution. The measurement of salt concentration immediately after the injection allows the base film flow rate, and consequently the liquid entrainment, to be determined. In the original application of the method, film samples were extracted and analysed (see Fig. 2.14). The use of conductance probes allowed salt concentration to be detected in situ, as reported by Schadel et al. (1990), with a noticeable simplification of the method. The tracer method has been perceived to be cumbersome and inaccurate, as also recently reported by Han et al. (2007). For this reason it has never been adopted for the study of SD flow and very few times for vertical annular flows.

A modified version of the tracer method has been proposed by Han et al. (2007). They combined this method with the liquid film extraction in order to quantify the disturbances casued by the separation process. These authors designed a special component that removes the liquid layer from the flow using a static annulus slightly larger than the average film thickness. The drawback of this separator is the potential that part of the liquid carried by the crest of the disturbance waves (whose amplitudes are typically several times larger than that of the average film thickness) is physically sheared into the gas core by the separator itself. For this reason, a $CaCl_2$ solution was injected into the liquid film through a port just before the separator. The mass fraction of $CaCl_2$ appearing in the gas core after the extraction reflected the liquid portion that was sheared off from the liquid film. This new technique seems to provide reliable, consistent and repeatable data. However, it appears impossible to apply this kind of separator on non axisymmetric flows, and generally on flows whose liquid film thickness is not known a priori.

2.4 Entrainment and deposition rate measurement

The rates of droplet entrainment and deposition have been measured under developing or fully developed flow conditions. However, the situation

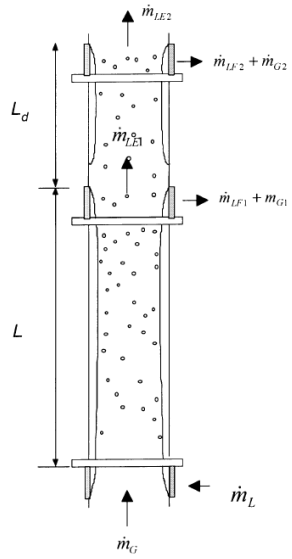

FIGURE 2.13 – Double film removal technique. The first extraction is used to measure the liquid entrainment. The second extraction is used to measure the deposition rate. (Taken from Lopez de Bertodano et al., 2001).

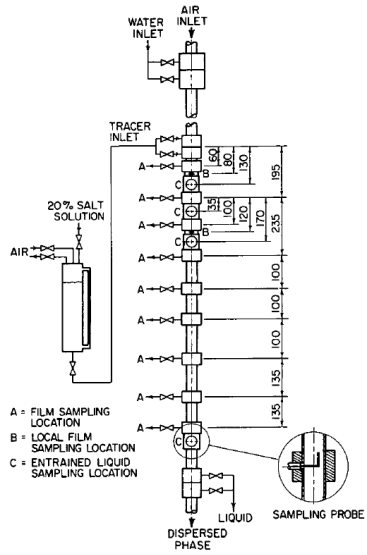

FIGURE 2.14 – Scheme of the experimental apparatus used by Andreussi (1983) for the measurement of liquid entrainment and droplet exchange with the tracer method.

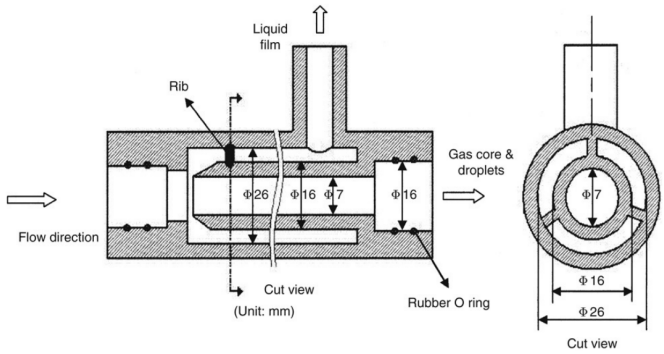

FIGURE 2.15 – Front and side view of gas-liquid separator developed by Han et al. (2007) for the removal of the liquid layer.

reported by Hewitt (1979) more than 30 years ago is still actual: there are no well established techniques for measuring these quantities even in a vertical pipe and very few new methods have been proposed in recent years. In the past, mainly two methods have been used: the double film extraction method and the tracer method, both already mentioned as techniques adopted to measure the liquid entrainment.

- The **Double Film Extraction Method** permits the measurement not only of the liquid entrainment, but also of the rate of deposition between the first and a second extraction, positioned downstream (see Fig. 2.13). As already explained above, this method suffers of a number of limitations and potential inaccuracies, but the main problem is that the deposition rate is measured under developing flow conditions, namely between the two extraction units. This makes the data analysis and the development of correlations a difficult task.

- Also the **Tracer Method** can be employed for the measurement of the rates of entrainment and deposition, if the salt concentration in the film is measured not only immediately after the injection, but also at different distances downstream, as depicted in Fig. 2.14. Mass balances are then used to relate the measurements of tracer concentration along the pipe to the rate of droplet interchange between the film and the initially unsalted liquid droplets carried by the gas. This implies the necessity of performing conductivity measurements at several axial and circumferential locations at the same time. As already mentioned, the use of conductance probes instead of liquid samples can simplify the method, allowing salt concentration to be detected in situ. Other methods could be adopted to measure the concentration of a tracer in the liquid layer, such as the Planar Laser Induced Fluorescence. However, the application of this method for the simul-

taneous measurement at several positions in the pipe would be much more expensive and complicated to be performed.

Very few alternatives can be found in literature for the measurement of droplet interchange. Among the new techniques, recently Damsohn and Prasser (2011) proposed a conductance method based on a sensor able to detect the impact of droplets on a thin horizontal liquid film. This sensor is the same illustrated in Section 2.2.3 for thickness measurement of a liquid layer. In order to detect smaller droplets, the droplet conductivity has been increased. In principle, the sensor developed by these authors allows the droplet deposition rate to be determined, but it seems difficult that this method be able to deal with thick films and/or large deposition rates, unless the method evolves towards the tracer method.

2.5 Conclusions

After this literature review on the methods used in the past to measure liquid film thickness, entrainment and rate of entrainment and deposition in annular or stratified dispersed flow, it is easier for us to justify the choice of the tracer method along with conductance probes in the present work.

For what regards the measurement of liquid film thickness, optical techniques or other electromagnetic radiation methods could be employed. These techniques present the advantage of being non-intrusive. However, they can be quite expensive and when using high energy radiation equipments, specific safety assurance is required. Furthemore, all these techniques can be used only in situations where all the liquid between emitter and detector is in the form of a single film. This provides a strong limitation since in our flow conditions the film can reach the top of the pipe covering all the circumference and liquid droplets entrainment in the airflow is also expected.

Precision in light absorption technique is heavily affected by scattering and refraction at the air/liquid interface. Since this happens in wavy flow, also in present experiment the use of this technique is not recommended. Another reason to disregard these methods for the present application is that it may be difficult to use the same method to measure not only the film thickness, but also the entrainment and liquid mass transfer rate.

Traditional conductance methods have the disadvantage of being intrusive. On the other hand, conductance probes are relatively cheap both in construction and in maintenance, they are easy to design and are probably the only instrument, among those presented above, that can be totally manifactured on one's own, excepted few electronic components. On the contrary of tomographic techniques, conductance probes do not need any reconstruction algorithm, as they just provide istantaneous values of conductance, and these values are limited by the number of adopted probes. The subsequent interpretation of the measurements is generally performed

in real-time using the characteristic curve of the sensors.

For what regards the measurement of entrainment and deposition rates, the tracer method still appears as the only viable technique to study complex flow patterns such as annular or SD flow in near horizontal pipes. This explains why the tracer method has been adopted in the present application: this choice has been made due to the lack of any possible alternative. As it will be clear from this work, the tracer method is really cumbersome and not particularly accurate, as perceived by the community, but it allows an unexpected insight into the structure of SD flow. This is because the tracer is a passive scalar and its transport in a complex flow system may reveal more details than the ones for which its use has been originally planned. Moreover, the experimental system developed to measure the tracer transport allows also different data to be taken.

To our knowledge the tracer method has never been adopted for the analysis of SD flow in near-horizontal pipes or for fluids other than water, but there are no reasons to suspect that the method will not be as effective in these cases. The main problem when dealing with SD flow is the asymmetric distribution of the liquid layer, which requires, on one hand, a circumferential distribution of the inlet tracer flow rate proportional to the local liquid film flow rate. On the other hand, that the tracer concentration be measured not only at various distances from the tracer injection, but also around the pipe wall.

The first task has been solved with an ad-hoc designed system of injection.The second requirement can be obtained with a series of conductance probes positioned at a number of axial locations and distributed all around the pipe circumference. The only alternative method to measure the concentration of a species dissolved in the fluid is the Planar Laser Induced Fluorescence. Anyway, the adaptation of this technique to perform measurements around the pipe wall at several axial positions, would reveal to be very complex to be performed and managed.

In conclusion, the combined use of the tracer method and conductance probes should be able to provide simultaneous measurements of film thickness, liquid entrainment and rates of liquid exchange in a stratified-dispersed flow.

For the present experiments, a non-conventional probe configuration has been chosen, in order to obtain the best results for all the flow conditions analysed. In the next chapter, this novel probe arrangement is described and the entire design of the test section is explained in detail.

I

Conductance Probes

Life is strange. When I was a child, they strictly recommended me not to play with water near electrical sources. Once graduated, they proposed me to work by playing with water and electrical current.

3

Development of the wire conductance probe test section

3.1 Introduction

In the present chapter, a conductance method based on the use of an array of non-conventional wire probes is proposed to measure the local thickness or conductivity of a liquid layer flowing at pipe wall. The test section has been developed to generate these data at flow conditions as close as possible to those of interest to the oil and gas industry in terms of pipe diameter and physical properties. The same experimental set-up can be adopted to study other flow patterns occurring in near-horizontal pipes besides stratified-dispersed flow, such as the flow of liquid slugs or elongated gas bubbles and, in general, developing or transient flow conditions. The range of liquid thicknesses that we expect to measure in an 80 mm pipe goes from a minimum of 0.05 mm to a maximum of 50-60 mm. Having this objective in mind, wire probes appear to be a better choice than flush-mounted probes, due to their intrinsic linearity, which allows the height of both thin and thick liquid layers to be measured with good accuracy. The expected measuring range of the proposed test section is very wide, but it can easily be attained using the same electronics by properly choosing the liquid conductivity. This represents a major advantage of wire probes when compared with flush-mounted probes or other methods adopted in the literature to measure the thickness of a liquid layer.

The main disadvantage of wire probes is that they are intrusive. This potential limitation of wire probes is examined into details in the present chapter, with a careful computation of the flow and the electric fields around the electrodes. A set of experiments relative to free falling films, which allowed the wire probes to be compared with the ring probes, is presented in the next chapter.

The idea is to adopt the same spatial configuration of Multiple Needle Contact probe presented in Section 2.2.3, replacing each radial point-electrode cluster with a wire probe. This change allows to move from a discrete to a continue measurement of liquid presence on the cross section.

The conductance probes proposed in the present work are made of three rigid wires spaced along the flow direction. A circumferential array of such probes is installed in a test section made of a non-conducting material which is part of a flow rig designed to operate at an appreciable pressure, composed of metallic pipes electrically connected to the ground potential. A common excitation signal is fed to all the central electrodes (transmitting electrodes) of the array, while the external electrodes (receiving electrodes) are actively kept at the same, ground potential. This allows to minimize current losses towards ground and to mitigate possible interferences between adjacent probes. The simultaneous operation of all the probes of the array, without multiplexing, is also useful to obtain a good circumferential resolution of film thickness or conductivity measurements.

A three electrode geometry of conductance probes has been used by other authors. For instance, Kim et al. (2009) developed a three electrode flush-mounted probe to compensate the temperature effects on thickness measurements. A three layer wire mesh has been developed by Richter et al. (2002) to measure the velocity of the gas bubbles crossing the mesh. In both cases, the objectives of these authors were substantially different from those of the present method.

In this chapter, a thorough description of the multi-probe test section, the electrical behavior of the probes and the data acquisition system is reported.

3.2 Conductance Probes

3.2.1 Basic Theory

Brown et al. (1978) showed that the impedance between two electrodes immersed in a conducting liquid is mainly resistive and does not depend on the frequency of the signal applied to the electrodes when this frequency is high enough to make double-layer effects negligible. In this case, the electrical potential generated around the electrodes can be computed by integrating the Laplace equation:

$$\nabla^2 \phi = 0 \ \ on\, \Omega \, ; \quad \phi = \phi_0 \ \ on\, \partial\Omega \, , \tag{3.2.1}$$

where ϕ is the electrical potential, Ω the domain, $\partial\Omega$ the domain boundary and ϕ_0 the value that the potential assumes at the boundary. Once the spatial distribution of the electrical potential has been determined, it is possible to calculate the electrical current density vector, $\overrightarrow{J}$, with the following

relationship:

$$\overrightarrow{J} = -\gamma \cdot \nabla\phi \,, \tag{3.2.2}$$

where γ is the electric conductivity of the medium. The conductance between the electrodes can be derived as the ratio between the current and the potential difference.

The main advantage of wire probes is that the conductance between the electrodes, G, is a linear function of the film height, h, and the liquid conductivity, γ,

$$G = k \cdot \gamma \cdot h \,, \tag{3.2.3}$$

where k is a constant related to the probe geometry. Brown et al. (1978) have shown that at increasing frequency of the applied electrical signal, k tends to the value:

$$k = \frac{\pi}{ln\left[(d-r)/r\right]} \,, \tag{3.2.4}$$

where r is the radius of the wires and d is the distance between them.

The present flow rig has been designed to operate at significant pressure (the design pressure is 40 Bar). This level of pressure can be easily sustained by the non-conducting sections of the pipe used to install the conductance probes. However, these sections are part of a metallic rig connected to the electrical ground and this may represent a threat to the integrity of the probe signals. This potential limitation of the experimental method has been faced by adopting a novel probe geometry which consists of three rigid wire electrodes spaced along the flow direction. In these probes the central electrode is set at a given potential and the two side electrodes are actively set at the same reference potential of the metallic pipe. In practice, with this probe configuration the side electrodes act as screens to current dispersion towards the metallic pipe.

For an unbounded liquid film the conductance of a three wire probe can be theoretically derived from the Laplace equation. In this case the constant k assumes the value

$$k = \frac{4\pi}{3\ln\left[(d-r)/r\right] - \ln\left[(2d-r)/(d+r)\right]} \,. \tag{3.2.5}$$

This equation allows the probe and the related electronics to be properly designed when the probe is installed in an insulated pipe. When d and r are assigned, a comparison between Eqs. 3.2.4 and 3.2.5 shows that with two receiving electrodes the current signal increases by about 40%. The other advantages related to the three-electrode configuration and the use of an array of conductance probes, operating without multiplexing, are discussed in the next section.

3.2.2 Estimation of current dispersion

The conductance measurement between wire electrodes can be significantly altered by the presence of nearby probes and/or side currents directed towards the metallic sections of the pipe set at the ground potential. The probe conductance and the side currents can be derived from the numerical integration of Laplace equation with the appropriate boundary conditions. In the following examples, this integration has been performed for the probe geometry (electrode diameter and distance between the transmitting and receiving electrodes) reported in Section 3.2.3.

TABLE 3.1 – Fractions of current dispersed to ground.

	Three electrodes	Two electrodes
Single Probe	0.40	0.61
Probe Array	0.05	0.16

In Fig. 3.1, the electric field relative to a single three-wire probe immersed in a liquid film of constant height is compared with the case of a two-wire probe. In these computations, the film height is equal to 8 mm, the electrodes are aligned along the flow direction, the distance between the terminal sections of the liquid film (connected to ground) and the film width are both equal to 314 mm and the external one or two electrodes are kept at ground potential. From this figure, the difference between the two electric fields can be detected at least from a qualitative point of view. In Table 3.1, the current dispersion expressed as fraction of the total current transmitted by the central electrode to the terminal sections of the liquid film is reported. As can be seen from Table 3.1, in both cases the current dispersion is relevant, though it is significantly smaller for the three-electrode probe.

In Fig. 3.2(a), the electric field relative to an array of three-electrode probes spaced at a distance of 13.8 mm is shown. As can be seen from this figure, the side probes bound the electric field of all the probes of the array into a restricted volume of liquid. A comparison with the case of a single three-electrode probe shown in Fig. 3.1(a) is useful to understand the effect of side probes. A similar evaluation is made in Fig. 3.2(b) for a two-electrode probe. Fig. 3.2 clearly shows the significant contribution of the active adjacent probes to the confinement of the electrical field of all the probes. As reported in Table 3.1, also the current dispersion is significantly reduced. For a three-wire probe, the fraction of current dispersion decreases from 0.40 for a single probe to 0.05 for a probe array. For a two-wire probe from 0.61 to 0.16. In both cases the effect of side probes is relevant and, in particular, a three-electrode array, without multiplexing, is able to minimize the current dispersion to ground. This explains why this probe configuration has been chosen.

The case of stratified flow in a circular pipe is considered in Fig. 3.3,

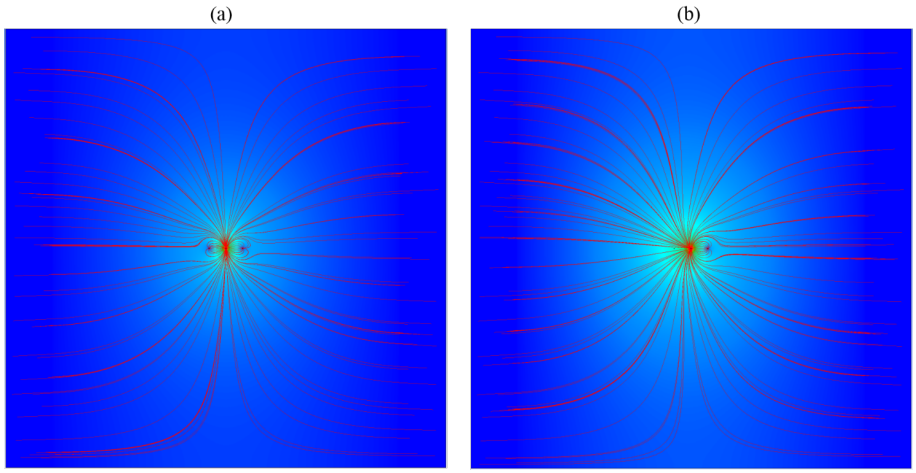

FIGURE 3.1 – Electric fields of single three-wire probe (a) and two-wire probe (b) immersed in a liquid film of constant thickness.

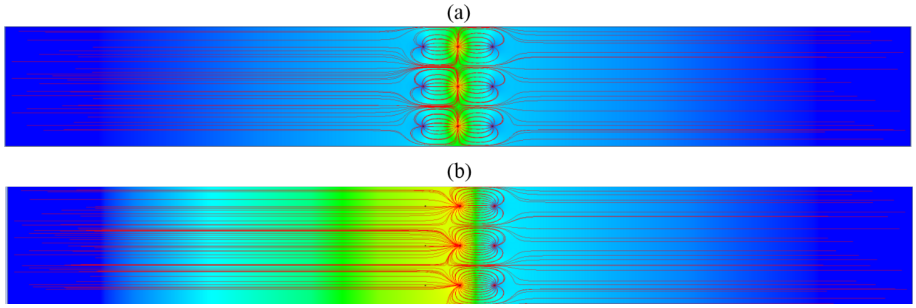

FIGURE 3.2 – Electric fields of three-wire probe (a) and two-wire probe array (b) immersed in a liquid film of constant thickness.

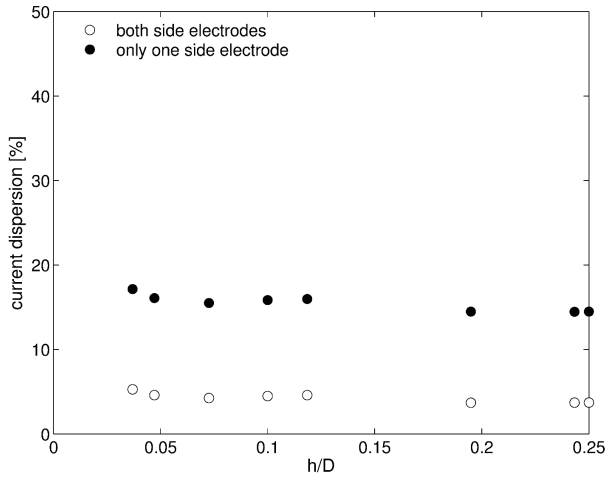

FIGURE 3.3 – Fraction of the electrical current going to the conducting pipe sections obtained by numerical simulations. Wire probe in stratified condition.

where the current dispersion is plotted vs the dimensionless liquid height, h/D, for three and two-electrode arrays. The geometry of the system is described in Section 3.2.3. As can be seen from Fig. 3.3, for a three-electrode array, the current dispersion is approximately constant and about equal to 4% in the range 0 <h/D <0.3. This value rises to about 15% for a two-electrode array. These values are very similar to the case considered above of a constant thickness film.

A careful probe calibration may account for the current dispersion towards the flanges when the height of the liquid layer does not significantly change with time or along the pipe, but the signal would be distorted when large waves or liquid slugs pass through the test section. In order to clarify this point, the simple case of a square wave crossing the test section is considered. In this example, the square wave ranges from a base value h/D = 0.1 to the value h/D = 0.25. In Fig. 3.4, the dimensionless conductance of the central probe derived from the numerical integration of Laplace equation is plotted as a function of the wave position along the test section. The conductance is normalized with respect to the value at h/D = 0.25. In this figure the readings relative to three or two- wire probes are compared. As can be seen from Fig. 3.4, the current dispersion significantly affects the reading of the two-wire probe, deforming the wave shape in particular on the side not screened by the receiving electrodes. The measurement of the three-wire probe is more localized, and the only deviation from the actual wave shape occurs when the wave crosses the probe. This deviation is due to the distance between the wires along the flow direction. This aspect of the probe geometry represents a potential limitation of the present measuring system. However, considering that the transit time of a wave or a liquid

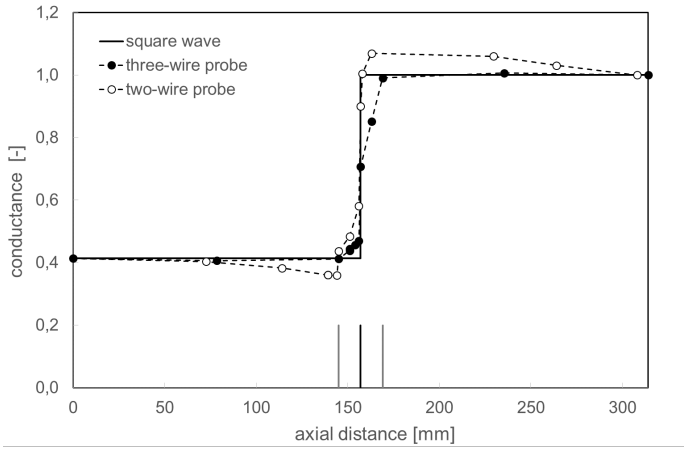

FIGURE 3.4 – Dimensionless conductance of the vertical probe as a function of a square wave position crossing the test section. In the two-wire configuration the receiving electrode not active is that on the right.

slug passing through the probes is of the order of 0.01 s, and the sampling frequency of the present measuring system is typically less than 100 s^{-1} , it is clear that this is a minor problem.

3.2.3 Wire probes

Fig. 3.5 (a) shows the wire probe section developed for the present work. From this figure it can be seen that the test section consists of three arrays of 15 wire electrodes installed on three planes normal to the axis of the tube. For clarity, in Fig. 3.6 also a 3-D view of probes 1 and 2 (vertical and first lateral probe) of the test section is shown. Each probe consists of three parallel, stainless steel, rigid wires, 0.3 mm in diameter, aligned along the flow direction. The spacing along the flow direction between the wires is equal to 12 mm. With reference to Fig. 3.5 (a), the short vertical wire (Probe 1) can be replaced with cross-sectional wire. This probe arrangement leads to a constant factor of $k \simeq 1$ (see Eq. 3.2.5). The electronic circuit has been designed to measure a rate of electrical current up to 1 mA and the potential difference applied across transmitting and receiving electrodes is 1 V. Given these parameters and following Eq. 3.2.3, when the liquid height is 5 mm (typical value expected at pipe bottom) the maximum liquid conductivity admittable is 2000 $\mu S/cm$, while the minimum one required by the electronics sensitivity is about 50 $\mu S/cm$. This wide operative range of liquid conductivity allows to perform flow tests with the salty tracer under several operative conditions.

The body of each measuring section is made of a PET plastic (Arnite), which is characterized by good mechanical properties, an excellent resistance

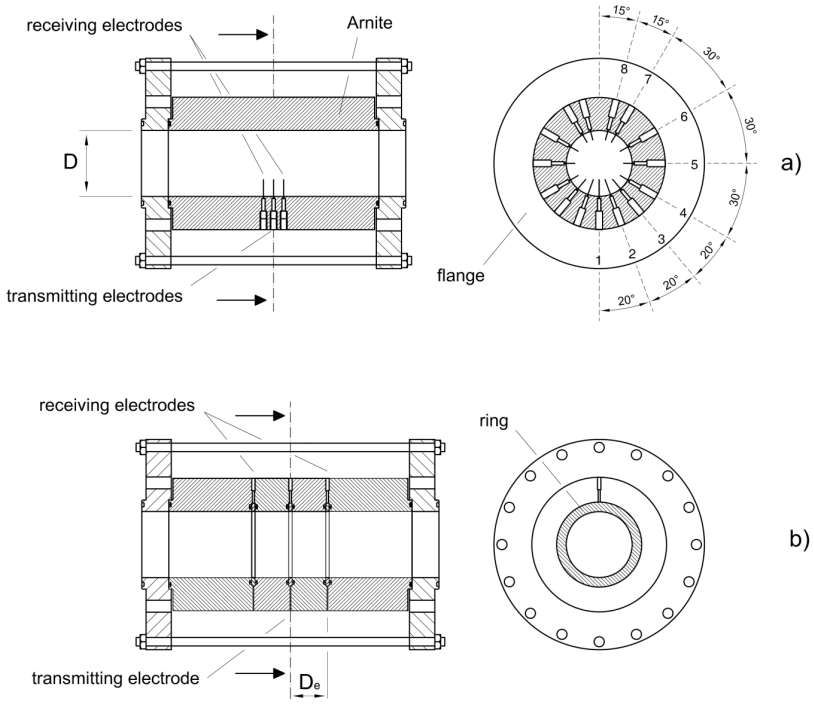

FIGURE 3.5 – Test sections developed in the present work. Wire probes (a) and ring probes (b).

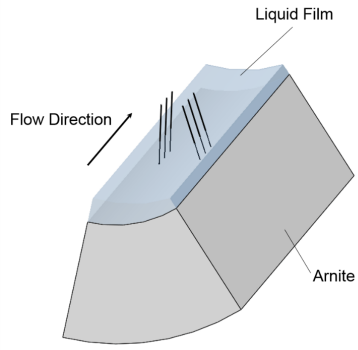

FIGURE 3.6 – Three dimensional view of the vertical and first lateral wire probes.

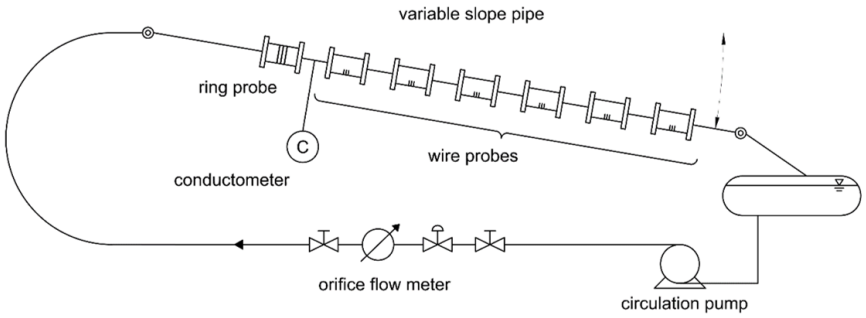

FIGURE 3.7 – Simplified chart of the flow loop used for probe validation: gravity driven flow in inclined pipe.

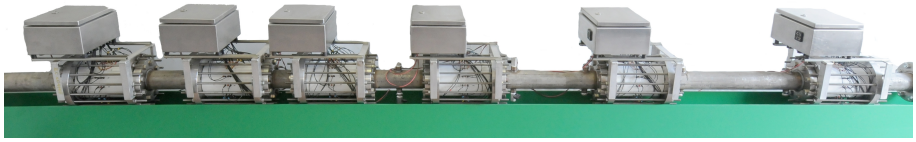

FIGURE 3.8 – Sequence of the six wire measuring sections used in present experiments. Each section has a box containing the dedicated electronics.

to chemical agents and a maximum operating temperature equal to 120 ℃. Each measuring section is connected to the rest of the pipe with stainless steel flanges set at the ground potential. This allows the test section to be employed at appreciable pressure. O-ring static seals have been used in order to avoid liquid leaks between the main body of the measuring section and the stainless steel rods that support the wires.

The overall experimental set-up consists of 6 measuring sections similar to that shown in Fig. 3.5 (a). The distance among the measuring sections can be varied by means of a set of spacers. One of the possible configurations of the system is shown in Fig. 3.7, where also a ring probe section is shown. The set of measuring sections can also be used to study transient or developing flow conditions, such as the motion of interfacial waves, liquid slugs or elongated gas bubbles. In Fig. 3.8 a picture of the sequence of the six wire measuring sections is shown. The box above each section contains the dedicated electronics.

In a measuring section, the linearity of each probe is conserved also in presence of nearby probes and terminal flanges. This can be seen from Fig. 3.9, which reports the electrical response of the central probe computed by

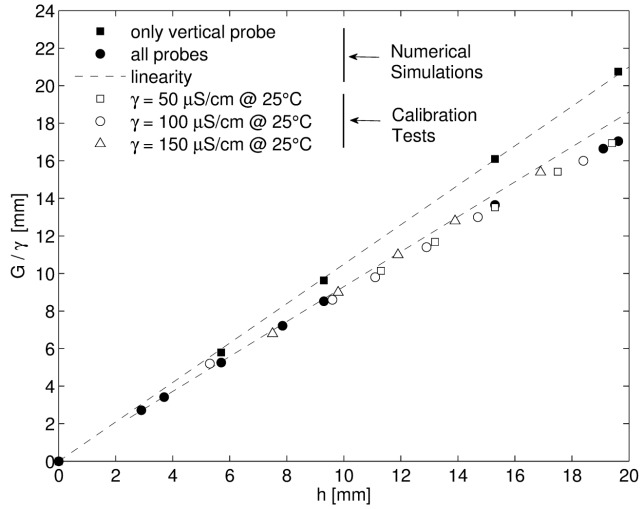

FIGURE 3.9 – Response of the vertical probe in stratified condition. Comparison between numericalmsimulations and calibration tests.

the numerical integration of Laplace equation for the two cases: a) only the vertical probe is active, b) all probes are active. As can be seen from this figure, the presence of nearby probes alters the electrical response of the vertical probe. Nonetheless this probe maintains a linear behaviour up to film heights of 10 mm. Above this height the linearity slightly decays and a more careful probe calibration is required. An example of probe calibration is reported in the same figure, for three different values of the liquid conductivity. As can be seen from this figure, the calibration tests agree quite well with the numerical predictions, with a scatter of less than ±2%. Also for the inclined probes, the conductance is a linear function of the wetted length of the probe, which, for the present probe geometry and in stratified or annular flow, is equal for all the electrodes of the same probe.

3.2.4 Probe calibration

In practical applications, probe calibration is used to derive the relation between the liquid height and the measured conductance, while the theoretical computations are mainly used in order to design the probes and optimize their geometry. The static calibration of a probe can be performed by closing both ends of the non-conducting duct where the probe is installed with blind flanges and filling it with known volumes of liquid, thus simulating stratified flow conditions. In the calibration tests, the flanges are metallic and connected to ground in order to take into account the current dispersion. The liquid conductivity and temperature are carefully monitored. The

results obtained with this method can be checked with the direct measurement of the liquid height performed with a needle contact probe (see Section 2.2.3). As explained above, this instrument is equipped with a thin needle, which allows an electrical loop to be closed when the needle tip touches the liquid surface. In successive validation tests the two methods agreed with a typical scatter of less than 0.1 mm and no systematic error was noticed.

When all measuring sections are installed in the main pipe, the needle contact probe (or micrometric head) is used to measure the film height at various positions along the pipe. The objective of these measurements is to check probe calibrations and to verify if all measuring sections are aligned in the horizontal position. This is done by closing the outlet valve of the pipe, which is then filled with controlled volumes of liquid.

3.2.5 Effect of wires on liquid flow

Three-wire probes guarantee a good circumferential resolution of the measurements because the probes are aligned along the flow direction and the electric field generated by each probe is bound by nearby probes into a restricted volume. However, they are more intrusive than conventional probes, considering the presence of three electrodes rather than two. This potential limitation of the probes deserves some attention.

The issue of flow disturbances induced by wire electrodes presents two distinct aspects: on one hand, the electrodes and in particular three arrays of 15 electrodes may modify the flow structure of the liquid layer. In order to limit this effect, the construction of the measuring sections allows single probes to be easily removed, when necessary. For instance, a three wire probe can be transformed into a two wire, accepting an increase of current dispersion toward the metallic pipe, or all the probes installed on the upper pipe wall can be removed when the liquid deposition on the upper wall is negligible.

On the other hand, the disturbances generated by the probes may alter the probe signal, thus causing an error in the film height readings. This effect has been analyzed by determining the flow field of the liquid phase around the probe. To this objective, the VOF multiphase model of a 3-D flow simulator (Ansys Fluent) has been used to determine the flow field around a three wire probe immersed in a falling film 10 mm high. The average velocity of the liquid around the probe is equal to 0.94 m/s. The results obtained are shown in Fig. 3.10, where both the side and front views of the gas-liquid interface are represented. As can be seen from this figure, the modifications of the interface around the wires are of the order of the wire diameter (0.3 mm) and increase in size going from the first electrode to the last.

The overall effect of the flow disturbance caused by the electrodes on the probe conductance can be determined by solving the Laplace equation for the distorted shape of the gas-liquid interface. The result obtained for the

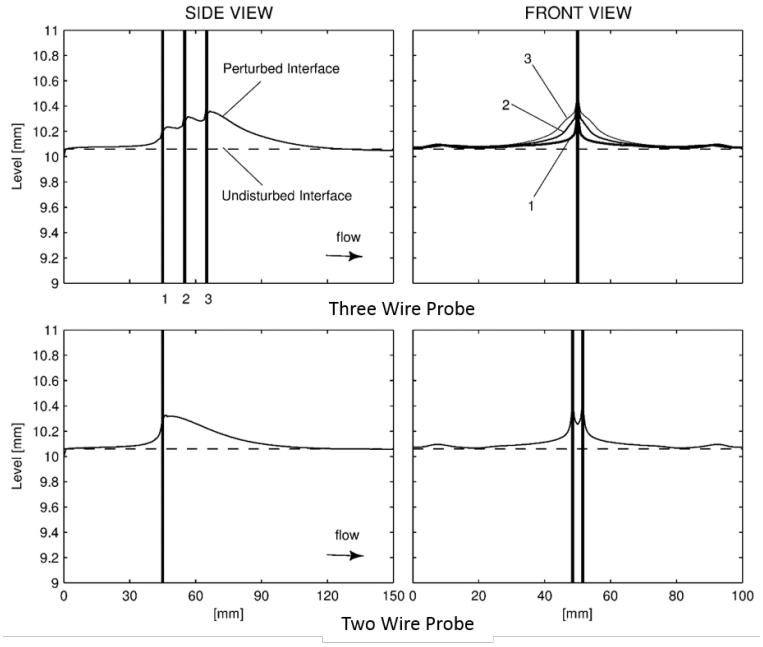

FIGURE 3.10 – Side and front view of the perturbed gas-liquid interface in presence of wire probes: three wire probe (top) and two wire probe (bottom).

case considered in Fig. 3.10 is an increase of the probe signal equal to 2.3% of the original, undisturbed signal. This value is significant because this potential source of error should be added to the others, such as the error associated with probe calibration, the measurement of the liquid conductance or the measurement of pipe inclination.

As shown in Fig. 3.10, the effect of wire-flow interactions is also significant for a conventional probe made of two 0.3 mm wires normal to the flow direction and spaced 3 mm apart. This distance appears to be the correct choice when a good circumferential resolution is required. The error caused by the flow disturbance for this conventional probe is smaller (1.8%), but, in practice, quite similar to the three wire case. It may be concluded that the problem of wire-flow interactions exists, but it is not specific of the probe configuration proposed in this work. To this it may be added that the use of wire electrodes to determine the increase of liquid conductivity due to the injection of a tracer, once the film height has been measured, is exempt from this type of error.

3.2.6 Ring probe

Andreussi et al. (1988) showed that the conductance between two ring electrodes is a linear function of the hold-up of the continuous liquid phase when the distance between the electrodes is larger than about two pipe diameters, independently on the shape of the wall layer. For shorter distances, these authors extended the theoretical solution determined by Coney (1973) for flush-mounted, rectangular electrodes to ring electrodes. Devia and Fossa (2003) found a very good agreement between their numerical solution of the Laplace equation and the simplified model proposed by Andreussi et al. (1988).

In the present work, a ring probe has been used along with the wire probes to measure the hold-up of falling liquid films in near-horizontal pipes. This allows the effect of wire probe intrusiveness to be verified. In order to screen the probe from the metallic sections of the pipe, a three ring probe has been adopted. The probe is made of three 4 mm stainless steel rings spaced 40 mm apart. The body of the probe has been built with the same plastic material as the wire probes. The relatively short distance between the rings limits the range of the probe at which the conductance is a linear function of the liquid hold-up. In Fig. 3.5 (b) the drawing of the ring probe developed in the present work is shown.

In Fig. 3.11 the theoretical value of the dimensionless conductance G^* obtained by the numerical integration of Laplace equation for the present geometry of the ring probe is compared with the results of the static calibration. In this figure the dimensionless conductance G^* is the conductance normalized with respect to the conductance for $\alpha_L = 1$. As can be seen from this figure, the agreement between the numerical computations and the results of probe calibration is excellent. In the same figure also the pre-

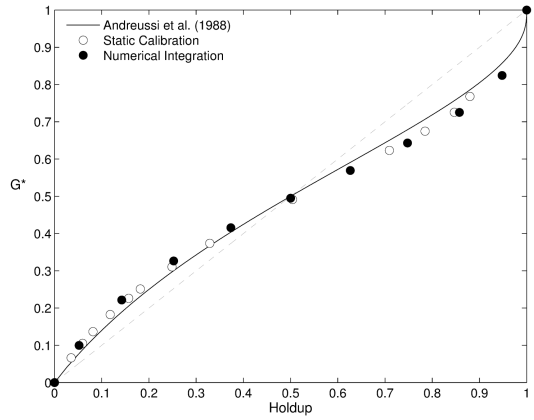

FIGURE 3.11 – Static calibration and numerical integration for a three ring probe compared with the theoretical model of Andreussi et al. (1988).

dictions of the simplified model of Andreussi et al. (1988) are reported. In this case the agreement between data and predictions is not as good. This may depend on different reasons, such as the different probe configuration, with three electrodes rather than two and the signal distortion due to the flanges connected to the ground potential.

3.3 Architecture of the Measurement System

Up to six measurement sections can be installed in the test rig. A measurement section consists of the following components:

- One array of wire probes, each consisting of three rigid wires aligned along the flow direction.
- The analog front-end connected to the relative probes.
- The local data acquisition system, which collects the signals originated by the front-end.

The number of voltage signals produced by the whole system can be as large as 90 at a maximum sampling frequency of 100 Hz per signal. In order to deal with these data, a workstation acts as data logger and interface to the human operator (HMI). A simplified block diagram, giving a general view of the whole measurement system is shown in Fig. 3.12.

For each measuring section, the array of 15 wire probes can be seen as a matrix made of three arrays of electrodes. The signals fed to the three arrays are handled as follows:

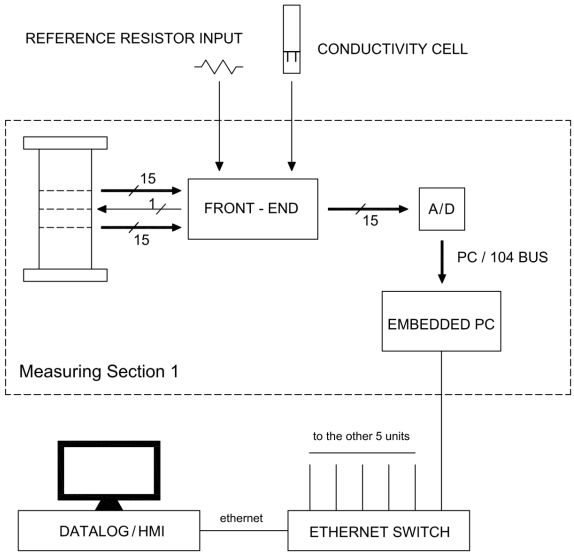

FIGURE 3.12 – Simplified block diagram of the measuring system.

- A common excitation signal is fed to all the electrodes of the central array. Such signal is in the form of an alternated voltage signal.
- The two external electrodes are connected in pairs and are actively set to the same potential of the grounded pipe, which corresponds to the zero voltage level of the excitation signal.
- All the other conductive surfaces of the experimental set-up (flanges, etc.) are also tied to the same potential, which is treated as a voltage reference.
- The observable parameter is the total current flowing into each pair of electrodes belonging to the external arrays, by closing the current loop of the excitation signal.

The reference potential can be considered as a virtual ground, actively generated by a particular configuration of the analog front-end, which sources or sinks current in order to tie the potential of the controlled node (one side electrode) to a pre-determined value. This configuration permits to keep the two external arrays in a substantially equipotential plane, thus minimising the signal dispersion due to the external conductive components of the flow loop (because tied at the same potential of the electrodes) and probe-to-probe cross-talk (because adjacent electrodes belonging to the same array are actively forced to adhere to the same potential).

This configuration enables the simultaneous operation of the 15 measurement probes without multiplexing, thanks to the substantial absence of

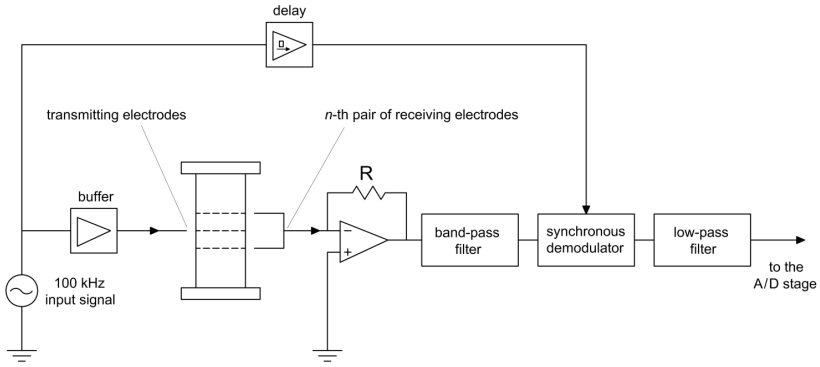

FIGURE 3.13 – Simplified structure of a measurement channel belonging to the analog front-end.

cross-talk between the different probes. The absence of multiplexing represents a noticeable advantage of the present set-up as it enhances signal integrity in the signal processing chain and binds the signals generated by the central array of electrodes into a limited volume of the liquid layer, due to the presence of nearby active electrodes. This feature of the system allows a more localized conductance measurement to be obtained and significantly limits current dispersion to ground.

3.3.1 Electronic circuit

The electronics of the sensor units (i.e., the analog front-end and the data conversion devices that interface the workstation with the analog signals) has been conceived and developed specifically for this application. Each sensor unit has a front-end and data conversion electronics mounted locally. The excitation signal supplied to the central array of electrodes (transmitting electrodes) is generated by a low distortion sinusoidal oscillator, set to a frequency of 100 kHz. Each front-end board is provided with a dedicated oscillator, and has the option to use an external source, e.g., a digital synthesis generator shared by all the measuring sections.

The two external arrays (receiving electrodes) are connected to dedicated wideband current-input circuits (trans-impedance amplifiers), followed by a demodulation stage, which performs simultaneous conversions of all the channels by an array of coherent demodulators, thus providing a rectified output after cutting-off the residual ripple. The 100 kHz working frequency has been chosen as a trade-off between high frequency needs (to cut-off demodulation ripple and make double layer effect negligible) and low frequency requirement (to limit the impact of jitter and switching noise of demodulators on the rectified output).

As specified in the previous section, this configuration does not require the use of a multiplexed scheme, with relevant advantages in terms of noise reduction and response to transients. In fact, such current-input stages tie their input potential to the reference potential of the whole electronic front-end, assuming the ideal Operational-Amplifier approximation and applying the virtual short circuit principle as a consequence. As mentioned above, such reference potential corresponds also to the zero voltage level of the excitation signal, and is tied to the ground potential. In addition to that, as this equipotential array of current-input electrodes can be placed at the same potential of the other conductive wet surfaces of the experimental set-up, the unwanted currents flowing between each probe and the rest of the test apparatus can be limited. Moreover, since the excitation source generates a zero-averaged symmetrical and alternating signal, there is no DC component across any electrodes or across different probes that can potentially produce unwanted electrolytic effects. It must be noted that all the electrodes of the transmitting array are fed by in-phase signals having the same amplitude, thus further eliminating residual currents between the electrodes.

Fig. 3.13 presents the simplified structure of a measurement channel belonging to the analog front-end. The current signals coming from each pair of receiving electrodes are handled by a signal processing chain, which consists of the following stages: i) current to voltage conversion, ii) band-pass filter, iii) synchronous demodulation, iv) low-pass filter. Signals are then forwarded to the Analog to Digital (A/D) converter, a 16 bits, 16 channels, 200 ksamples/second A/D board, based on the industry- standard PC/104 bus. Such board is directly interfaced with a local controller, a SBC (Single Board Computer embedded PC), which buffers the data, performs further digital filtering, and handles the communication with the datalog/HMI (Human to Machine Interface) workstation, where the operator can control how the experiment evolves in real-time. The workstation also performs proper logging of all the collected data during each experiment. The local A/D conversion, which is performed in each sensor unit, permits to transmit all the acquired information in digital form, avoiding the transmission of analog signals over relatively long lines, which are prone to loss of information due to interferences, noise pick-up and distortion by the transmission line.

As shown in Fig. 3.13, the analog front-end is connected to a reference resistor and an optional conductivity cell, in addition to the connections with the probes. The conductivity cell is used as a reference measurement in specific parts of the whole experimental apparatus, and is physically connected to the nearest sensor unit. Such conductivity cells perform a direct measurement of a liquid sample drained from any measuring section. The reference resistor input connects a high precision resistor to a generic measurement channel (identical to those used for the electrode probes), which is used as a reference channel. The high matching between identical channels in the front-end and the normalisation of the acquired measurements with

respect to this reference channel, result in an improved immunity to drifts in the front-end electronics.

For what regards the analog signal processing chain shown in Fig. 3.13, the current signal is first converted to a voltage signal by a trans-impedance amplifier, based on a classical Operational Amplifier configuration. Such input stage provides the virtual ground reference mentioned earlier in this section. A second order high-pass and a smooth first order low-pass filter are respectively used to damp the mains supply noise and the radio-frequency noise picked-up by the cabling, forming a band-pass filtering, in the whole. The demodulator is synchronized with a delayed version of the excitation signal, in order to compensate for the phase shift due to the reactive component in the impedance of the probe-cabling-filter arrangement. After the final low-pass filtering, the signal is fed to the data acquisition board (A/D board), which provides digital conversion with a resolution of 16 bits, locally to each sensor unit.

All the sensor units share the same function generator, which provides a common source for the excitation signals used by all the probes (transmitting electrodes). The selected generator is characterised by a direct digital synthesis, ensuring an excellent stability and spectral purity of the generated sine-wave.

3.3.2 Data acquisition and display

A "Single Master-Multiple Slave"software architecture has been developed in order to monitor and acquire data at maximum speed, without having data loss and misalignment. The main functionalities implemented by the software can be summarized as follows:

- Real-time data acquisition. It is possible to monitor the overall system activity, access any sensor unit and manage every acquisition channel individually.
- Graphical User Interface and real-time data representation. Software architecture is split into an Acquisition Control Program, executed by the embedded-pc, and an Administration and Monitoring Tool, which displays data using graphical interfaces.
- Data storing and retrieving using a database interface. The Monitoring Tool handles communication with all the sensor units and stores data to a SQL database continuously.
- Online diagnostic tests capability.

The Administration and Monitoring Tool acts as a Single-Master and is executed on a dedicated workstation with multi-homed network configuration: one Gigabit Ethernet interface is dedicated to the communication with the multiple-slave set, another GBit Eth connects the workstation to local

network for remote access. The communication module (DLL) implements data exchange using multiple sockets interfaces:

- UDP Server Socket for discovery operations and network topology self-arrangement.
- TCP Sockets for connection-oriented one-to-one communication with slaves; TCP ensures a reliable channel for data exchange with respect of the right flowing order for the data-communication messages.

The Acquisition Program runs on the embedded-PC and manages the low-level hardware interaction with High Performance A/D subsystem and the data dispatch to the workstation.

3.3.3 Signal processing

Acquired signals are voltage levels directly related to the measured conductance between each pair of electrical nodes, represented by one electrode belonging to the central array (transmitting electrode) and the two corresponding electrodes belonging to the side arrays (receiving electrodes), which are shorted together and sink the loop current that goes through the conducting liquid phase. As specified in Section 3.3.1, in order to limit the experimental errors, such signals are normalized with respect to a reference signal obtained by closing the current loop of a generic input channel with a reference resistor. This operation is performed by the data-collecting workstation, since it is preferred to transmit raw data from the local SBCs.

The normalization step is expressed by the following relation, where all the variables represent the instantaneous values taken by the parameters that they represent:

$$V_N(j,k) = \frac{V(j,k)}{V_{REF}(j)} - V_{OFF}(j,k) \ . \tag{3.3.1}$$

In Eq.3.3.1, j identifies the measuring section and k the conductance probe, $V(j,k)$ is the voltage measured by the generic probe, $V_{REF}(j)$ is the normalized reference voltage measured at section j, $V_{OFF}(j,k)$ is the normalized offset voltage pertaining to each probe, $V_N(j,k)$ is the normalized voltage signal. The latter is expected to be proportional to the conductance between the electrodes. Recalling Eq.3.3.1, $V_N(j,k)$ can be expressed as:

$$V_N(j,k) = f'(h_{j,k})\,\gamma_j \ , \tag{3.3.2}$$

where f' is a function of $h_{j,k}$, the local value of the liquid height.

Eq.3.3.2 can be used to measure the local liquid film height when the function f' has been determined by probe calibration and the liquid conductivity is known or is measured. To this purpose, a dedicated conductivity

cell is used. The signal measured by this cell undergoes the same normalization step as the other conductance probe signals. The value of the liquid conductivity at the j-th location, γ_j, can then be obtained by calibration of the conductivity cell with liquids of known conductivity. In addition, all the electrodes are calibrated via a characteristic function that transforms the corrected data into a wet-length for each of the electrodes. Such functions are individually determined for each probe.

3.4 Conclusions

The development of a test section for the study of stratified and stratified-dispersed flow required a great amount of theoretical and experimental work to be carried on, besides the work required by the mechanical and electrical design of the measuring system. The main activities of the present project and the conclusions that can be drawn are the following:

1. **Definition of probe geometry.** Among the different geometries proposed in the literature, wire electrodes have been selected because they guarantee a linear response at varying over a very wide range the film thickness and the average liquid conductivity. In the present work non-conventional wire and ring probes based on the use of three-electrodes spaced along the flow direction have been adopted for the measurement of the circumferential film thickness distribution and for the average liquid hold-up, respectively. This choice is related to the application of conductance probes to the measurement of the film thickness in metallic pipes, designed to operate at an appreciable pressure (40 Bar) and electrically connected to the ground potential. In the present application, the probes are installed in a non-conducting duct and the external electrodes of each probe are actively kept at the ground potential. This arrangement allows the current dispersion to the external conductive components of the test rig to be minimized and substantially eliminates probe-to-probe interference. The wire probes are installed all around the pipe circumference, in order to provide local measurements of film height or liquid conductivity.

2. **Prediction of probe conductance.** The analytical or numerical integration of Laplace equation has been used to determine the probe conductance and optimize the geometry of the test section. The results obtained indicate that the theoretical predictions are quite accurate and agree very well with the static calibration of the probes. The integration of Laplace equation also allows the dispersion of the electrical current toward the conducting parts of the pipe to be estimated with good accuracy. A new theoretical equation (Eq. 3.2.5) has been derived to predict the conductance of a three-wire probe immersed in an unbounded liquid film.

3. **Computation of the interactions between wire electrodes and liquid flow.** The integration of Navier-Stokes equations using the VOF multiphase model allowed the disturbance generated by a set of wire electrodes to be evaluated. This disturbance can produce an error in the measurement of the film height about equal to 2% for the flow condition examined in the present work. The magnitude of this error does not change significantly when comparing the present three wire configuration with the conventional one based on two wires.

4. **Design of the front-end electronics.** The three electrode configuration enables the simultaneous operation of the 15 wire probes without multiplexing. The absence of multiplexing represents a noticeable advantage of the present set-up: it allows most of the demodulated signal bandwidth to be exploited and eliminates most sources of electrical switching noise and subsequent errors. In addition to enhancing signal integrity in the signal processing chain, this configuration binds the signals generated by the central array of wires into a limited volume of the liquid layer, providing a more localized measurement in the circumferential direction.

4

Probe validation: gravity driven flow in inclined pipe

4.1 Introduction

The study of free falling liquid layers in a circular duct has been chosen as preliminary application of the measuring section developed in the present work. The reason being that it represents the simplest case of stratified liquid flow in a pipe and is one of the few flow conditions which can be very well described with a semi-empirical method or by the numerical integration of Navier-Stokes equations. Analytical solutions of the Navier-Stokes equations for this flow condition are also available (Giovine et al., 1991). In Fig. 4.1 a reference scheme of gravity driven flow is depicted, along with the main parameters tipically involved for its description.

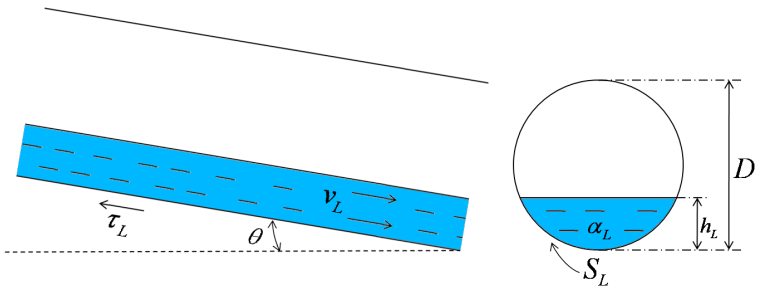

FIGURE 4.1 – Simplified scheme of gravity driven flow.

4.2 Flow test

4.2.1 Free falling liquid layers

The semi-empirical method is based on the force balance

$$-\tau_{WL} S_L + \rho_L A_L g sin\theta = 0 \,, \tag{4.2.1}$$

where τ_{WL} is the shear stress at pipe wall, ρ_L the liquid density, g the gravity and θ the angle between the pipe and the horizontal. Taitel and Dukler (1976) expressed τ_{WL} in terms of the friction factor f_L as

$$\tau_{WL} = \frac{1}{2} f_L \rho_L u_L^2 \,. \tag{4.2.2}$$

In this equation, u_L is the mean liquid velocity and f_L is assumed to be the same function of the liquid Reynolds number, Re_L, as in single phase flow, with Re_L defined as

$$Re_L = \frac{4A_L}{S_L} \frac{u_L}{\nu_L} \,, \tag{4.2.3}$$

where ν_L is the liquid kinematic viscosity. f_L can be predicted with the equations:

$$Re_L \leq 2000 \quad f_L = \frac{16}{Re_L} \,, \tag{4.2.4}$$

$$Re_L > 2000 \quad f_L = 0.046 Re_L^{-0.2} \,. \tag{4.2.5}$$

Andreussi and Persen (1987) derived from Eq.4.2.2 the following relation for the dimensionless liquid flow area, A_L^+:

$$A_L^+ = \frac{4A_L}{S_L \nu_L} \left(\frac{\tau_{WL}}{\rho_L} \right)^{\frac{1}{2}} = \left(\frac{f_L}{2} \right)^{\frac{1}{2}} Re_L \,. \tag{4.2.6}$$

According to this equation, A_L^+ is only a function of the liquid Reynolds number.

Giovine et al. (1991) have shown that the analytical solutions of Navier-Stokes equations relative to single phase laminar flow in inclined pipes obtained for h/D = 0.5 and h/D $\longrightarrow$ 0, almost coincide with the solution based on Eqs.4.2.1 - 4.2.4. These authors also noticed that the numerical integration of N-S equations computed by Buffham (1968) for laminar flow is very similar to the Taitel and Dukler solution and concluded that the simplified approach to the problem reported above has a general validity for laminar flow conditions.

For turbulent flow, the Taitel and Dukler solution of the falling film problem is compared in Fig. 4.2 with the numerical integration of Navier-Stokes equations made with the VOF multiphase model of Fluent. In this

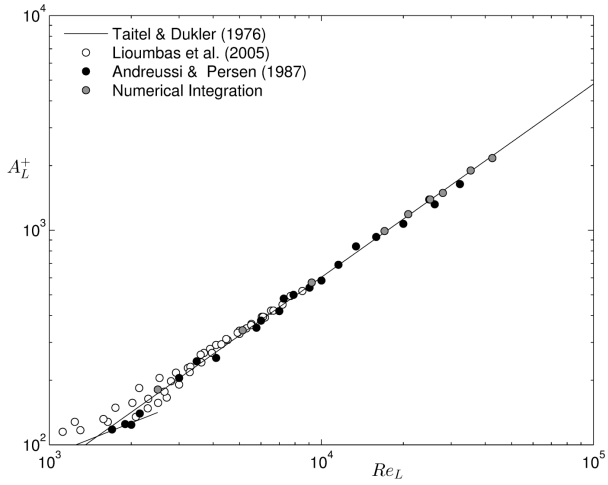

FIGURE 4.2 – Dimensionless liquid flow area vs liquid Reynolds number for a free falling liquid layer in a circular duct.

computation the standard $k - \varepsilon$ model of turbulence has been used. As can be seen from Fig. 4.2, the simple solution of the falling film problem proposed by Taitel and Dukler (1976) almost coincides with the results of the numerical integration also for turbulent flow, thus suggesting that in this simple case of stratified flow the theoretical predictions should be reliable.

In Fig. 4.2, the experimental measurements of Andreussi and Persen (1987) and Lioumbas et al. (2005) are also reported. As can be seen from this figure, for $Re_L > 3000$ the theoretical predictions provide a very good fit to the experimental measurements. For $Re_L < 3000$, the dispersion of the experimental measurements of Lioumbas et al. (2005) is relevant. This may be due to the fact that at these Reynolds numbers the transition between laminar and turbulent flow occurs, but it is useful to recall that, on one hand, the relative error of film height measurements can be larger for thin rather than thick films; on the other hand, that Lioumbas et al. (2005) state in their paper that the estimated average uncertainty of their measurements is equal to 10%. At low Reynolds numbers, the scatter of the data shown in Fig. 4.2 is well above 20%.

4.2.2 Experiments

The experiments have been conducted in the Multiphase Flow Laboratory of TEA Sistemi, a spin-off company of the University of Pisa. A simplified chart of the flow loop is shown in Fig. 3.7. The test section is approximately 5 m long and the pipe internal diameter is 80 mm. In present experiments the pipe is inclined on its support and its inclination with respect to the horizontal is carefully measured. This also requires the horizontal position

of the test section to be identified. The final value of the pipe inclination can be determined with an overall accuracy which is estimated to be better than 0.04°. At the small inclinations investigated in the present work, this level of accuracy may generate an error of the order of 1-2% in the measurement of the film thickness. In the flow loop used by Andreussi and Persen (1987), the pipe was 26 m long. This allowed a better measurement of its inclination, with an uncertainty estimated by these authors equal to 0.02°.

The working liquid is demineralized water whose conductivity has been risen to the desired level by adding known amounts of KBr. In these tests a salt concentration of 150 mg/lt led to a liquid conductivity of about 200 $\mu S/cm$. The final conductivity and temperature of the water phase has been carefully measured and the expected uncertainty of conductance measurements is about equal to 2%. The overall accuracy of the present measurements is not expected to be better than 4%. Possibly most of the published film thickness measurements are affected by similar or larger uncertainties, as it appears from the work of Lioumbas et al. (2005). This level of uncertainty is partially related to the conductance method which requires an accurate measurement of the liquid conductivity.

4.2.3 Results and Discussion

The experimental measurements are relative to tests performed by two different operators who adopted different experimental procedures and set-ups. In particular, two methods have been used for probe calibration.

TEST A. The test section was assembled with 6 measuring sections, was set in the horizontal position and the vertical wire probes were calibrated simultaneously by closing both ends of the pipe and filling the pipe with different volumes of water. In this case the liquid level was only measured near each probe with the micrometric head described in Section 3.2.4. The micrometric head was also used to determine the horizontal position of the test section by measuring the liquid level at various positions along the section. It is useful to remark that it is very difficult to avoid minor misalignments (0.1-0.2 mm) among the different sections of the pipe. The liquid used for the calibration was the same liquid used for the tests. Its temperature was always carefully measured and the conductivity corrected for temperature variations both during the calibration and the tests. This procedure almost reduces to zero the error associated with the measurement of the liquid conductivity. The same procedure was followed by Andreussi and Persen (1987).

TEST B. The test section was assembled with 3 measuring sections. Each measuring section was calibrated individually on the bench following the procedure described in Section 3.2.4. The section was filled with known volumes of water and the liquid height was also determined with the micrometric head. This procedure allows the calibration to be extremely accurate. In particular, any possible uncertainty about the inclination of

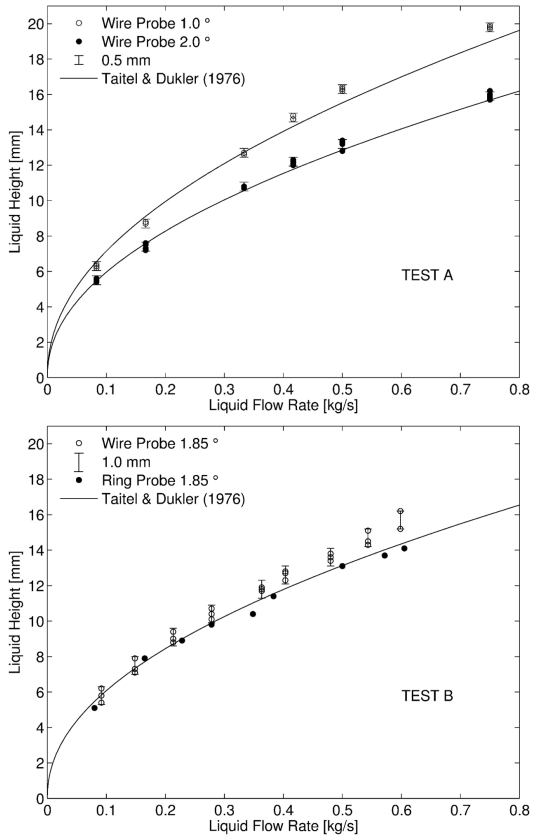

FIGURE 4.3 – Raw measurements for three pipe inclinations.

the section with respect to the horizontal is reduced to zero because the probes are at the centre of the section. However, the liquid used for the calibration was not the same liquid used in the experiments and this leaves a possible source of error. The ring probe was also calibrated on the bench and used in this series of experiments.

The raw measurements are shown in Fig. 4.3, which reports the liquid height read with the central probe as a function of the liquid flow rate for three pipe inclinations. The multiple readings reported for each flow rate are relative to the 6 or 3 measuring sections used in tests A and B, respectively. In this figure it is reported that the dispersion of film height measurements is equal to 0.5 mm for test A and 1.0 mm for test B. This difference is due to the independent calibration performed for each probe in test B and provides an estimate of the uncertainty of the calibration procedure. From Fig. 4.3 it can be noted that the dispersion of the measurements appears to be independent from the film height, thus indicating that at low film heights

the relative error of the measurements can be significant.

In Fig. 4.3, the measurements obtained with the ring probe and the theoretical predictions are also reported. The overall fit of the data is fairly good, in particular the ring probe data are only slightly below the predictions. The wire probe data appear to be affected by systematic, minor deviations in the range of large film heights. This difference is less than 4%, in case A and goes up to values about equal to 6% in case B. As the expected uncertainty of present measurements has been evaluated by taking into account only the results of the static probe calibration, the increased values of the experimental error can be attributed to the effects of the disturbances generated by wire probes at the gas-liquid interface. These disturbances are expected to increase at increasing liquid velocity, and of course do not regard the ring probe measurements.

4.3 Conclusions

The flow test performed as a benchmark for the validation of the test section regarded the case of free falling liquid layers in a circular duct. The semi-empirical solution proposed by Taitel and Dukler (1976) has been compared with a 3-D flow simulation and a very good agreement has been found between these solutions of the problem. Published data agree with the predictions at large Reynolds numbers, but the scatter of measurements is significant at low film heights, in a range of liquid Reynolds numbers corresponding to the transition between laminar and turbulent flow. For this case the experiments reported by Lioumbas et al. (2005) are affected by a deviation from the theoretical predictions greater than 20%, which can be due to experimental errors.

Present measurements are affected by systematic, low deviations from the theoretical predictions. The magnitude of these deviations is quite small for ring probes and changes according to the calibration method for wire probes. It seems possible that the scatter of present measurements be related to the measurement of the electrical conductivity, minor errors affecting the pipe inclination and, finally, for the case of wire probes, the disturbances generated by the interactions between the vertical wires and the liquid flow.

II

Tracer Method

Life is curious. When I was a child, they carefully teached me how much salt to put in water to cook a good pasta. Once at work, they carefully teached me how much salt to put in water to study stratified-dispersed flow.

5

The tracer method applied to stratified-dispersed flow: design of experiment

5.1 Introduction

As stated in Section 2.5, for what regards the measurement of droplet exchange, the tracer method appears as the only viable technique to study complex flow patterns such as annular or stratified-dispersed flow in near horizontal pipes. The principal problem, when dealing with SD flow, is the asymmetric distribution of the liquid layer, due to the effect of gravity. This fact requires a circumferential distribution of the inlet tracer flow rate proportional to the local liquid film flow rate, and that the tracer concentration be measured not only at various distances from the tracer injection, but also all around the pipe periphery.

In this chapter we explain how the tracer method is combined with the test section introduced in Chapter 3 to obtain simultaneous measurements of film thickness, liquid entrainment and rate of liquid exchange. Particular effort has been given in the proper design of the tracer injection system and in the research of the best procedure to minimize experimental errors.

5.2 Model of tracer transport

Tracer transport in vertical annular flow has been described by one-dimensional tracer conservation equations based on the assumption that tracer mixing in the wall layer after its injection is almost instantaneous (Quandt, 1965). The experiments reported by Cousins et al. (1965) and Jagota et al. (1973) apparently contradict this assumption. The theoretical analysis of tracer mixing in a turbulent liquid film reported by Andreussi and Zanelli (1976)

and a set of experiments described by Andreussi (1983) indicate that tracer mixing in the radial direction is very efficient, while the circumferential liquid film distribution and tracer concentration can be poor, even in vertical flows. These effects may explain the experimental observations of Cousins et al. (1965) and Jagota et al. (1973).

The tracer conservation equations proposed by Quandt (1965) are based on the assumption that fully developed flow conditions are reached. These conditions can be approached in long insulated pipes, when a gas-liquid mixture flows at thermodynamic equilibrium under a moderate pressure gradient.

In fully developed annular flow, the rate of droplet deposition becomes equal to the rate of entrainment and the liquid film and the entrained droplets flow rates tend to assume a constant value along the pipe. When a tracer is injected into the wall layer, the mass balances relative to tracer transport can be written as:

$$\rho_L \alpha_F u_F \frac{dC_F}{dz} = -\Phi_I \left(C_F - C_D\right), \tag{5.2.1}$$

$$\rho_L \alpha_D u_D \frac{dC_D}{dz} = \Phi_I \left(C_F - C_D\right), \tag{5.2.2}$$

where C_F , C_D are the tracer concentrations in the film and the entrained droplets, z the axial coordinate and Φ_I the rate of droplet interchange. It is useful to notice that in vertical annular flow, the rates of droplet entrainment and deposition are usually expressed as mass flow rates per unit area, R_A , R_D , which are related to Φ_A , Φ_D by the relation

$$R_i = \frac{D_t}{4} \Phi_i, \tag{5.2.3}$$

where D_t is the pipe diameter. Eqs. 5.2.1 and 5.2.2 are based on the assumption that the flow structure of the liquid phase can be simulated by two distinct fields, the wall layer, with mean velocity equal to u_F and hold-up α_F and the entrained liquid, with mean velocity equal to u_D and hold-up α_D.

This simple two-field model for the liquid phase has also been adopted by Bendiksen et al. (1989) and by Bonizzi at al. (2009) to describe transient or developing SD and annular flow conditions. However, in SD flow, due to the effect of gravity, the flow of the liquid phase is more complex and the experimental observations may suggest a different description of the flow structure.

The integration of Eqs. 5.2.1 and 5.2.2 is straightforward and the results can be expressed in terms of the dimensionless tracer concentration $p\left(z\right)$ defined as

$$p\left(z\right) = \frac{C_F\left(z\right) - C_e}{C_e}, \tag{5.2.4}$$

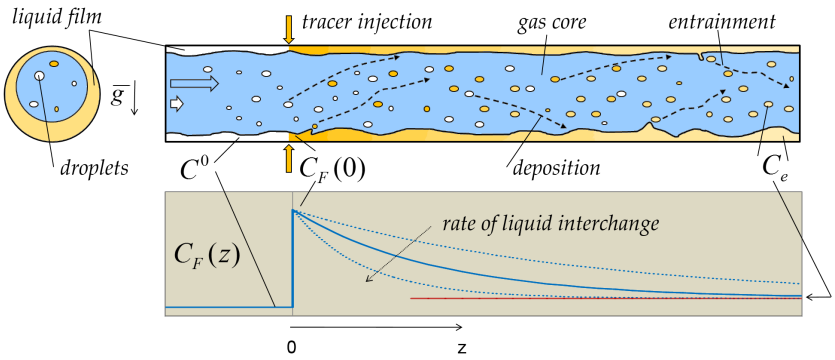

FIGURE 5.1 – Sketch of the tracer method applied to a SD flow in horizontal pipe (top) and qualitative solution of differential equations 5.2.1 and 5.2.2 (bottom).

where C_e is the limiting tracer concentration attained in a long pipe. C_e is related to the tracer concentration in the liquid film immediately after the injection, $C_F(0)$, through the mass balance

$$\alpha_F u_F C_F(0) = C_e(\alpha_F u_F + \alpha_D u_D). \tag{5.2.5}$$

It is obtained

$$p(z) = \frac{1-f_F}{f_F} exp\left[-\frac{\Phi_I}{\rho_L}\left(\frac{1}{\alpha_F u_F} + \frac{1}{\alpha_D u_D}\right) z\right], \tag{5.2.6}$$

where f_F is the fraction of liquid flowing in the film. From this equation it can be seen that f_F can be immediately obtained from the intercept of $p(z)$ at $z = 0$ and, once f_F is derived, Φ_I is simply proportional to the slope of $p(z)$ vs z in a semi-log plot. As the measurement of tracer concentration tends to be more accurate close to tracer injection, Φ_I can also be computed from the value of the derivative of $p(z)$ for zß0 which, from Eq. 5.2.6, is found to be

$$\frac{dp(z)}{dz}|_{z=0} = -\frac{A\Phi_I}{W_L f_F^2}, \tag{5.2.7}$$

where W_L is the overall liquid flow rate and A the pipe cross section.

In Fig. 5.1 a sketch of the application of tracer method to a SD flow in horizontal pipe is shown along with a qualitative solution of differential equations 5.2.1 and 5.2.2.

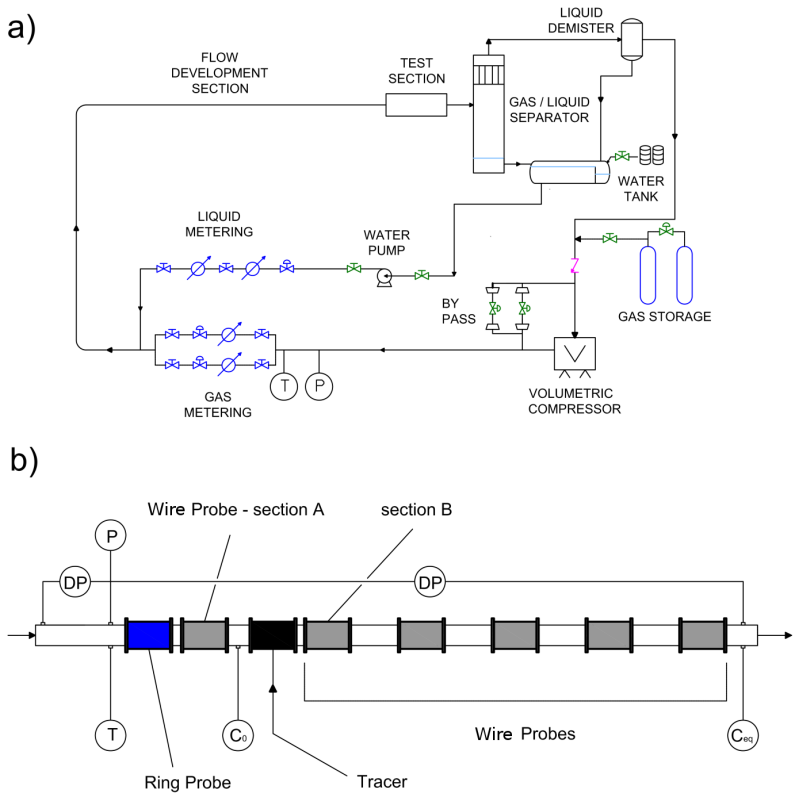

FIGURE 5.2 – a) Multiphase Flow Loop: Schematic Diagram. b) Test section: conductance probes and other instruments.

5.3 Experimental system

5.3.1 Flow Loop

The experiments have been conducted in the Multiphase Flow laboratory of TEA Sistemi (Pisa). A simplified chart of the flow loop is shown in Fig. 5.2 (a). The gas (nitrogen, air or SF_6) is circulated in the loop through a volumetric compressor, which can operate up to a pressure of 25 bar and allows a differential pressure of 5 bar, at a maximum flow rate of 400 m^3/h. A set of three pumps with maximum flow rates of 5, 30 and 65 m^3/h permits a wide range of operating conditions and the simultaneous use of two liquids (water, water-propanol, liquid hydrocarbons). Single phase gas and liquid streams pass through dedicated skids, where the flow rates are measured and controlled using the instrumentation reported in Table 5.1

TABLE 5.1 – (a) Operating conditions, (b) reference instrumentation

Panel (a)	
Loop Operating Pressure	2 - 40 bar
Loop Operating Temperature	2 - 40 °C
Pipeline ID	80 mm
Length of Test Section	25 m
Loop Max Pressure Drop	5 bar
Max. Superficial Gas Velocity	22 m/s (30 bar)
Max. Superficial Liquid Velocity	5.5 m/s (Single Phase)
Installed Power	400 kW
Panel (b)	
Oil	1″ Coriolis Meter 3″ Orifice Meter
Water	$\frac{1}{4}$″, $\frac{1}{2}$″, 1″, 3″ Magnetic Flow Meters
Gas	1″, 3″ Venturi Meters $\frac{1}{2}$″, $1\frac{1}{2}$″ Vortex Meters $\frac{3}{8}$″ Orifice Meter

The test section adopts a set of conductance probes for the measurement of the liquid hold-up and the liquid film distribution around the pipe wall and two differential pressure transmitters for the measurement of the pressure gradient. Ahead of the test section, a pipe of about 40 m allows fully developed flow conditions to be reached. The test section, which is approximately 10 m long, is installed in the terminal part of the pipe, for

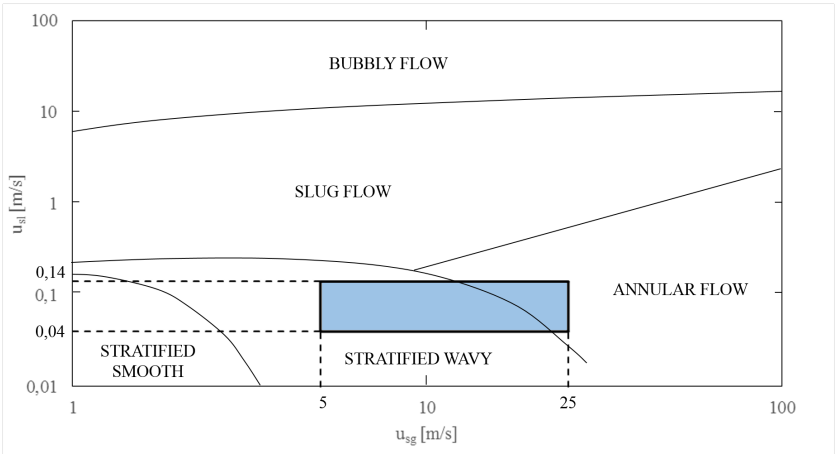

FIGURE 5.3 – Working range of present experiments (blue area) is shown on the flow pattern map of Taitel and Dukler.

an overall pipe length of approximately 50 m. The pipe internal diameter is 80 mm.

In present experiments the pipe is horizontal and the working fluids are water and nitrogen at 5 bar. The maximum gas velocity that can be attained at this pressure is 25 m/s. The range of gas and liquid flow rates examined in this work is $u_{sg} = 5 - 25$ m/s and $u_{sl} = 0.04 - 0.14$ m/s. In Fig. 5.3 this operative area is superposed to the flow pattern map of Taitel and Dukler for horizontal lines. The map regards gas-liquid flow at standard conditions and fluid properties. The effect of fluid properties on two-phase flow phenomena has been studied by a number of investigators. In particular, Hoogendoorn and Buitelaar (1961) and recently Tzotzi et al. (2011) found that an increase in gas density decreases significantly the onset of atomization. Following this consideration, the working range chosen for present experiments falls in the transition area between stratified wavy and annular flow. The maximum liquid flow rate has to be limited to avoid slug flow, while the maximum gas flow rate is imposed by compressor performances. Future work will be carried on with water and water-propanol mixtures to simulate light hydrocarbon flow, and gas densities in the range 6-60 kg/m^3, using nitrogen or SF_6.

5.3.2 Test Section

The test section adopted in this study is shown in Fig. 5.2 (b). It consists of the same conductance measuring sections (six wire-electrode and one ring-electrode) already used in Chapter 4 for gravity driven flow test. In addition, the section for tracer injection is mounted after the first wire-electrode probe section.

As explained in Section 3.2.1, the conductance readings of wire probes, G, is strictly proportional both to the local film height, h, and the liquid conductivity, γ, (Eq. 3.2.3)

$$G = k \cdot \gamma \cdot h \ , \tag{5.3.1}$$

where k is a constant related to the probe geometry. The liquid conductivity, at low tracer concentration, is proportional to the salt concentration, C_S,

$$\gamma = \lambda \cdot C_S \ , \tag{5.3.2}$$

where λ is a function of the liquid temperature.

The linear behaviour of wire probes both with the liquid height and conductivity makes very simple the measurement of the tracer concentration in a flowing liquid. If we indicate with G^0 the conductance of a probe when the tracer flow is switched off, the ratio G/G^0 immediately allows the ratio C_S/C_S^0 to be determined, provided that the film height does not change. The concentration of the tracer added to the liquid stream, measured by a generic conductance probe can then be computed as

$$C = C_S - C_S^0 = \left(\frac{G}{G^0} - 1 \right) C_S^0 \ . \tag{5.3.3}$$

The first wire section encountered by the gas-liquid mixture along the pipe (section A in Fig. 5.2 (b)) is used to determine the liquid film distribution around the pipe wall. This section is also used to correct the readings of all conductance probes for variations with time of the liquid conductivity. During a typical experiment these variations are less than 5% and are caused by slow variations of the salt concentration with time (the water phase operates in a closed loop) and minor variations (1 - 2 ℃) of the water temperature.

In order to correct for conductivity variations, in each experiment, before starting with the salt injection, the average conductance values $G_{i,j}^0$ are measured at each probe (i indicates the test section, i = A, B, ...; j indicates the angular position of the probe, j = 1, 2, ..., where 1 indicates the central vertical probe, 2 the probe at an angle of 20°, etc.). $G_{i,j}^0$ values are normalized with respect to the corresponding values at section A,

$$\widetilde{G}_{i,j}^0 = \frac{G_{i,j}^0}{G_{A,j}^0} \ . \tag{5.3.4}$$

When tracer injection is switched on, each value of $G_{A,j}^0$, taken at time t_k, $G_{A,j}^0(t_k)$ is used to derive the corresponding value of $G_{i,j}^0(t_k)$ as

$$G_{i,j}^0(t_k) = \widetilde{G}_{i,j}^0 \cdot G_{A,j}^0(t_k) \ . \tag{5.3.5}$$

This allows the tracer concentration at probe i,j, $C_{i,j}(t_k)$, to be determined with Eq. 5.3.3 as

$$C_{i,j}(t_k) = \left(\frac{G_{i,j}(t_k)}{G^0_{i,j}(t_k)} - 1 \right) \cdot C^0_{i,j}(t_k) \ , \tag{5.3.6}$$

with $C^0_{i,j}(t_k)$ computed as

$$C^0_{i,j}(t_k) = \widetilde{G}^0_{i,j} \cdot C^0(t_k) \ , \tag{5.3.7}$$

where $C^0(t_k)$ is the concentration of the wall layer obtained by the continuous conductivity measurement in a section ahead of tracer injection, using an in-line conductivity meter.

5.3.3 Tracer injection

The tracer used in present experiments is a solution (10 g/lt) of pure (99.5%) KBr in distilled water. The solution is obtained by dissolving an accurately weighted quantity of dried KBr into a known volume of water. The final uncertainty of the tracer concentration in the solution is estimated to be better than 1.0%.

The water phase flowing in a closed loop is made of de-ionized water whose conductivity at the beginning of each cycle of tests is raised to a value at which the probe conductance could be correctly read (approximately 100 μS/cm) by adding the required amount of KBr. During a cycle of tests the conductivity of the water phase slowly rises up to the value at which the relation between salt concentration and conductivity starts to deviate from linearity. When this happens, a new batch of de-ionized water is introduced into the flow loop.

In present experiments, the tracer flow rate into the wall layer has always been kept below 2.5% of the overall liquid flow. This is a compromise between a minimum signal increment on the first wire probe section after the injection (section B) and the need of reduce the perturbation induced on the liquid layer in the pipe. This aspect is explained in detail in Appendix A. Fig. 5.4 shows a schematic of the tracer injection system, which details (1), (2) and (3) are reported in Fig. 5.5. The system consists of the following components:

Tracer Vessel. It is a 200 lt vessel operating at atmospheric pressure. Inside the tank, a rotating mixer maintains the liquid homogeneous. The tracer is extracted from the vessel with two volumetric pumps. Immediately before, the tracer temperature and conducibility are constantly measured.

Tracer Distribution System. It is the core of injection system and has been designed following precise criteria. In Appendix A the design procedure is explained in detail. Fig. 5.6 shows bottom and frontal view of the section, while in Fig. 5.7 a three-dimensional view of the object is reported.

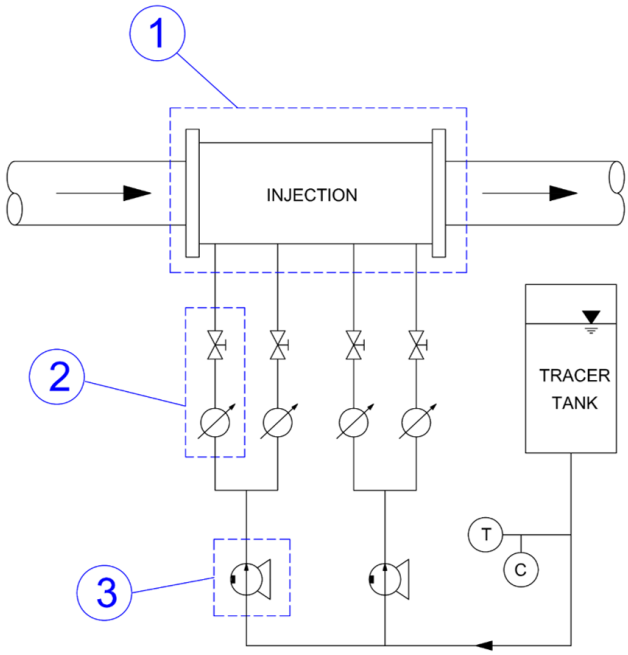

FIGURE 5.4 – Schematic of the tracer injection system.

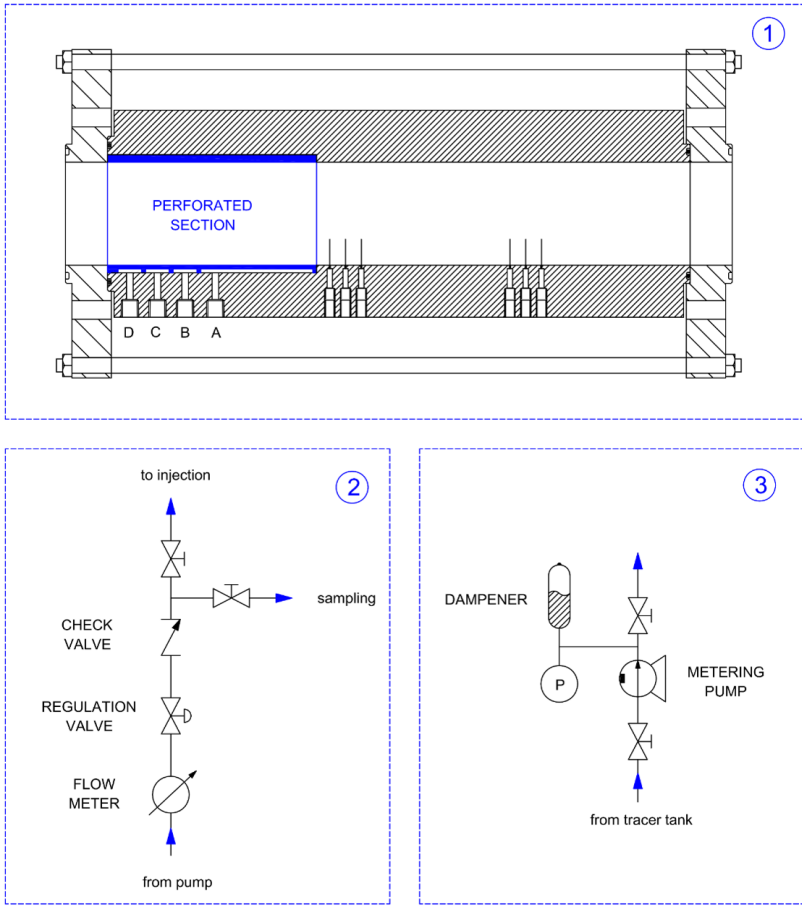

FIGURE 5.5 – Details of the tracer injection system sketched in Fig. 5.4: tracer distribution system (1), tracer control system (2) and metering pumps (3).

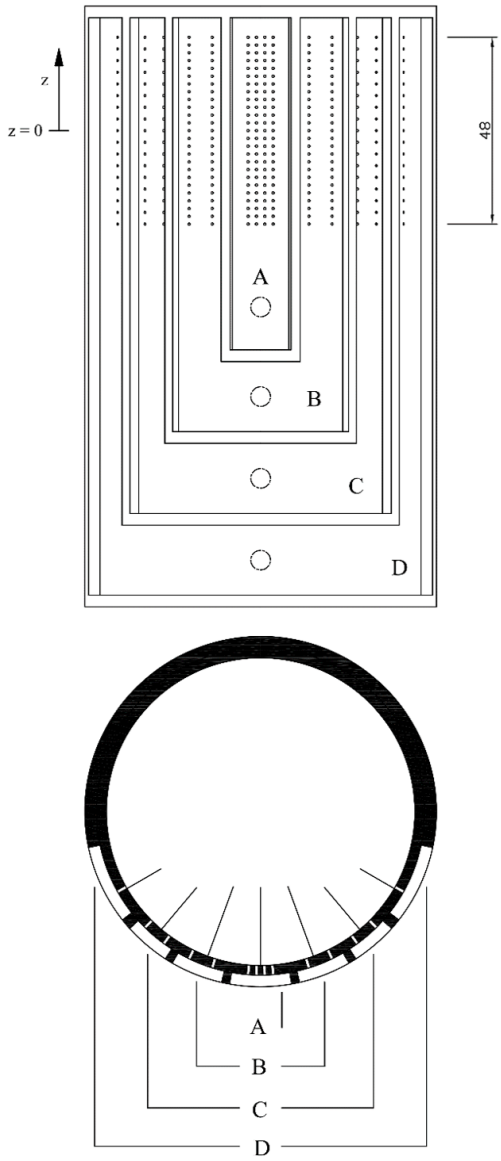

FIGURE 5.6 – Bottom and frontal view of the porous section for tracer injection. For clarity, also the first 7 wire-electrodes are shown.

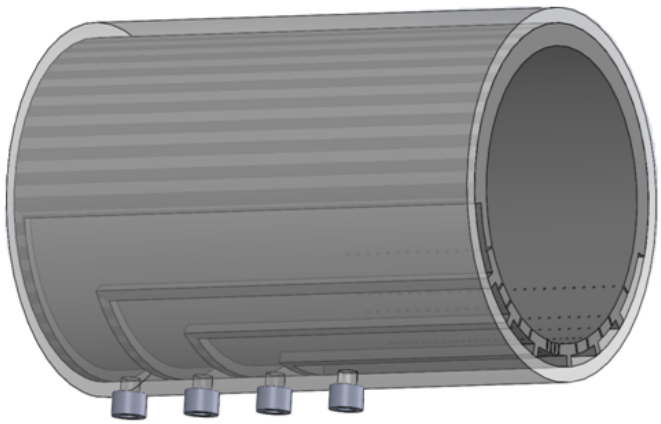

FIGURE 5.7 – Three-dimensional view of the porous section for tracer injection.

The tracer is injected only in the lower part of the pipe, where experimental observations indicate that most of the continuous liquid phase is flowing. The overall tracer flow is subdivided into four streams which are injected at different, symmetric locations around the pipe. The streams enter separately in four independent chambers, from which the tracer penetrates in the liquid film by a series of small holes. In order to monitor the concentration in the liquid layer immediately after the injection, the perforated section is mounted on the same block which hosts the second wire-electrode probe. The distance between the probe and the porous section has been minimized. As depicted in Fig. 5.6, the four chambers are positioned at the same azimuthal angles at which the first 7 electrodes of wire probes are located (0°, ±20°, ±40°, ±60°). In this way the signal provided by each of these electrodes is quite proportional to the tracer flow rate injected by the corresponding chamber, and can be used as feedback in order to achieve an uniform liquid concentration in the wall layer. Fig. 5.8 has the objective of clarify this concept.

As shown in Fig. 5.5 (1), also the third wire measuring section is mounted on this block, and its function is to provide the first experimental measurement of concentration decay in the liquid layer, due to the combined actions of entrainment and deposition. For what regards the electric requirements, the distance between probes and flanges has been kept the same of the standard probe configuration presented in Section 3.2. The numerical integration of Laplace equation has shown that, if the two probe sections are axially spaced of the same distance, their mutual interaction is negligible.

Metering Pumps. At the outlet of the tracer vessel, the flow is subdivided into two streams by two volumetric alternative pumps, having different operational ranges. The highest flow rate is dedicated to the injection

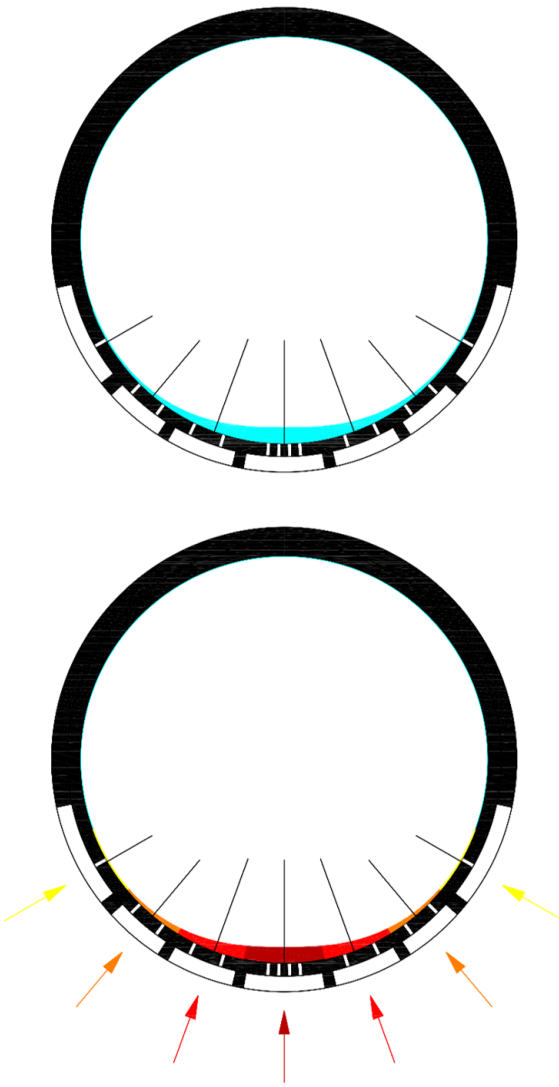

FIGURE 5.8 – Frontal view of the porous section. In the bottom image the volumes of liquid layer served by the four chambers are pictured in different colors. For clarity, also the first 7 wire-electrodes are shown. $u_{sg} = 20.8m/s; u_{sl} = 0.068m/s$.

at the bottom part of the pipe, where the thickness and the flow rate of the liquid layer are more pronounced (chambers A and B). The other tracer stream is addressed to the lateral wall of the pipe, which hosts a minor part of the continuous liquid fraction (chambers C and D). As depicted in Fig. 5.5 (3), each pump is assisted by a dampener, which transforms the pulsating flow into a more continuous stream. This task is very important in the present application, since a pulsating injection could spread the tracer directly into the gas core in the form of droplets. It is clear that such an event would invalidate any subsequent measurements.

Tracer Control System. The objective of the Control System is to obtain a uniform tracer concentration around the pipe wall immediately after tracer injection. To this purpose the tracer flow rate at each injection section is controlled with a set of valves, as shown in Fig. 5.5(2). A mini ovalgear flowmeter measures accurately the tracer flow rate and a regulation valve allows to split the flow coming from a common pump into two streams at the desired proportion.

Test Procedure.

It must be pointed out that the test procedure is very delicate, especially for what regards the stabilization of tracer flow rates at the desired values. Much efforts have been made to tune the procedure in order to gain the best results in terms of reproducibility and ease of execution. As an example, results were not good when the total tracer over liquid flow rate ratio W_T/W_L was kept below 0.02, probably because the quantity was not enough to permit an adequate homoegeous diffusion in the liquid film. An other essential task was the minimization of execution time. In fact, since the water circulated in a closed loop, after a certain period of time the liquid conductivity at the test section began to rise, due to the recirculation of the tracer injected. This period depended primarly on the water flow rate and on the total water amount inside the loop and was generally of the order of few minutes. Then, the tracer flow rate regulation had to be performed as faster as possibile.

We remind also that when the liquid concentration reached a certain value, the entire salty liquid had to be substituted with a new batch of de-ionized water. This operation was necessary not only because the relation between salt concentration and conductivity started to deviate from linearity, but also because the experimental uncertainty rised up to prohibitive levels. This happened because, at constant tracer concentration, the increment of liquid film concentration

$$\frac{C_{i,j}\left(t_k\right)}{C^0_{i,j}\left(t_k\right)} = \frac{G_{i,j}\left(t_k\right)}{G^0_{i,j}\left(t_k\right)} - 1 \tag{5.3.8}$$

(see Eq. 5.3.6) caused by the injection decreased at increasing the liquid concentration $C^0\left(t_k\right)$ ahead of the injection. The concentration ratio of

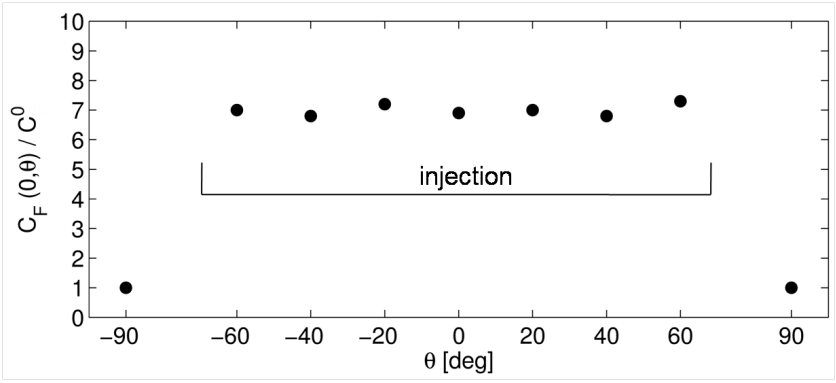

FIGURE 5.9 – Example of circumferential tracer concentration immediately after injection. C^0 is the salt concentration in the base film before tracer injection.

Eq. 5.3.8 was close to 7 at the beginning of a test cycle, as in the example reported in Fig. 5.9. Such a value allowed to capture the concentration decay along the pipe with a good precision. When the concentration ratio became equal to 2, this trend was affected by a strong uncertainty and it was necessary to change the liquid in the loop.

Unluckily, the operation of water refilling is quite time-consuming. The entire loop must be depressurised, the water tank and the "dead-points" of the loop (risers, bends, syphons, everywhere the water cannot be removed by the action of a single-phase gas flow) are emptied, a new volume of liquid (400 lt) is introduced in the tank and the loop is re-pressurised. This procedure requires about half a day and represents another strong motivation to minimize the amount of tracer injected in the liquid stream, in other words to reduce as much as possibile the time required for each test. Despite the work done to optimize the process, it was not possibile to do more than 5-6 tests with the same water.

Having these objectives in mind, the main steps followed during an experiment are listed here:

1. The tracer solution is pumped into the injection system and recirculated in the vessel through the sampling valve shown in Fig. 5.5(2). This keeps the solution concentration at a constant value.

2. The gas-liquid flow is established at desired conditions. After a period of time the temperature, and consequently the water conductivity, stabilizes at a constant value.

3. At the actual flow conditions, the four tracer flow rates required at the injection are estimated (see Appendix A) and established acting on the Control System, as explained above. The tracer is still recirculated into the vessel.

4. The "blank-conductance" $G^0_{i,j}$ is acquired and the water conductivity is measured.

5. The sampling valves are closed and tracer streams are forced to go into the distribution system. The check valve shown in Fig. 5.5(2) automatically opens when the pressure of the injection system equals the pressure of the loop.

6. The liquid film concentration measured in the second measuring section (section B in Fig. 5.2 (b)) is read in the display of the Data Acquisition System. The tracer flows are regulated until these concentrations become uniform. An example of the tracer concentration around pipe wall obtained according to this procedure is shown in Fig. 5.9. The uniform tracer concentration shown in this figure guarantees that any tangential tracer exchange be limited and that the tracer injected at each position be proportional to the local film flow rate. When the conditions shown in Fig. 5.9 are reached, data from all the measuring probes are ready to be taken.

7. At the end of data acquisition, the injection is immediately stopped. Before to start the consecutive experiment, the gas-liquid flow is circulated in the loop until water concentration settles at a new "blank" value.

5.4 Conclusions

In this chapter we have explained how the tracer method is combined with the conductance probes to obtain simultaneous measurements of film thickness, liquid entrainment and rate of liquid exchange. The main task was to design a system of tracer injection that allows a circumferential distribution of the inlet tracer flow rate proportional to the local liquid film flow rate. This system has been conceived to operate in a wide range of flow conditions, i.e. $u_{sg} = 5 - 25$ m/s and $u_{sl} = 0.04 - 0.14$ m/s.

The first conductance measuring section, located immediately downstream the injection area, is used to provide a feedback of tracer distribution along the pipe periphery, then to adjust the local tracer flow rates in order to reach an uniform injection in terms of liquid concentration. This regulation is possible in real time and this makes the experimental procedure particularly practice, fast and precise.

In the next chapter the first experimental results obtained in stratified-dispersed flow are analysed and discussed.

6

Flow test: results and discussion

6.1 Introduction

In this chapter the first experimental results obtained with the set-up described in previous chapter is presented and analysed. Measurements have been taken both about film thickness, liquid entrainment and deposition rate.

As stated in Chapter 5, the tuning of the experiment has been difficult and time consuming. For this reason, the data obtained with sufficient reproducibility regard a limited set of flow conditions.

6.2 Results and discussion

6.2.1 Circumferential Film Distribution

In Fig. 6.1 the time averaged values of the local film thickness are plotted in polar coordinates. The same data are shown in a semi-log plot in Fig. 6.2. The circumferential values of the film thickness, $h(\theta)$, allow the mean liquid hold-up, α_F, defined as

$$\alpha_F = \frac{1}{\pi R^2} \int_{A_F} r dr d\theta \,, \tag{6.2.1}$$

where A_F is the flow area of the continuous liquid layer flowing at pipe wall, to be computed by the numerical integration of the equation

$$\alpha_F = \frac{2}{\pi} \int_0^{2\pi} \frac{h(\theta)}{D_t} \left(1 - \frac{h(\theta)}{D_t}\right) d\theta \,. \tag{6.2.2}$$

Hereafter we consider the circumferential "zero" coordinate, $\theta = 0$, to be located at the pipe bottom. The results obtained are represented in Fig. 6.1 as the equivalent height of a stratified liquid layer. The average hold-up

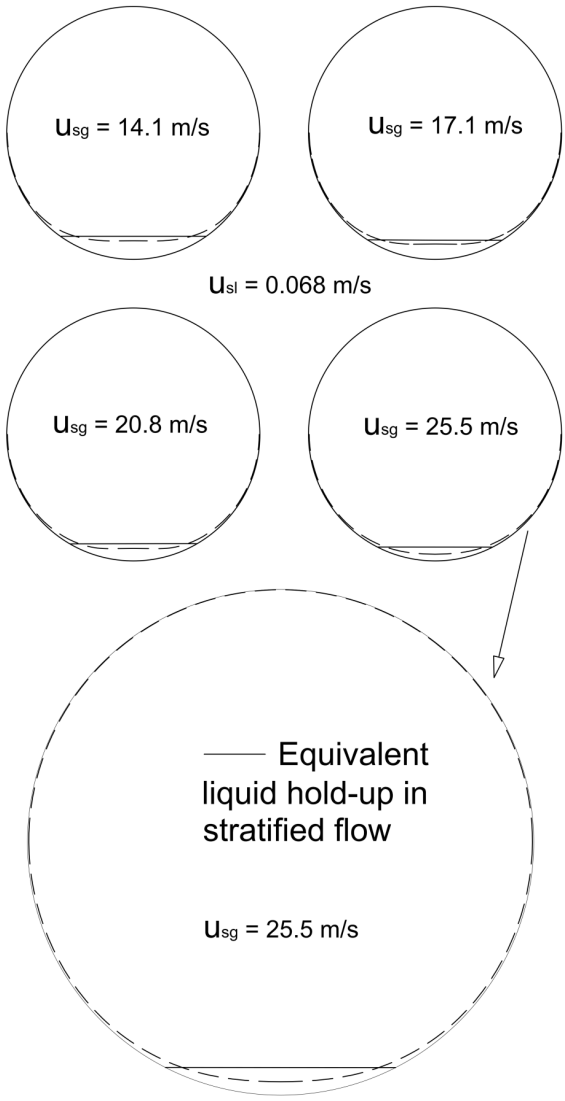

FIGURE 6.1 – Circumferential film thickness distribution in polar coordinates.

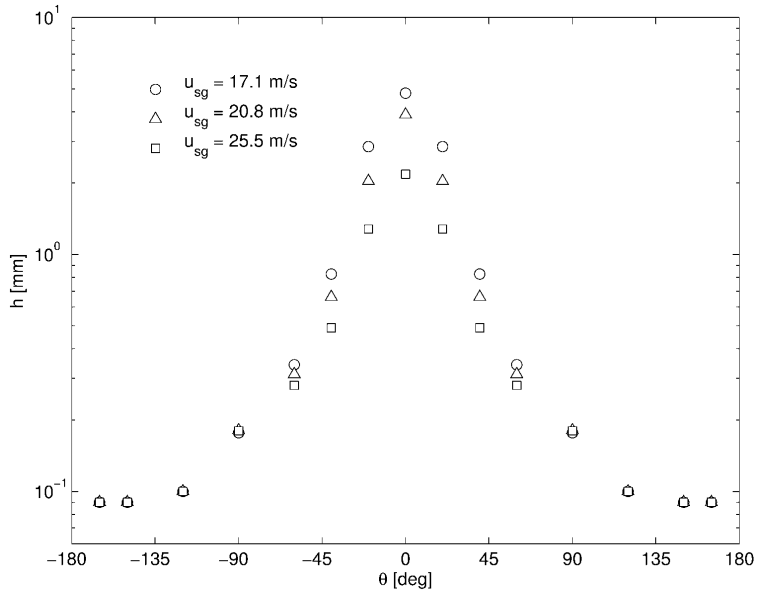

FIGURE 6.2 – Circumferential film thickness distribution. $u_{sl} = 0.068\ m/s$.

measured with the ring probe almost coincides with the wire probe data shown in Fig. 6.1, at least in the range of gas velocities at which SD flow is observed. The good agreement between wire and ring probes confirms that the set of wire only introduces a minor disturbance to liquid flow.

The graphs shown in Fig. 6.1 and Fig. 6.2 clearly indicate that, in the range of gas velocities considered in present experiments, the continuous liquid layer is made of a thick film which entirely flows in the lower part of the pipe (base film) and of a much thinner film flowing along the upper pipe wall (upper film). This observation confirms previous work by Paras and Karabelas (1991), Williams et al. (1996) and Geraci et al. (2007), among others, and is interesting because it suggests that at least the flow of the base film can be simulated as an extension to large gas velocities of the model and closure equations developed for stratified flow. This is already made in one-dimensional transient flow models, see for instance, Benkinsen et al. (1991), or Bonizzi et al. (2009). According to the experiments by Geraci et al. (2007), this seems to be possible for pipe inclinations up to of 45°. For larger inclinations, the wall layer tends to be more similar to annular flow in a vertical pipe.

In the present work, the circumferential wire probes also allowed a deep insight into the flow structure. For instance, Fig. 6.3 reveals the presence of long wave-length, 2-D waves flowing on the base film. The amplitude of these waves decreases at increasing values of the angle at which the probe is located and the waves disappear at the 90° probe. This can

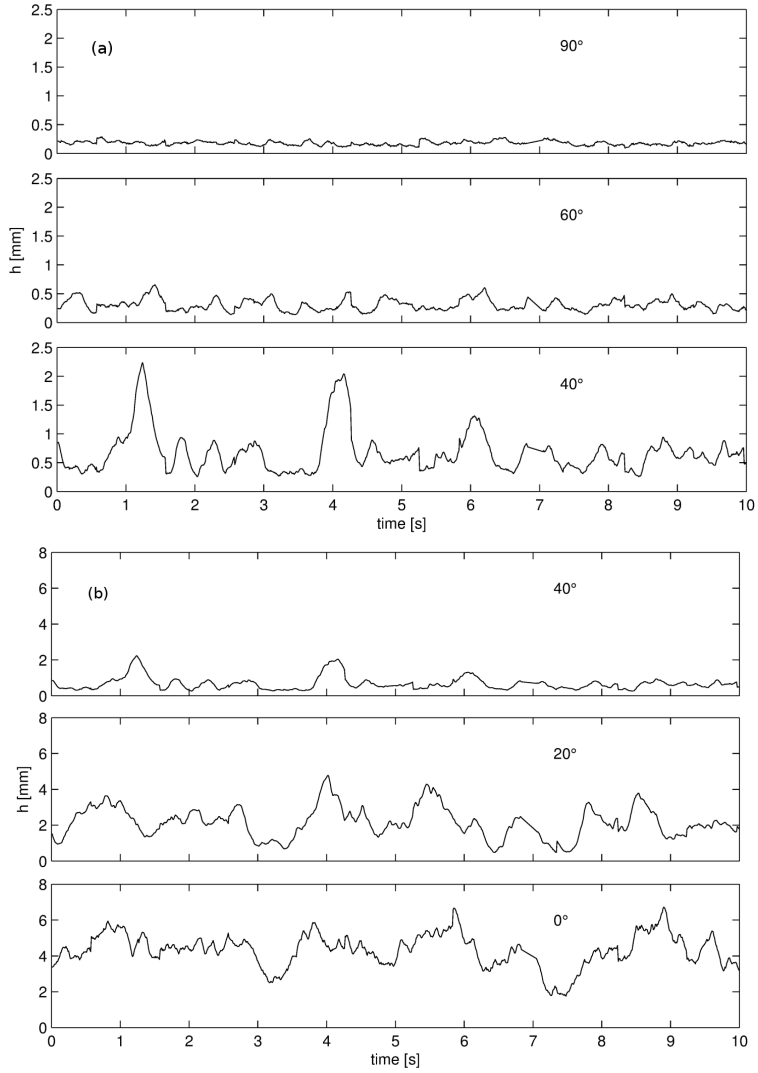

FIGURE 6.3 – Time traces of film thickness at varying θ. $usl = 0.068\ m/s$, $usg = 20.8\ m/s$. (a) is a 3x enlargement with respect to (b).

be clearly seen from the time traces reported in Fig. 6.3, which is split in two parts. In the upper part a blow-up of the traces at 40°, 60° and 90° is shown. In the lower part, for comparison, the time trace at 40° is represented again using the same scale as the traces at 0° and 20°. As in annular and stratified- dispersed flows the onset of heavy entrainment is usually associated with the transition between the so called "ripple"and "large disturbance wave"regimes (see for instance, Asali et al., 1985), the time traces shown in Fig. 6.3 are an indication that the upper liquid film is not atomizing.

The data presented in Fig. 6.1, 6.2 and 6.3 clearly indicate that the thin film flowing all around the upper pipe wall is not generated by the flow of large 2-D waves on the base film. The other mechanism which has been proposed to explain the formation of this film, is related to the secondary flow of the gas phase around the pipe wall. This requires that the secondary flow be directed upward at pipe wall and downward at the center plane. However, Dykhno et al. (1994) showed that in stratified-dispersed flow the gas secondary flow is directed in the opposite direction and enhances the drainage of the film rather than causing its formation (see Fig. 6.9 (b)). It may be concluded that the upper liquid film is generated by the deposition of entrained droplets.

The data relative to the circumferential liquid film distribution around the pipe wall shown in Fig. 6.2 reveal a potentially interesting feature, in particular when these data are compared with the similar plot presented by Williams et al. (1996). The better spatial resolution of the present data (5 probes in the range 0-90°, compared with 3 probes) helps to see from Fig. 6.2 that the angle at which the local film thickness tends to assume an almost constant, low value, for all flow conditions, is about equal to ±70° from the bottom of the pipe.

The data presented by Williams et al. (1996), relative to the film height distribution in a horizontal pipe of similar diameter and flow conditions, apparently confirm that this is the case for the extensive set of gas and liquid flow rates investigated by these authors. This observation can be important because it may be used to develop a simplified model of the liquid flow around the pipe. It has also been very useful in the design of the tracer injection section, because from Fig. 6.1, 6.2 and 6.3 it seems that the thick atomizing film at pipe bottom is bound by gravity to flow between ±70° from the vertical.

6.2.2 Circumferential tracer distribution

In Fig. 6.4 the time averaged values of the local tracer concentration around the pipe wall are plotted for various distances downstream of the tracer injection. An interesting feature of these experiments is that at the lateral positions where the tracer is not injected, for instance at 90°, the tracer concentration is close to zero not only immediately after tracer injection,

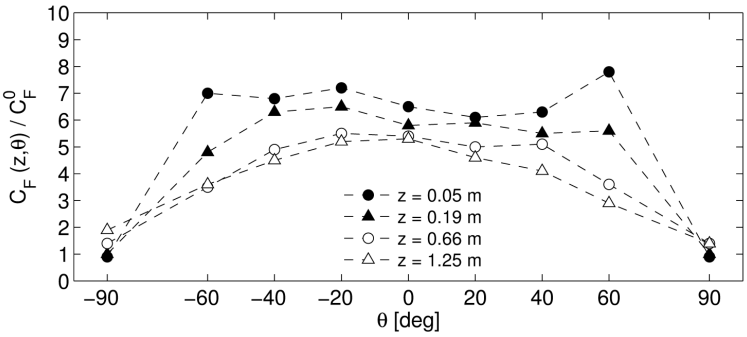

FIGURE 6.4 – Circumferential tracer concentration along the pipe. C_F is the salt concentration in the base film before tracer injection. $usl = 0.068\ m/s$, $usg = 25.5\ m/s$

but also at the following measuring sections. This result can be due to a small rate of droplet deposition on the upper pipe wall and, eventually, to a significant delay between droplet entrainment and their deposition on the upper film, with a consequent delay of the deposition on the side wall of salted droplets. It also reveals poor circumferential mixing of the tracer and the presence of a downward flow of the lateral liquid film, which tends to dilute the base film.

It can be assumed that the drainage of the upper film be determined by gravity. The possible contribution of gas secondary flows cannot be excluded. The measurements shown in Fig. 6.4 do not clarify this point, but suggest that if the secondary flows are directed in the downward direction next to the side pipe wall, as proposed by Dykhno et al. (1994), the low tracer concentration in the lateral film can be better justified than the assumption of secondary flow acting in the opposite direction.

When the motion of a thin laminar film is mainly determined by gravity, the film thickness depends on the cubic root of the film flow rate and on the pipe inclination. This may explain why the thickness variations around the pipe wall in the present and as well in Williams et al. (1995) experiments are relatively small in the range 180°- 90° and only increase appreciably at lower inclinations.

6.2.3 Tracer concentration along the pipe

The tracer flow rate in the continuous liquid at any position along the pipe, $W_T(z)$, can be computed as

$$W_T(z) = \int_{A_F} C_F(z,r,\theta)\, u_F(r,\theta)\, r\, dr\, d\theta\ , \tag{6.2.3}$$

where C_F and $u_F(r,\theta)$ are the local tracer concentration and liquid velocity. In this equation, u_F is only function of r and θ, as fully developed

flow conditions are assumed. According to Andreussi (1983), tracer mixing in the radial direction is complete a few centimeters after the injection. Therefore, in Eq. 6.2.3 $C_F(z,r,\theta)$ is independent from r at any axial and circumferential position, $C_F(z,r,\theta) = C_F(z,\theta)$.

In present experiments tracer injection is controlled in order to obtain a uniform tracer distribution around the pipe circumference. This implies that immediately after tracer injection, $C_F(0,\theta) = C_F^0$ and Eq. 6.2.3 can be written as

$$W_T(0) = C_F^0 \int_{A_F} u_F(r,\theta)\, r\, dr\, d\theta \,. \tag{6.2.4}$$

It is useful to introduce the volumetric flow rate per unit length of the liquid film, $\Gamma(\theta)$, defined as

$$\Gamma(\theta) = \frac{1}{R} \int_{R-h(\theta)}^{R} r u_F(r,\theta)\, dr \,. \tag{6.2.5}$$

In terms of $\Gamma(\theta)$, $W_T(z)$, and the film flow rate, W_F, can be written as

$$W_F = R\rho_L \int_{-\theta_F}^{\theta_F} \Gamma(\theta) \;, \tag{6.2.6}$$

$$W_T(z) = R \int_{-\theta_F}^{\theta_F} C_F(z,\theta)\, \Gamma(\theta) \;, \tag{6.2.7}$$

where, as reported above, θ_F is the angle around the pipe perimeter which encloses the base film ($\theta_F = \pm 70$ %). Beyond this angle both $\Gamma(\theta)$ and $C_F(z,\theta)$ assume values close to zero. At tracer injection, the tracer flow rate injected at any circumferential position, $W_T(\theta_i)$ is carefully measured and is equal to

$$W_T(\theta_i) = C_F^0 \Gamma(\theta_i)\, R\Delta\theta \,. \tag{6.2.8}$$

From this equation, $\Gamma(\theta_i)$ can easily be computed. This also allows W_F to be determined as

$$W_F = R\rho_L \Delta\theta \sum_{i=1}^{n} \Gamma(\theta_i) \;. \tag{6.2.9}$$

In Table 6.1, the flow rates of the bottom liquid layer derived from the initial tracer concentration are compared with the values obtained using the tracer balance equations. As can be seen from this table, the use of Eq. 6.2.9 to derive W_F does not seem to be very accurate. Moreover, the values of W_F appear to be always smaller than the values determined with the tracer balance equations. This is due to the minor tracer dilution occurring in the few centimeters of pipe which separate the injection section from the first measuring section.

TABLE 6.1 – $usl = 0.068\ m/s$, $usg = 25.5\ m/s$ for all tests. Measurement of f_B by data interpolation or direct tracer balance.

f_B		
Test	Tracer balance equation	Initial tracer concentration
A	0.57	0.47
B	0.56	0.55
C	0.57	0.56

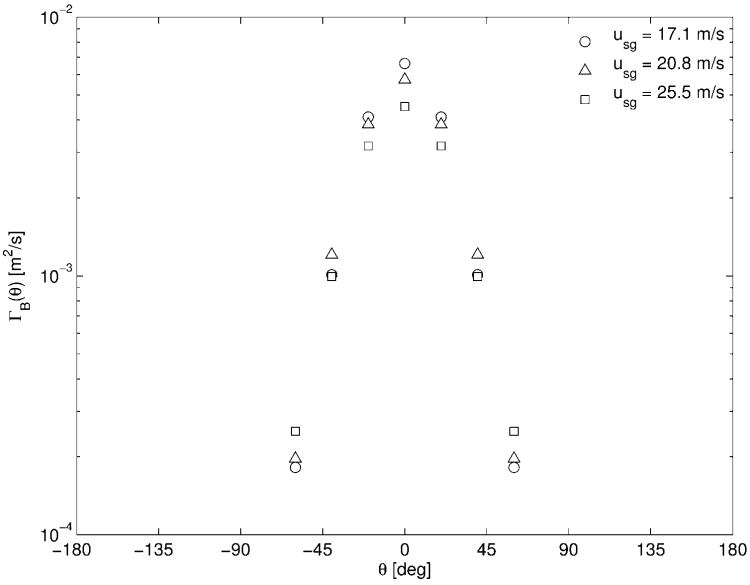

FIGURE 6.5 – Local film flow rate $\Gamma_B(\theta)$ vs θ. $usl = 0.068\ m/s$ for all tests.

The set of values of the local film flow rate $\Gamma(\theta_i)$ determined as indicated above, immediately after tracer injection, can be used to determine the time and circumferential average tracer concentration at any axial position, $\langle C_F(z)\rangle$, defined as

$$\langle C_F(z)\rangle = \frac{\int_{-\theta_F}^{\theta_F} C_F(z,\theta)\,\Gamma(\theta)\,d\theta}{\int_{-\theta_F}^{\theta_F} \Gamma(\theta)\,d\theta}\ . \tag{6.2.10}$$

$\langle C_F(z)\rangle$ can be computed as

$$\langle C_F(z)\rangle = \frac{\sum_{i=1}^{n} C_F(z,\theta_i)\,\Gamma(\theta_i)}{\sum_{i=1}^{n} \Gamma(\theta_i)}\ . \tag{6.2.11}$$

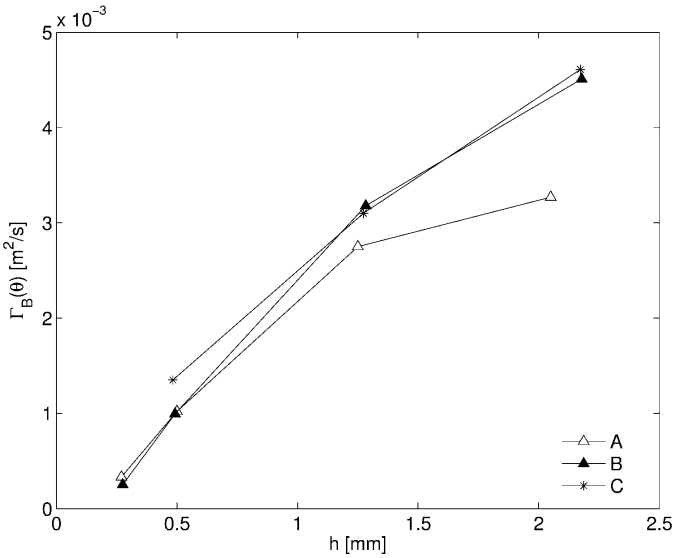

FIGURE 6.6 – Local film flow rate vs film thickness. $usl = 0.068\ m/s$, $usg = 25.5\ m/s$

The values of $\Gamma(\theta_i)$ determined in a set of preliminary tests are represented in Fig. 6.5 as a function of θ. As can be seen from this figure, the local film flow rate has only been measured at angles up to $\pm 60°$ from the vertical. This is because the tracer is only injected up to these angles. Nonetheless, the trend of $\Gamma(\theta_i)$ values indicates that the local film flow rate in the base liquid layer tends to zero for angles of about $\pm 70°$, thus confirming the previous observation on the angular distribution of the base film.

The measurements of $\Gamma(\theta_i)$ are represented in Fig. 6.6 as a function of the local film height, $h(\theta_i)$. This graph is interesting because it allows to test the models proposed in the literature to describe the flow of thin liquid films sheared by the gas. The data reported in Fig. 6.6 cover, in a single experiment, a wide range of film heights, also in presence of a significant component of gravity acting in a direction normal to the main flow.

For each test, the limiting tracer concentration in the liquid phase for $z \longrightarrow \infty$, C_e, can be computed as

$$C_e = \frac{W_T(0)}{W_L}\ , \tag{6.2.12}$$

where $W_T(0)$ is the measured tracer flow rate at inlet and W_L the overall liquid flow rate fed to the system. The measured values of $\langle C_F(z) \rangle$ and C_e allow the dimensionless tracer concentration $p(z)$ defined in Eq. 5.2.4 to be estimated. The results relative to three different tests conducted at the same conditions are shown in Fig. 6.7, where a tentative linear interpolation

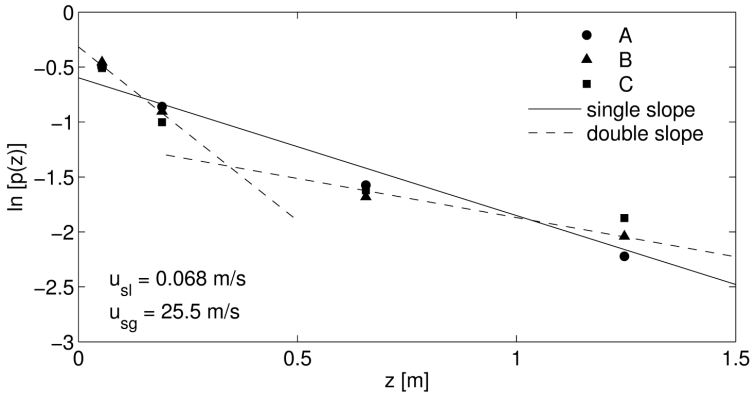

FIGURE 6.7 – Dimensionless tracer concentration along the pipe.

of the measurements is also reported. The objective of these multiple tests has been to verify how good the reproducibility of the present experiments is.

As can be seen from Fig. 6.7, the trend of $p(z)$ vs z in a semi-log plot deviates appreciably from the linear behavior predicted by Eq. 5.2.6. The only parameter that can be derived from this graph is the value of the base film fraction f_B , which can be immediately related to the value of $p(z)$ for $z \longrightarrow 0$. The interpolation of the experiments with two straight lines (also shown in Fig. 6.7) is simple, considering that the data are only available at four axial locations. Still, this interpolation helps to compare the present data with the results obtained by Andreussi (1983) for the vertical flow experiments conducted at low gas velocities (37 - 44 m/s).

The trend of the dimensionless tracer concentration along the pipe observed by this author was attributed to the presence of two different mechanisms of droplet deposition, trajectory and turbulent diffusion. According to Andreussi & Azzopardi (1983), the rate of deposition can be different in these two cases and this difference may explain the trend of the tracer concentration plot.

In horizontal pipes, the flow structure is quite different, due to the presence of the upper film. As discussed above, this film appears to be generated by droplet deposition on the upper pipe wall. The tracer concentration measured in this film along the pipe is low, as shown in Fig. 6.4, thus indicating that the tracer exchange between this film, the layer flowing at pipe bottom and the entrained drops is also low. It is concluded that in SD flow two different processes of tracer mixing may co-exist, a fast droplet exchange between the base film and the gas core and a slow transfer between the entrained droplets, the upper film and the base film.

6.3 Three-field model of tracer transport

The experimental observations presented in the previous section indicate that the simple one-dimensional two-field model adopted for the liquid phase may be not accurate enough to describe SD flow. A possible improvement may rely upon the development of a three dimensional model of this flow pattern, based on local measurements of flow parameters such as the circumferential film thickness distribution and the phase velocities and volume fractions in the gas core. The 3-D model finally obtained should then be integrated into a more conventional 1-D transient flow model, which is, at present, the only possible choice for the simulation of gas-liquid flow in long pipelines.

A possible alternative would be to maintain the one-dimensional description of SD flow and adopt a three-field model for the liquid phase. This new model can be considered as an evolution of the two-field model proposed for vertical annular flows, whereby, in near horizontal flow, the simultaneous presence of a significant fraction of short-living droplets traveling close to the gas-liquid interface and of smaller droplets fully entrained by the gas and characterized by a much lower deposition velocity, is explicitly accounted for. It can be expected that the short- living droplets be ejected from the base film with an appreciable velocity, as found by James et al. (1980) for vertical annular flow, but then, due to their size and the action of gravity, deposit on the base film after a short distance from their entrainment. Therefore, their contribution to the formation of the upper wall layer is expected to be small, at least for pipe diameters larger than 0.08-0.1 m, as those adopted in the present experiments and by Williams et al. (1996).

The formation of the upper film layer can then be attributed to the deposition of smaller droplets. This assumption can be supported by the presence of a significant secondary flow of the gas phase directed in the upward direction at the centre of the pipe, as discussed in Section 6.2.1. The magnitude of this flow can be of the order of 10% of the gas velocity, as reported, among others by Van't Westende et al. (2007), and the gas flowing in the upward direction may be able to extract the smaller drops from the massive liquid entrainment occurring at the gas-liquid interface. The size of these droplets is likely to be such that they can be fully entrained by the gas, their deposition is then appreciably delayed and mainly occurs on the upper and side pipe wall, due to the combined effects of the vertical momentum and the centrifugal acceleration provided by the gas secondary flow. This leads to the formation of the thin non-atomizing film observed in the present experiments and suggests that appreciable fractions of the liquid phase, the small droplets and the thin circumferential film, do not actively participate to the process of tracer mixing.

An estimate of the upper film flow rate, knowing its mean height, is possible using the semi- empirical correlations proposed by Asali et al. (1985) to predict the thickness of very thin, non-atomizing films shared by the

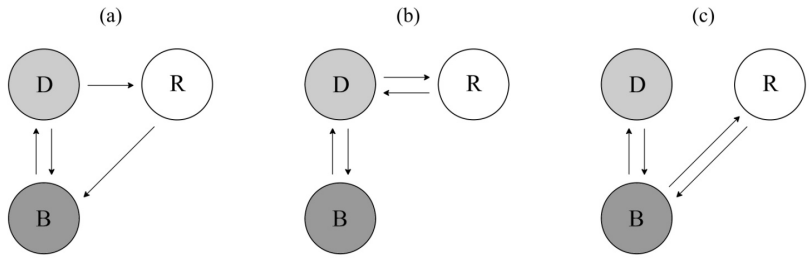

FIGURE 6.8 – Possible schemes of mass transfer among the liquid fields. Base film (B), short-living droplets (D) and droplets fully entrained by the gas phase (R).

gas flow. This estimate indicates that this flow rate be much less than the flow rates of the other three fields, As both this liquid layer and the small droplets provide a similar, minor contribution to the process of tracer mixing, in the analysis of tracer experiments it is convenient to include the upper film into the small droplets field with the objective of closing the overall mass balance.

It can be added that the presence of the upper wall layer cannot be ignored because on one hand, this film delays the liquid mixing process, on the other, Asali et al (1985) showed that even a very thin liquid layer may cause an appreciable increase of the gas phase friction factor. For this reason, future work on stratified-dispersed flow should also regard the data acquisition and the development of specific models to describe the upper film flow behaviour.

The three field scheme of the liquid flow outlined above requires the velocities u_B, u_D , u_R and the liquid hold-ups α_B, α_D, α_R to be introduced, where subscript B indicates the base film, D the short-living droplets and R the droplets fully entrained by the gas phase. The definition of the three main fields characterizing liquid flow is not sufficient to model the system because different schemes of liquid transfer among these fields can be proposed. The schemes which can better describe the present observations are shown in Fig. 6.8. In all these schemes only field B can produce liquid entrainment with rate Φ_B. In scheme (a) and (b), field R is generated by field D. From a physical stand-point, this can be attributed to the effect of gas secondary motions. Field R transfers back to field B in scheme (a) and to field D in scheme (b) the mass received from field B. Finally, in scheme (c), the exchanges of liquid between field B and field D and between field B and field R are entirely independent. In all the three cases sketched in Fig. 6.8, the phenomenon controlling tracer transport is the mass exchange between fields B and D, while Φ_R is expected to be much smaller than Φ_B. With this assumption, the three schemes considered above are very similar. Therefore, in the following only the tracer balances relative to scheme (a)

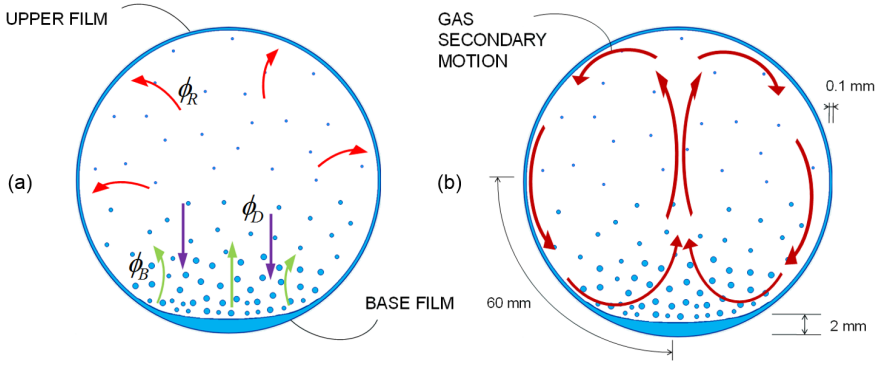

FIGURE 6.9 – Pictorial representation of (a) three field liquid transfer (scheme *a* of Fig. 6.8) and (b) gas secondary motion, oriented as measured by Dykhno et al. (1994).

are reported. Fig. 6.9 (a) shows a pictorial representation of this scheme. The other cases can be easily derived from this and the values of the unknown parameters (flow rates of the fields and mass exchange rates) derived from the best fit of the experimental measurements of tracer transport are almost identical for the three schemes considered in Fig. 6.8.

According to scheme (a), in fully developed flow, the rate of liquid entrainment from the base film Φ_B is equal to

$$\Phi_B = \Phi_D + \Phi_R \,, \tag{6.3.1}$$

where Φ_D is the rate of deposition on the base film of the short-living droplets and Φ_R of the smaller droplets. Φ_R includes the drainage of the upper circumferential film. The tracer conservation equations can be written as

$$\rho_L \, \alpha_B \, u_B \, \frac{dC_B}{dz} = -\Phi_B C_B + \Phi_D C_D + \Phi_R C_R \,, \tag{6.3.2}$$

$$\rho_L \, \alpha_D \, u_D \, \frac{dC_D}{dz} = \Phi_B \left(C_B - C_D \right) \,, \tag{6.3.3}$$

$$\rho_L \, \alpha_R \, u_R \, \frac{dC_R}{dz} = \Phi_R \left(C_D - C_R \right) \,, \tag{6.3.4}$$

where C_B, C_D, C_R represent the tracer concentrations in the respective fields. This system of linear differential equations can be expressed in terms of the two functions x, y defined as

$$x\left(z\right) = C_B\left(z\right) - C_D\left(z\right) \,, \tag{6.3.5}$$

$$y\left(z\right) = C_D\left(z\right) - C_R\left(z\right) \,. \tag{6.3.6}$$

It is obtained

$$\frac{dx}{dz} = -\left(\frac{\Phi_B}{\rho_L\,\alpha_B\,u_B} + \frac{\Phi_B}{\rho_L\,\alpha_D\,u_D}\right) x - \frac{\Phi_R}{\rho_L\,\alpha_B\,u_B}\,y\,, \tag{6.3.7}$$

$$\frac{dy}{dz} = \left(\frac{\Phi_B}{\rho_L\,\alpha_D\,u_D}\right) x - \frac{\Phi_R}{\rho_L\,\alpha_R\,u_R}\,y\,, \tag{6.3.8}$$

Eqs. 6.3.7 and 6.3.8 can easily be integrated with boundary conditions

$$x = C_B^0,\;\; y = 0 \;\; @ \;\; z = 0\,, \tag{6.3.9}$$

The result of the integration can be expressed as

$$x = \frac{C_B^0}{\lambda_2 - \lambda_1}\left[(\lambda_2 - c_1)\,exp\{\lambda_1 z\} - (\lambda_1 - c_1)\,exp\{\lambda_2 z\}\right]\,, \tag{6.3.10}$$

$$y = \frac{C_B^0}{\lambda_2 - \lambda_1}\frac{(\lambda_2 - c_1)\,(\lambda_1 - c_1)}{c_2}\left(exp\{\lambda_1 z\} - exp\{\lambda_2 z\}\right)\,, \tag{6.3.11}$$

where λ_1, λ_2 are the eigenvalues of the system of linear differential equations

$$\frac{dx}{dz} = c_1 x + c_2 y\,, \tag{6.3.12}$$

$$\frac{dy}{dz} = c_3 x + c_4 y\,, \tag{6.3.13}$$

and c_i the coefficients of x and y in Eqs.6.3.7 and 6.3.8. The dimensionless tracer concentration $p\,(z)$ can easily be derived from x and y as

$$p\,(z) = (1 - f_B)\,\frac{x}{C_e} + f_R\frac{y}{C_e}\,, \tag{6.3.14}$$

where f_B and f_R are the fractions of liquid flow in fields B and R. Finally, the value of $p\,(z)$ at $z = 0$ is

$$p\,(0) = \frac{1 - f_B}{f_B}\,, \tag{6.3.15}$$

which is the same value found for the two field model. The initial slope of $p\,(z)$ is

$$\frac{dp}{dz}|_{z=0} = -\frac{1 - f_B}{f_B}\left(\frac{\Phi_B}{\rho_L\,\alpha_B\,u_B} + \frac{\Phi_B}{\rho_L\,\alpha_D\,u_D}\right) + \frac{f_R}{f_B}\left(\frac{\Phi_B}{\rho_L\,\alpha_D\,u_D}\right)\,. \tag{6.3.16}$$

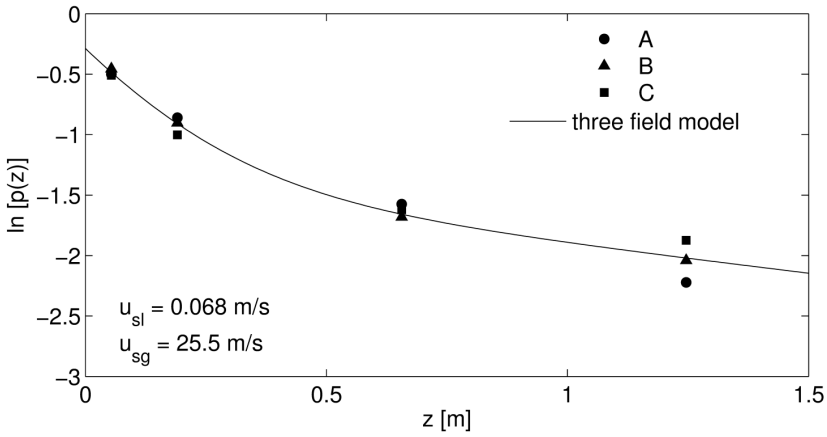

FIGURE 6.10 – Dimensionless tracer concentration along the pipe. Comparison between three-field model and experiments.

In this equation, if we replace f_R with $1 - f_B - f_D$ it can easily be shown that the initial slope of $p(z)$ becomes equal to the value found for the two field model, Eq. 5.2.7, with f_B replacing f_F.

In principle, the values of Φ_R and f_R can be estimated from the trend of $p(z)$ for large values of z. Unfortunately, at large distances from tracer injection C_B approaches C_e and $p(z)$ tends to zero. It then happens that small absolute errors in the measurement of the tracer concentration will introduce large errors in the values of $p(z)$. In order to evaluate the full set of parameters of the three-field model, it is possible to look for the best fit of the experimental values of $p(z)$ with the analytical solution of model equations. Also this procedure is questionable, due to the limited number of tracer concentration measurements and their appreciable uncertainty.

It is useful to remark that at least the values of the liquid film flow rate and the rate of entrainment are expected to be fairly accurate because, as explained above, these parameters are evaluated from the value of $p(z)$ and its derivative for $z \to 0$.

TABLE 6.2 – $usl = 0.068\ m/s$, $usg = 25.5\ m/s$ for all tests. Parameters of the three-field model.

Test	f_B	f_D	f_R	Φ_B	Φ_R
A	0.57	0.17	0.26	62	13
B	0.56	0.26	0.18	71	5
C	0.57	0.23	0.20	80	5
All	0.57	0.21	0.22	68	8

Fig. 6.10 reports the same data shown in Fig. 6.7, along with the best fit of these data with Eq. 6.3.14. The values of model parameters for each of the experiments are reported in Table 6.2, where also the case of a unique fit of all the experiments is shown. Table 6.2 confirms that the value of f_B is fairly stable in all the experiments. The variability of Φ_B, the rate of droplet entrainment, and f_R are limited to $\pm 20\%$. The uncertainty affecting the remaining parameter, Φ_R, is significant. This parameter needs to be determined with a distinct experiment, or predicted with a physical model. It is also possible to increase the number of measuring sections in the present experiment, but also the accuracy of tracer concentration measurements should increase.

The values of Φ_R and f_R reported in Table 6.2 deserve some comment, even if it is expected that the actual values of these parameters may be different. Φ_R is more than 10 times smaller than Φ_B. Such a difference of the two rates explains the trend of the dimensionless tracer concentration shown in Fig. 6.7. It can be noted that the change of slope in the present experiments appears to be more severe than that reported by Andreussi (1983) for vertical annular flow.

The large value estimated for f_R does not seem to be justified by the hold-up of the upper wall layer. Apart from the accuracy of this estimate, it seems that the overall fraction of liquid marginally involved in the tracer exchange be significant: about 20% of the total liquid flow.

The rate of entrainment determined in present experiments, Φ_B, is equal to the rate of deposition over the entire pipe wall, $\Phi_B = \Phi_R + \Phi_D$. In vertical flows the rate of droplet deposition is usually expressed as

$$\Phi_D = \frac{4}{D_t} k_D C_E \ , \tag{6.3.17}$$

where k_D is the deposition velocity. According to present measurements, the value of k_D is about equal to 2 m/s, which is one order of magnitude larger than in vertical flows. This result can only be explained assuming that the droplets generated at the gas-liquid interface in horizontal flow, due to gravity, tend to deposit back on the base film after a short trajectory in the gas core. Only a limited amount of entrained drops is able to fly to the upper part of the pipe and then fall back on the base film or the side wall.

6.4 Conclusions

The tracer method, originally developed by Quandt (1965) to determine the liquid transfer between the wall layer and the gas core in vertical annular flow, has been applied to the case of stratified-dispersed flow in a horizontal pipe. This required the development of a specially designed test section (described into details in Chapter 3), used to detect the film thickness and

the tracer concentration around the pipe wall at a number of axial locations, and a differential tracer injection method, which guarantees uniform tracer concentration in the wall layer immediately after its injection.

This experimental set-up has been able to provide valuable data, even if the observed flow structure appears to be more complicated than expected. For this reason, the analysis of the experimental measurements required the development of a new three-field model of the liquid phase. In the present formulation, the model holds for steady, fully developed flow conditions and is based on a one-dimensional description of the flow system, whereby the three liquid fields are characterized by single velocity and hold-up values. The model accounts for the simultaneous presence of a significant fraction of short-living droplets traveling close to the gas-liquid interface and smaller droplets, fully entrained by the gas, characterized by a much lower deposition velocity. The continuous liquid layer is also split into two fractions, the thick atomizing layer at pipe bottom and the upper layer which appears to be generated by droplet deposition. The hold-up and flow rate of the upper layer appear to be small. This allows the presence of this film to be neglected, as far as the overall liquid mass balance concerns, but it is expected that its presence delays the transport processes among the liquid fields and significantly affects the frictional pressure gradient. The new model of the liquid flow can replace the conventional scheme adopted in one dimensional flow simulators (Bendiksen et al., 1991), which assumes, also for stratified-dispersed flow, that the liquid phase be only divided between the film at pipe wall and the entrained droplets.

The main experimental results can be summarised as follows:

1. The circumferential film thickness distribution confirms the experimental observations reported, among the others, by Williams et al. (1996). The better spatial resolution of present measurements also allowed the circumferential position at which the local film height assumes an almost constant, low value to be detected. This position ($\pm 70^\circ$ with respect to the vertical) appears to be independent of the gas and liquid flow rates and can be considered as the position at which the thin film generated by droplet deposition on the upper pipe wall merges with the thick liquid layer flowing at pipe bottom.

2. The time traces of the local film height show the presence of large waves whose amplitude decreases at increasing the angle at which the probe is located. These waves can hardly be detected at 60° inclination and disappear at 90° (there are no intermediate readings). This confirms what reported above and also that the thin film around the pipe wall is not generated by the large waves.

3. The circumferential distribution of the tracer concentration at various axial positions indicates that the droplet deposition on the thin lateral film and the draining of this film into the thick bottom layer are slow

processes which delay tracer mixing. This obliges to take explicitly into account the presence of this film and of a consistent fraction of entrained droplets characterized by a slow deposition rate on the upper pipe wall.

4. The differential tracer injection around the pipe wall allowed the local film flow rate to be measured. These data, along with the values of the local film thickness, may provide some insight into the flow of thin liquid layers under the gas shear along the main flow direction and the force of gravity acting in the normal direction.

5. The rate of droplet transfer has only been measured with some accuracy (three distinct tests and a wide number of preliminary tests performed in order to tune the system) for one set of flow conditions. The results obtained indicate that the flow rate of the thick liquid layer flowing at the pipe bottom can be measured with good accuracy. The reproducibility of the measurements of the droplet entrainment rate and the two flow rates of entrained droplets are within $\pm 20\%$. The error affecting the estimate of the deposition rate of small drops appears to be relevant.

6. The result obtained for the single case considered in this work is interesting because the value of the deposition coefficient appears to be one order of magnitude larger than the values relative to vertical annular flow. This can be explained considering the relevant effect of gravity on droplet deposition in a horizontal flow system.

The development and validation of the experimental method presented in this work has been difficult, time consuming and expensive. The results obtained indicate that the number of tracer measuring sections should increase. This requires an upgrade of the experimental system. The overall experience made in this work confirms that the tracer method is cumbersome, as initially reported in Section 2.3, but also able to provide very valuable information about the flow structure of stratified-dispersed flow.

7

Conclusions and future work

7.1 Conclusions

The main objective of the present work was the development of a new experimental method to study stratified-dispersed flow in near horizontal pipes, at flow conditions as closer as possible to those of natural gas pipelines. To this aim, the test section has been conceived to operate at an appreciable pressure (40 Bar) and a relatively large diameter pipe size of 80 mm has been chosen.

The main conclusions that can be drawn have already been listed at the end of each chapter. Here we briefly summarise the principal considerations.

Part I was dedicated to the development of the conductance probe test section:

- Conductance probes have been adopted because of their limited cost when compared with other methods proposed in the literature. Moreover, they can be used to obtain measurements of both film thickness and liquid film flow and deposition rate by means of the tracer method. Among the different geometries proposed in the literature, wire electrodes have been chosen because they guarantee a linear response at varying over a very wide range the film thickness and the average liquid conductivity. The probes were positioned all around the pipe circumference, following an arrangement never investigated before.

- The design of the test section required a huge amount of theoretical and experimental work. A new theoretical equation (Eq. 3.2.5) has been derived to predict the conductance of a three-wire probe immersed in an unbounded liquid film. The numerical integration of Laplace equation has been used to determine the probe conductance and optimize the geometry of the test section. It turns out that the circumferential distribution of the electrodes eliminates probe-to-probe interference, enabling the simultaneous operation of the 15 wire probes without multiplexing. The absence of multiplexing represents

a noticeable advantage of the present set-up: it allows most of the demodulated signal bandwidth to be exploited and eliminates most sources of electrical switching noise and subsequent errors.

- Non-conventional wire probes based on the use of three-electrodes spaced along the flow direction have been adopted. This geometry allows the current dispersion to the external conductive components of the test rig to be minimized and the measure to be more localised.

- The integration of Navier-Stokes equations using the VOF multiphase model allowed the disturbance generated by a set of wire electrodes to be evaluated. This disturbance can produce an error in the measurement of the film height about equal to 2% for the flow condition examined in the present work. The magnitude of this error does not change significantly when comparing the present three wire configuration with the conventional one based on two wires.

- The test section has been validated on a free falling liquid layer. The measurements are affected by systematic, low deviations from the theoretical predictions. The magnitude of these deviations changes according to the calibration method and reaches a maximum of 6%. The principal source of error seems to be related to the measurement of the electrical conductivity, while the disturbances generated by wire-flow interactions are less pronounced. Anyway, possibly most of the published film thickness measurements are affected by similar or larger uncertainties, as it appears from the work of Lioumbas et al. (2005).

Part II deals with the application of the tracer method to SD flow:

- The tracer method, never adopted before to study SD flow, has been combined with the conductance probes to obtain simultaneous measurements of film thickness, liquid entrainment and rate of liquid exchange. The main task was to design a system of tracer injection that allows a circumferential distribution of the inlet tracer flow rate. This system has been conceived to operate in a wide range of flow conditions. Particular efforts have been made to tune the test procedure in order to gain the best results in terms of reproducibility and ease of execution.

- The circumferential film thickness distribution confirms the experimental observations reported, among others, by Williams et al. (1996). The thin liquid film on the upper part of the pipe wall seems to be generated by droplet deposition.

- The circumferential measurement of tracer concentration at various axial positions indicates that the droplet deposition on the thin lateral

film and the draining of this film are slow processes and must be taken into account in data interpretation. A new, three-field model of tracer transport is proposed.

- The differential tracer injection around the pipe wall allowed the local film flow rate to be measured with good accuracy.

- The error affecting the measurements of droplet entrainment and deposition rate is more relevant. Anyway, these measurements are interesting because the value of the deposition coefficient appears to be one order of magnitude larger than the values relative to vertical annular flow. This is probably due to the relevant effect of gravity on droplet deposition in a horizontal flow system.

The overall experimental activity confirms that the tracer method is cumbersome, as perceived by the community, but also able to provide very useful information about the flow structure of stratified-dispersed flow.

7.2 Future Work

Despite the enormous efforts and costs directed to the design, construction, validation and tuning of the new experimental methodology, this work can be considered just as a starting point for future improvements and extensions of such technique. In particular, these aspects should be considered in the next steps of the research:

- The first experimental upgrade can be obtained by adopting a higher number of measuring sections, located as closer as possible each other immediately after the injection. This allows to collect a higher number of measurements in the first transient of tracer exhange between droplets and liquid layer and then to obtain a more robust fit of experimental data with the three-field model. This modification could be gained by extending the plastic block of the tracer distribution system, so that it can host more than two wire measuring sections.

- The use of flush-mounted probes - such as pin electrode probes - can be adopted to measure with better accuracy the very thin film at the upper parts of the pipe. This modification of the measuring test section should be relatively easy and cheap. The configuration of three-electrode probes should be maintained, then an accurate calibration at low liquid heights is the only task required.

- An extensive test campaign should be performed in order to collect data over a wider range of flow conditions and gas and liquid physical properties. In this perspective, we remind that the test section developed in the present study is designed to operate at a pressure

of 40 Bar. Gaseous phase properties can be varied also using a different gas, such as nitrogen or SF_6, while water can be replaced by water-propanol mixtures to simulate light hydrocarbon flows.

- Once a significant amount of data have been recorded, the research must evolve toward the development of physically based closure laws for (i) gas/liquid interfacial friction factor, (ii) liquid film holdup and wetted perimeter, (iii) rates of droplet entrainment and deposition. These closure laws will allow the one-dimensional, multi-field, gas-liquid flow models to predict with more accuracy the multiphase flow conditions encountered in many industrial applications, expecially in the Oil&Gas Industry.

A

Design of the perforated section for tracer injection

The section is designed to operate in the range of gas and liquid flow rates explored in the present work: $u_{sg} = 5 - 25$ m/s and $u_{sl} = 0.04 - 0.14$ m/s. In these flow conditions, the film thickness distribution around the circumference is measured during preliminary experiments. The obtained profiles are the same presented in Fig. 6.2. Even though the liquid layer is detected at all the circumferential positions, it should be very difficult to inject tracer where the thickness is measured to be lower than few hundreds microns. For this reason the maximum circumferential coordinate of injection is chosen to be ± 60 °.

The criteria followed in designing the perforated section are listed here:

1. The axial length of injection must be minimized, in order to approximate it with a localized axial coordinate ($z = 0$).
2. Any liquid film flow disturbances must be minimized. This implies:
    a. to minimize the diameter of injection holes;
    b. to limit the tracer flow rate;
    c. to limit the tracer velocity while exiting from the holes. As a consequence, a minimum number of holes is established.

Conservatively, the system is designed as it should work in the most severe condition:

- maximum film flow rate $W_{Fmax} \longrightarrow$ maximum tracer flow rate W_{Tmax};
- minimum film thickness $h(\theta)_{min}$.

With the aim of obtain an uniform circumferential increase of concentration in the wall layer, the tracer flow rate must be proportional to the local film flow rate. This latter quantity is not known a priori, as it is one of

the parameters to be measured with the tracer method. It is then estimated that the local film flow rate could be expressed as a function of the local film thickness,

$$W_{Fi} = a h_i^n \ , \tag{A.0.1}$$

where i is a counter for the electrodes (and the corresponding chambers), a is a constant of proportionality and the exponent n depends on the flow regime. Since

$$W_F = \sum_i W_{Fi} = a \sum_i h_i^n \ , \tag{A.0.2}$$

we can derive the local film flow rate:

$$W_{Fi} = W_F \frac{h_i^n}{\sum_i h_i^n}. \tag{A.0.3}$$

It has been demonstrated that the exponent n varies between 1.1 for a turbulent flow and 2.0 for a laminar flow. In the present case this parameter has been arbitrarily set to 1.4. From an estimate of the maximum film flow rate in the pipe and considering a tracer over film flow rate ratio of 0.02, the maximum tracer flow rate at each chamber is derived. As requested by criterium 2.c., it is essential to limit the injection velocity of the tracer, to avoid part of the tracer jet to penetrate the liquid substrate and to be spread directly in the gas core in the form of droplets, as already said in Section 5.3.3.

Table A.1 – Parameters of the perforated section.

chamber	hole diameter [mm]	n°of rows	n°of holes per row	distance between holes [mm]
A	0.6	4	25	2
B	0.6	4	25	2
C	0.6	4	17	3
D	0.6	2	17	3

When the kinetic energy of the tracer flow equals the hydrostatic pressure of the liquid film

$$\frac{1}{2} v_T^2 = gh \ , \tag{A.0.4}$$

the maximum velocity v_{Tmax} can be found. Combining v_{Tmax} with the required flow rate, the total area of injection per chamber is obtained. The choice of hole diameter falls as a compromise between intrusiveness

reduction and machining limitations. These latter impose also the distance between adjacent holes. Each chamber can hold a number of hole rows, dependent on its circumferential extension. The higher the number of rows, the shorter the axial length of the perforated section. In Fig. 5.6 the final configuration is shown and in Table A.1 the corresponding parameters are reported.

B

List of Publications

Referred Journal Publications

J1 **Pitton**, **E.**, Ciandri, P., Margarone, M., Andreussi, P., 2014. An experimental study of stratified-dispersed flow in horizontal pipes. *Int. J. Multiphase Flow* **67**, 92-103.

J2 Andreussi, P., **Pitton**, **E.**, Ciandri, P., Picciaia, D., Vignali, A., Scozzari, A., 2014. Measurement of liquid film distribution in near-horizontal pipes with an array of wire probes. Under review.

Advanced Courses

1. Non-spherical particles and aggregates in fluid flows, CISM, Udine (Italy), June 17-21, 2013. Coordinated by: C. Marchioli (University of Udine, Italy) and F. Toschi (Eindhoven University of Technology, The Netherlands).
2. FLOW Summer School on Numerical Methods for Multiphase Flows, Linn FLOW Centre, KTH Royal Institute of Technology, Stockholm (Sweden), September 3-7, 2012 Coordinated by: Dr. Philipp Schlatter and Prof. Luca Brandt (KTH Royal Institute of Technology, Sweden)
3. Stochastic Methods in Fluid Mechanics, CISM, Udine (Italy), July 2-6, 2012. Coordinated by: S. Chibbaro (University Pierre et Marie Curie, Paris, France) and J. P. Minier (R&D EDF, Chatou, France).
4. 2011 GRICU PhD National School, S. Margherita di Pula, Cagliari (Italy), 26-29 September 2011. Coordinated by: P. Perego (University of Genoa, Italy)
5. Noise sources in turbulent Shear Flow, CISM, Udine (Italy), April 18-22, 2011. Coordinated by: R. Camusso (University of Rome "Roma Tre", Italy).
6. Euromech Colloquium 513: Dynamics of non Spherical Particles in fluid Turbulence, CISM, Udine (Italy), April 6-8, 2011. Coordinated by: H. I. Andersson (Norwegian University of Science and Technology, Norway) and A. Soldati (University of Udine, Italy).

Acknowledgments

My first gratitude goes to my advisor, Prof. Alfredo Soldati, for having given me the opportunity to seriously experiment myself as a scientist in a long term activity. And for having introduced me to Prof. Paolo Andreussi, which dedicated me a huge amount of his precious time, showing me the right approaches to solve the innumerable problems that I continuously found in my project. I think I've really learned a lot from your great capabilities in performing and managing engineering research.

I would like to thank Paolo Ciandri for his useful suggestions, expecially when technical issues found me unprepared due to my lacks of experience. I also thank Prof. Marina Campolo for her remote support from Udine. A big smile goes to my laboratory colleagues, with whom I had the pleasure to spend nice time in the lab; a special thank is directed to Alex: you have been my personal trainer, I hope I'm not disappointing you with my English now ... I also thank the colleagues of Milano, in particular Daniele, Andrea and Alessia, for their constant help in information technology and CFD simulations.

I acknowledge the city of Pisa, which hosted me during this experience, and anyone who has contributed to make me feel at home. In particular: Pietro, in you I really found a friend; Maria, Laura, Lorenzo, Elisabetta, Sonia, Paolo, and all the friends of Santa Croce.

A deep thought goes to my ex fellow students and/or doctoral candidates Giulio, Andrea, Simone, Gabriele, Enrico; our "meetings" beat the pace of these years. I hope the rhythm still survive in the future. Thanks to my closer PhD colleague Luca, your presence and support have been fundamental in this experience.

I thank my dear historical friends Luca(Muci), Mario and Franco; even though the distance keep us rather separated, your existence is priceless.

Finally, I hug my family: mamma, papà, se da un lato le cose che ci accomunano vanno scemando nel tempo, una cosa potremo condividere sempre più: l'essere adulti. Grazie per il vostro bene incondizionato. Stringo forte nonna Linda, e la ammiro per la sua - forse inconscia - volontà di resistere alle avversità. Anto e Luca, la vostra casa è sempre aperta, anche alle visite non programmate; grazie per il vostro esempio. Il mio ultimo pensiero, sorriso e abbraccio va a mio nipote Giulio, fedele compagno di piccoli/grandi giochi che aiutano entrambi a (ri)scoprire i piccoli/grandi segreti della fe-

licità. E a te, che ancora stai nel grembo, ma che già hai detto sì alla Vita: grazie in anticipo per tutto quello che sarà.

Bibliography

[1] Ambrosini, W., Anhorn, I., Forgione, N., Oriolo, F. and Vigni, P., 1998. Surface characteristics of a water film falling down a flat plate in the laminar-wavy regime. *Third International Conference on Multiphase Flow*, ICMF '98, Lyon, France, June 8-12.

[2] Andreussi, P., 1983. Droplet Transfer in Two-Phase Annular Flow. *Int. J. Multiphase Flow* **9**, 697-713.

[3] Andreussi, P., Asali, J.C., Hanratty, T.J., 1985. Initiation of roll waves in gas-liquid flow. *AIChE J.* **31**, 119-126.

[4] Andreussi, P., Azzopardi, B.J., 1983. Mathematical Modelling of Droplet Deposition and Interchange in Annular Flows. *Int. J. Multiphase Flow* **9**, 681-695.

[5] Andreussi, P., Di Donfrancesco, A., Messia, M., 1988. An Impedance Method for the Measurement of Liquid Hold-up in Two-Phase Flow. *Int. J. Multiphase Flow* **14**, 777-785.

[6] Andreussi, P., Persen, L.N., 1987. Stratified Gas-Liquid Flow in Downwardly Inclined Pipes. *Int. J. Multiphase Flow* **13**, 4, 565-575.

[7] Andreussi, P., Zanelli, S., 1976. Liquid Phase Mass Transfer in Annular Gas-Liquid Flow. *Ing. Chim. Ital.* **12**.

[8] Andritsos, N., Hanratty, T.J., 1987. Interfacial instabilities for horizontal gasliquid flows in pipelines. *Int. J. Multiphase Flow* **13**, 583-603.

[9] Asali, J.C., 1984. Entrainment in vertical gasliquid annular flow. Ph.D. thesis, Urbana (USA): University of Illinois.

[10] Asali, J.C., Hanratty, T.J., Andreussi, P., 1985. Interfacial drag and film height for vertical annular flow. *AIChE J.* **31**, 895-902.

[11] Assad, A., Jan, C.S., Lopez de Bertodano, M.A., Beus, S.G., 1998. Scaled entrainment measurements in ripple-annular flow in a small tube. *Nuclear Engineering and Design* **184**, 437-447.

[12] Barbosa, Jr J.R., Hewitt, G.F., Konig, G., Richardson, S.M., 2002. Liquid entrainment, droplet concentration and pressure gradient at the onset of annular flow in a vertical pipe. *Int. J. Multiphase Flow* **28**, 943-961.

[13] Barral, A.H., Angeli, P.,2014. Spectral density analysis of the interface in stratified oilwater flows. *Int. J. Multiphase Flow* **65**, 117-126.

[14] Bendiksen, K., Malne, D., Moe, R., Nuland, S., 1991. The Dynamic Two-Fluid Model OLGA: Theory and Application. *SPE Prod. Eng. J.* 171-180.

[15] Bezrodnyy, M.K. and Antoshko, Yu., 1992. An acoustic method for measuring the thickness of a flowing film. *Fluid Mechanics Research* **21**, 3, 1-5.

[16] Bieberle, A., Hoppe, D., Schleicher, E., Hampel, U., 2011. Void measurement using high-resolution gamma-ray computed tomography. *Nuclear Eng. and Design* **241**, 6, 2086-2092.

[17] Bonizzi, M., Andreussi, P., Banerjee, S., 2009. Flow regime independent, high resolution multi-field modelling of near-horizontal gasliquid flows in pipelines. *Int. J. Multiphase Flow* **35**, 34-46.

[18] Brown, R.C., Andreussi, P., Zanelli, S, 1978. The use of wire probes for the measurement of liquid film thickness in annular gas-liquid flows. *The Canadian J. of Chemical Engineering* **56**, 6, 754-757.

[19] Buffham, B.A., 1968. Laminar flow in open circular channels and symmetrical lenticular tubes. *Trans. Inst. Chem. Engrs* **46**, T153.

[20] Chang, J.S., Ichikawa, Y. and Irons, G.A., 1982. Flow regime characterization and liquid film thickness measurement in horizontal gasliquid two-phase flow by an ultrasonic method. *Measurements in Polyphase Flow* **7**, 7-12.

[21] Cherdantsev, A.V., Hann, D.B., Azzopardi, B.J., 2014. Study of gassheared liquid film in horizontal rectangular duct using high-speed LIF technique: Three-dimensional wavy structure and its relation to liquid entrainment. *International J. Multiphase Flow* **67**, 52-64.

[22] Clark, W.W., 2002. Liquid Film Thickness Measurement. *Multiphase Science and Technology* **14**, 1, 1-74.

[23] Collier, J.G. and Hewitt, G.F., 1964. Film thickness measurements. *UKAEA*, Report AERE-R 4684.

[24] Coney, M.W.E., 1973. The theory and application of conductance probes for the measurement of liquid film thickness in two-phase flow. *J. Phys. E: Scient. Instrum.* **6**, 903-910.

[25] Cousins, L.B., Denton, W.H., Hewitt,G.F., 1965. Liquid mass transfer in annular two-phase flow. *Atomic Energy Research Establishment* R6426, Harwell, England.

[26] Cousins, L.B.,Hewitt,G.F., 1968. Liquid Phase M ass Transfer in Annular Two-Phase Flow: Droplet Deposition and Liquid Entrainment. *UKAEA*, Report AERE-R 5657.

[27] Cravarolo, L., Hassid, A. and Villani, S., 1961. A beta-ray attenuation method for density measurements of liquid-gas mixtures in adiabatic flow. *Energia Nucleare* **8**, 12, 751-757.

[28] Dallman, J.C., 1981. Application of ultrasonics to the measurement of thin liquid films. *Transactions of the American Nuclear Society* **39**, 1039-1041.

[29] Damsohn, M., Prasser, H.-M., 2009. High-speed liquid film sensor for two-phase flows with high spatial resolution based on electrical conductance. *Flow Meas. and Instrumentation* **20**, 1-14.

[30] Damsohn, M., Prasser, H.-M., 2011. Droplet deposition measurement with high-speed camera and novel high-speed liquid film sensor with high spatial resolution. *Nuclear Eng. and Design* **241**, 2494-2499.

[31] Devia, F., Fossa, M., 2003. Design and optimisation of impedance probes for void fraction measurements. *Flow Meas. and Instr.* **14**, 45, 139149.

[32] Dykhno, L.A., Williams, L.R., Hanratty, T.J., 1994. Maps of mean gas velocity for stratified flows with and without atomization. *Int. J. Multiphase Flow* **20**, 4, 691-702.

[33] Dukler, A.E. and Bergelin, O.P., 1952. Characteristics of flow in falling liquid films. *Chemical Engineering Progress* **48**, 11, 557-563.

[34] Fore, L.B., Dukler, A.E., 1995. Droplet deposition and momentum transfer in annular flow. *AIChE J.* **41**, 9, 2040-2046.

[35] Fossa, M., 1998. Design and performance of a conductance probe for measuring the liquid fraction in two-phase gas-liquid flows. *Flow Meas. and Instrum.* **9**, 103109.

[36] Geraci, G., Azzopardi, B.J., van Maanen, H.R.E., 2007. Effect of inclination on circumferential film thickness variation in annular gas/liquid flow. *Chemical Eng. Science* **62**, 3032-3042.

[37] Gill, L.E., Hewitt, G.F., Hitchon, J.W., Lacey, P.M.C., 1963. Sampling probe studies of the gas core in annular two-phase flow-I: The effect of length on phase and velocity distribution. *Chemical Engineering Science* **18**, 8, 525-535.

[38] Gill, L.E., Hewitt, Lacey, P.M.C., 1964. Sampling probe studies of the gas core in annular two-phase flow-II: Studies of the effect of phase flow rates on phase and velocity distribution. *Chemical Engineering Science* **19**, 9, 665-682.

[39] Giovine, P., Minervini, A., Andreussi, P., 1991. Stability of liquid flow down an inclined tube. *Int. J. Multiphase Flow* **17**, 4, 485-496.

[40] Han, H., Gabriel, K.S., Wang, Z., 2007. A new method of entrainment fraction measurement in annular gas-liquid flow in a small diameter vertical tube. *Flow Measurement and Instrumentation* **18**, 79-86.

[41] Hewitt, C.F., 1979. Liquid mass transport in annular two-phase flow. Momentum Heat and Mass Transfer in Chemical Process and Energy Engineering Systems. Edited by F. Durst, C.G. Tsiklauri and N. Afgan, Hemisphere McGraw-Hill, Washington, DC.

[42] Hewitt, G.F., King, I. and Lovegrove, P.C., 1961. Holdup and pressure drop measurements in the two-phase annular flow of air-water mixtures. *UKAEA*, Report AERE-R 3764.

[43] Hewitt, G.F., King, R.D. and Lovegrove, P.C., 1962. Techniques for liquid film and pressure drop studies in annular two-phase flow. *UKAEA, Report AERE-R 3921.*

[44] Hewitt, G.F. and Lovegrove, P.C., 1962. The application of the light absorption technique to continuous film thickness recording in annular two-phase flow. *UKAEA*, Report AERE-R 3953.

[45] Hewitt, G.F., Lovegrove, P.C. and Nicholls, B., 1964. Film thickness measurement using a fluorescence technique. Part I: Description of the method. *UKAEA*, Report AERE-R 4478.

[46] Hoogendoorn, C.J., Buitelaar, A.A., 1961. The Effect of Gas Density and Gradual Vaporization on Gas-Liquid Flow in Horizontal Pipes. *Chem. Eng. Sci.* **16**, 208.

[47] Hughmark, G.A., Pressburg, B.S., 1961. Holdup and pressure drop with gas-liquid flow in a vertical pipe. *AIChE J.* **7**, 4, 677-682.

[48] Ishii, M., Grolmes, M.A., 1975. Inception criteria for droplet entrainment in two-phase concurrent film flow. *AIChE J.* **21**, 308-318.

[49] Ito, D., Prasser, H.-M., Kikura, H., Aritomi, M., 2011. Uncertainty and intrusiveness of three-layer wire-mesh sensor. *Flow Meas. and Instrumentation* **22**, 249256.

[50] Jagota, A.K., Rhodes, E., Scott, D.S., 1973. Tracer measurements in two-phase annular flow to obtain interchange and entrainment. *Can. J. Chem. Eng.*, **51**, 139-147.

[51] James, P.W., Hewitt, G.F., Whalley, P.B., 1980. Droplet motion in two-phase flow. *Atomic Energy Research Establishment*, R9711, Harwell, U.K.

[52] Kamei, T., Serizawa, A., 1998. Measurement of 2-dimensional local instantaneous liquid film thickness around simulated nuclear fuel rod by ultrasonic transmission technique. *Nuclear Engineering and Design* **184**, 349-362.

[53] Kang, H.C. and Kim, M.H., 1992a. The development of a flush-wire probe and calibration technique for measuring liquid film thickness. *International J. Multiphase Flow* **19**, 3, 423-437.

[54] Kang, H.C. and Kim, M.H., 1992b. Measurement of three-dimensional wave form and interfacial area in an air-water stratified flow. *Nuclear Engineering and Design* **136**, 347-360.

[55] Kim, J., Ahn, Y.-C., Kim, M.H., 2009. Measurement of void fraction and bubble speed of slug flow with three-ring conductance probes. *Flow Meas. And Instr.* **20**, 103-109.

[56] Koskie, J.E., Mudawar, I. and Tiederman, W.G., 1989. Parallel-wire probes for the measurement of thick liquid films. *Int. J. Multiphase Flow* **15**, 4, 521-530.

[57] Kvurt, Yu.P., Kholpanov, L.P., Malyusov, V.A. and Zhavoronkov, N.M., 1981. Influence of the alternating-current on the results of measurement of the thickness of liquid films by the conductivity method. *J. of Applied Chemistry in the USSR* **54**, 5, 872-876.

[58] Leman, G.W., Agostini, A., Andreussi, P., 1985. Tracer Analysis of Developing Two-Phase Annular Flow. *PhisicoChem. Hydrodynam.* **6**, 223-237.

[59] Leskovar, B., Sun, R.K., Kolbe, W.F. and Turko, B., 1979. Measurement of the thickness of liquid film by means of the capacitance method. Prepared for the *Electric Power Research Institute*. Research project 1379-1, Report No. NP-1212.

[60] Lioumbas, J.S., Paras, S.V., Karabelas, A.J., 2005. Co-current stratified gasliquid downflow Influence of the liquid flow field on interfacial structure. *Int. J. Multiphase Flow* **31**, 869896.

[61] Lopez de Bertodano, M.A., Jan, C.S., Beus, S.G., 1997. Annular flow entrainment rate experiment in a small vertical pipe. *Nuclear Engineering and Design* **178**, 61-70.

[62] Miya, M., Woodmansee, D.E., Hanratty, T.J., 1971. A model for roll waves in gas-liquid flow. *Chemical Engineering Science* **26**, 11, 1915-1931.

[63] Murav'ev, M.Yu., Vashak, F. and Kulov, N.N., 1984. Determination of the instantaneous thickness of a falling liquid film with a microelectrode. *Theoretical Foundations of Chemical Engineering* **17**, 6, 511-515.

[64] Nydal, O.J., Pintus, S., Andreussi, P., 1992. Statistical Characterization of Slug Flow. *Int. J. Multiphase Flow* **18**, 439-453.

[65] Ozgu, M.R., Chen J.C., and Eberhardt, N., 1973. A capacitance method for measurement of film thickness in two-phase flow. *Review of Scientific Instruments* **44**, 12, 1714-1716.

[66] Paras, S.V., Karabelas, A.J., 1991. Droplet Entrainment and Deposition in Horizontal Annular Flow. *Int. J. Multiphase Flow* **17**, 455-468.

[67] Prasser, H.-M., Bttger, A., Zschau, J., 1998. A new electrode-mesh tomograph for gasliquid flows. *Flow Meas. and Instrum.* **9**, 111119.

[68] Quandt, E.R., 1965. Measurement of Some Basic Parameters in Two-Phase Annular Flow. *AIChE J.* **11**, 311-318.

[69] Ritcher, S., Aritomi, M., Prasser, H.-M., Hampel, R., 2002. Approach towards spatial phase reconstruction in transient bubbly flow using wire-mesh sensor. *Int. J. Heat Mass Transfer* **45**, 10631075.

[70] Roy, R.P., Ku, J., Kaufman, I. and Shulda, J., 1986. Microwave method for measurement of liquid film thickness in gas-liquid flow. *Review of Scientific Instruments* **57**, 5, 952-956.

[71] Schadel, S.A., Leman, G.W., Binder, J.L., Hanratty, T.J., 1990. Rates of Atomization and Deposition in Vertical Annular Flow. *Int. J. Multiphase Flow* **16**, 363-374.

[72] Schubring, D., Ashwood, A.C., Shedd, T.A., Hurlburt, E.T., 2010a. Planar laser-induced fluorescence (PLIF) measurements of liquid film thickness in annular flow. Part I: Methods and data. *Int. J. Multiphase Flow* **36**, 10, 815-824.

[73] Schubring, D., Shedd, T.A., Hurlburt, E.T., 2010b. Studying disturbance waves in vertical annular flow with high-speed video. *Int. J. Multiphase Flow*, **36**, 385-396.

[74] Sekoguchi, K. and Mori, K., 1997. New development of experimental study on interfacial structure in gas-liquid two-phase flow. *Experimental Heat Transfer, Fluid Mechanics and Thermodynamics*, Edizioni ETS, pp 1177-1187.

[75] Sekoguchi, K., Takeishi, M., 1989. Interfacial structures in upward huge wave flow and annular flow regimes. *International J. Multiphase Flow* **15**, 3, 295-305.

[76] Sekoguchi, K., Takeishi, M. and Ishimatsu, T., 1985. Interfacial structure in vertical upward annular flow. *PhysicoChemical Hydrodynamics* **6**, 1-2, 239-255.

[77] Solesio, J.N., Flamand, J.C. and Delhaye, J.M., 1978. Liquid film thickness measurements by means of an x-ray absorption technique. Taken from *Topics in heat transfer and two phase flow*, by Bankoff, S.G., pp 193-198.

[78] Starkovich, V.S., Bird, P.F., Dallman, J.C. and Strong, R.D., 1980. Ultrasonic liquid film thickness measurements. *Transactions of the American Nuclear Society* **35**, 640-641.

[79] http://subseaworldnews.com/

[80] Sun, R.K., Kolbe, W.F., Leskovar, B. and Turko, B., 1982. Measurement of thickness of thin water film in two-phase flow by a capacitance method. *IEEE Transactions on Nuclear Science*, **29**, 1, 688-694.

[81] Swanson, R.W., 1966. Characteristics of the gas-liquid interface in two phase annular flow. Ph.D. Thesis, University of Delaware, Delaware.

[82] Tailby, S.R., and Portalski, S., 1960. The hydrodynamics of liquid films flowing on a vertical surface. *Trans. Instn Chem. Engrs.* **38**, 324-330.

[83] Taitel, Y., Dukler, A.E., 1976. A model for predicting flow regime transitions in horizontal and near horizontal gas-liquid flow. *AIChE J.* **22**, 47-55.

[84] Tayebi, D., Nuland, S., Fuchs, P., 2000. Droplet Transport in Oil/Gas Flow at High Gas Densities. *Int. J. Multiphase Flow* **26**, 741-761.

[85] Tzotzi, C., Bontozoglou, V., Andritsos, N., 2011. Effect of Fluid Properties on Flow Patterns in Two-Phase Gas-Liquid Flow in Horizontal and Downward Pipes. *Ind. Eng. Chem. Res.* **50**, 645655.

[86] Van't Westende, J.M.C., Belt, R.J., Portela, L.M., Mudde, R.F., Oliemans, R.V.A., 2007. Effect of secondary flow on droplet distribution and deposition in horizontal annular pipe flow. *Int. J. Multiphase Flow* **33**, 67-85.

[87] Vieira, R.E., Kesana, N.R., Torres, C.F., McLaury, B.S., Shirazi, S.A., Schleicher, E., Hampel, U., 2014. Experimental Investigation of Horizontal GasLiquid Stratified and Annular Flow Using Wire-Mesh Sensor. *J. of Fluids Engineering* **136**, 12, 1-16. In Press. Available online.

[88] Wallis, G.B., 1962. The onset of droplet entrainment in annular gas-liquid flow. General Electric Report no. 62 GL127.

[89] Webb, D.R., 1970. Studies of the characteristics of downward annular two-phase flow. Part 3. *UKAEA*, Report AERE-R6426.

[90] Whalley, P.B., Hewitt, G.F., Hutchinson, P., 1973. Experimental wave and entrainment measurements in vertical annular two-phase flow. *UKAEA*, Report AERE-R7521.

[91] Williams, L.R., Dykhno, L.A., Hanratty, T.J., 1996. Droplet Flux Distributions and Entrainment in Horizontal Gas-Liquid Flows. *Int. J. Multiphase Flow* **22**, 1-8.

[92] Wittig, S., Himmelsbach, J., Noll, B., Feld, D. J. and Samenfmk, W., 1992. Motion and evaporation of shear-driven liquid films in turbulent gases. *ASME-Journal of Engineering for Gas Turbines and Power* **114**, 395-400.

[93] Woodmansee, D.E., Hanratty, T.J., 1969. Base film over which roll waves propagate. *AIChE J.* **15**, 712-715.

[94] Xu, L., Han, Y., Xut, L.-A., Yangt, J., 1997. Application of ultrasonic tomography to monitoring gas/liquid flow. *Chemical Engineering Science* **52**, 13, 2171-2183.

[95] Zadrazil, I., Matar, O.K., Markides, C.N., 2014. An experimental characterization of downwards gasliquid annular flow by laser-induced fluorescence: Flow regimes and film statistics. *International J. Multiphase Flow* **60**, 87-102.

[96] Zhang, Z., Bieberle, M., Barthel, F., Szalinski, L., Hampel, U., 2013. Investigation of upward concurrent gas-liquid pipe flow using ultrafast X-ray tomography and wire-mesh sensor. *Flow Meas. And Instr.* **32**, 111-118.

[97] Zhao, Y., Markides, C.N., Matar, O.K., Hewitt, G.F., 2013. Disturbance wave development in two-phase gasliquid upwards vertical annular flow. *Flow Meas. And Instr.* **55**, 111-129.